STUDY OF THE PROPERTIES OF COMPACT STARS AND NUCLEAR REACTIONS OF ASTROPHYSICAL IMPORTANCE

By
DEBASIS ATTA
PHYS04201204008

Variable Energy Cyclotron Centre, Kolkata

A thesis submitted to the
Board of Studies in Physical Sciences

In partial fulfillment of requirements
for the Degree of
DOCTOR OF PHILOSOPHY
of
HOMI BHABHA NATIONAL INSTITUTE

August, 2018

Homi Bhabha National Institute[1]

Recommendations of the Viva Voce Committee

As members of the Viva Voce Committee, we certify that we have read the dissertation prepared by **Debasis Atta** entitled **"Study of the Properties of Compact Stars and Nuclear Reactions of Astrophysical importance"** and recommend that it may be accepted as fulfilling the thesis requirement for the award of Degree of Doctor of Philosophy.

Chairman - Prof. S. R. Banerjee		**Date:** 21/8/2018
Guide / Convener - Prof. D. N. Basu	D.N. Basu	**Date:** 21/08/2018
Co-guide - <Name> (if any)		**Date:**
Examiner – Prof. Rajeev Puri		**Date:** 21-8-2018
Member 1- Prof. Gargi Chaudhuri	Gargi Chaudhuri	**Date:** 21. 8. 2018
Member 2- Prof. Subinit Roy	Subinit Roy	**Date:** 21. 08. 2018

Final approval and acceptance of this thesis is contingent upon the candidate's submission of the final copies of the thesis to HBNI.

I/We hereby certify that I/we have read this thesis prepared under my/our direction and recommend that it may be accepted as fulfilling the thesis requirement.

Date: 21/08/2018

Place: Kolkata

<Signature>
Co-guide (if applicable)

D.N. Basu
Prof. D. N. Basu
Guide

[1] This page is to be included only for final submission after successful completion of viva voce.

Version approved during the meeting of Standing Committee of Deans held during 29-30 Nov 2013

STATEMENT BY AUTHOR

This dissertation has been submitted in partial fulfillment of requirements for an advanced degree at Homi Bhabha National Institute (HBNI) and is deposited in the Library to be made available to borrowers under rules of the HBNI.

Brief quotations from this dissertation are allowable without special permission, provided that accurate acknowledgement of source is made. Requests for permission for extended quotation from or reproduction of this manuscript in whole or in part may be granted by the Competent Authority of HBNI when in his or her judgment the proposed use of the material is in the interests of scholarship. In all other instances, however, permission must be obtained from the author.

Debasis Atta

Debasis Atta

DECLARATION

I, hereby declare that the investigation presented in the thesis has been carried out by me. The work is original and has not been submitted earlier as a whole or in part for a degree / diploma at this or any other Institution / University.

Debasis Atta
Debasis Atta

List of Publications arising from the thesis

Journal

1) Stability of β- eqilibrated dense matter and core crust transition in neutron stars, **Debasis Atta**, D. N. Basu, *Physical Review C 90, 035802 (2014).*

2) Fusion cross section for reactions involving medium and heavy nucleus-nucleus system, **Debasis Atta**, D. N. Basu, *Physical Review C 90, 064622 (2014).*

3) Yields of neutron rich nuclei by actinide photofission in the giant dipole resonance region, Debasis Bhowmick, **Debasis Atta**, D.N. Basu, Alok Chakraborty, *Physical Review C 91, 044611 (2015).*

4) Energy Dependence of exotic nuclei production cross sections by photofission reaction in GDR range, Debasis Bhowmick, F.A. Khan, **Debasis Atta**, D.N. Basu, Alok Chakraborty, *Can. J. Phys. 94, 243-248 (2016).*

5) Nuclear constraints on the core-crust transition and crustal fraction of moment of inertia of neutron stars, **Debasis Atta**, S Mukhopadhyay, D.N. Basu , *Ind. J. Phys. 91, 235-242 (2017).*

6) Landau Quantization and mass-radius relation of magnetized white dwarfs in general relativity, S. Mukhopadhyay, **Debasis Atta**, D.N. Basu, *Rom. Rep. Phys 69, 101 (2017).*

7) Compact bifluid hybrid stars: hadronic matter mixed with self-interacting fermionic asymmetric dark matter, S. Mukhopadhyay, **Debasis Atta**, K. Imam, D.N. Basu, C. Samanta, *Eur. Phys. J. C. 77, 440 (2017).*

8) Gravitational waves from isolated neutron stars: mass dependence of r-mode instability, S. Mukhopadhyay, Joydev Lahiri, **Debasis Atta**, K. Imam, D.N. Basu, *Physical Review C 97, 065804 (2018).*

9) Astrophysical S-factor for the deep sub-barrier fusion reactions of light nuclei, Vinay Singh, **Debasis Atta**, Md. A. Khan, D.N. Basu, *arXiv:1807.05815.*

Chapters in books and lectures notes

1. NA

2. NA

Conferences

1. Locating inner edge of neutron star crust from stability of neutron star matter, **Debasis Atta**, D.N. Basu, Proceedings of the DAE Symposium on Nuclear Physics, BHU University, Varanasi, UP, India, 59, 784-785 (2014).

2. Near barrier fusion cross sections for medium-heavy nuclei, **Debasis Atta**, D.N. Basu, Proceedings of the DAE Symposium on Nuclear Physics, BHU University, Varanasi, UP, India, 59, 384-385 (2014).

3. Exotic nuclei production by photofission at many energies, F. A. Khan, Debasis Bhowmick, **Debasis Atta**, D.N. Basu, M. Farooq, Alok Chakraborty, Proceedings of the DAE Symposium on Nuclear Physics, Satya Sai University, Andhra Pradesh, India, 60, 634-635 (2015).

4. Mass radius relation of magnetized white dwarfs, Somnath Mukhopadhyay, **Debasis Atta**, D.N. Basu, Proceedings of the DAE Symposium on Nuclear Physics, Satya Sai University, Andhra Pradesh, India, 60, 838-839 (2015).

5. Crustal fraction of moment of inertia of pulsars, **Debasis Atta**, Somnath Mukhopadhyay, D. N. Basu, Proceedings of the DAE Symposium on Nuclear Physics, Satya Sai University, Andhra Pradesh, India, 60, 854-855 (2015).

6. Interacting & non-interacting fermionic dark matter and quark matter compact stars, **Debasis Atta**, Somnath Mukhopadhyay, D.N. Basu, C. Samanta, Proceedings of the DAE Symposium on Nuclear Physics, Saha Institute of Nuclear Physics, Kolkata, India, 61, 890-891 (2016).

7. Astrophysical S factor for sub-barrier Fusion Reaction, Vinay Singh, **Debasis Atta** , Md. A. Khan, Proceedings of the DAE Symposium on Nuclear Physics,Saha Institute of Nuclear Physics, Kolkata, India, 61, 930-931 (2016).

Others

1. NA

Debasis Atta

Debasis Atta

ACKNOWLEDGEMENTS

It is a great pleasure to express my sincere thanks to Dr. D. N. Basu for his supervision throughout this work. I am greatly indebted to him for his keen interest, valuable suggestions and encouragement.

I am very grateful to Dr. C. Samanta, Dr. Alok Chakraborty, Dr. D. Bhowmik, Dr. A. Khan for fruitful collaboration with them.

I wish to thanks Dr (s) S. R. Bannerjee, J. Alam, G. Chowdhury, Subinit Roy, Tilak Ghosh for many helpful discussions and suggestions.

I am deeply moved to thank my parents and my wife Paramita for their constant love and encouragement.

At the end, I acknowledge with thanks the co-operation extended by the officials and friends of VECC physics group.

Version approved during the meeting of Standing Committee of Deans held during 29-30 Nov 2013

Homi Bhabha National Institute

SYNOPSIS OF Ph. D. THESIS

1. Name of the Student: Shri Debasis Atta

2. Name of the Constituent Institution: Variable Energy Cyclotron Centre

3. Enrolment No. : PHYS04201204008

4. Title of the Thesis: Study of the Properties of Compact Stars and Nuclear Reactions of Astrophysical importance

5. Board of Studies: Physical Science

SYNOPSIS

(Limited to 10 pages in double spacing)

The neutron star properties are studied using β-equilibrated neutron star matter obtained from the density dependent M3Y effective nucleon-nucleon interaction for a pure hadronic model. The results agree with the recent observations of the massive compact stars. The high-density behavior of symmetric and asymmetric nuclear matter satisfies the constraints from the observed flow data of heavy-ion collisions. The stability of the β-equilibrated dense nuclear matter is analyzed with respect to the thermodynamic stability conditions. The effects of the nuclear incompressibility on the core-crust transition density and pressure are investigated.

In a Fermi gas model of interacting nucleons, with isospin asymmetry $X = \frac{\rho_n - \rho_p}{\rho_n + \rho_p}, \quad \rho = \rho_n + \rho_p$, where ρ_n, ρ_p and ρ are the neutron, proton and nucleonic densities respectively, the energy per nucleon for isospin asymmetric nuclear matter can be derived as [1] $\epsilon(\rho, X) = [\frac{3\hbar^2 k_F^2}{10m}]F(X) + (\frac{\rho J_v C}{2})(1 - \beta\rho^n)$ where m is the nucleonic mass, $k_F{=}(1.5\pi^2\rho)^{\frac{1}{3}}$ which equals Fermi momentum in case of SNM, the kinetic energy per nucleon $\epsilon^{kin}{=}[\frac{3\hbar^2 k_F^2}{10m}]F(X)$ with $F(X){=}[\frac{(1+X)^{5/3}+(1-X)^{5/3}}{2}]$ and $J_v{=}J_{v00} + X^2 J_{v01}$, J_{v00} and J_{v01} represent the volume integrals of the t_{00}^{M3Y} and the isovector t_{01}^{M3Y} components of M3Y interaction.

The ϵ^{kin} can be differentiated with respect to ρ to yield equation for $X = 0$: $\frac{\partial\epsilon}{\partial\rho} = [\frac{\hbar^2 k_F^2}{5m\rho}] + \frac{J_{v00}C}{2}[1-(n+1)\beta\rho^n] - \alpha J_{00}C[1-\beta\rho^n][\frac{\hbar^2 k_F^2}{10m}]$. Then energy/baryon and its derivative with the saturation condition $\frac{\partial\epsilon}{\partial\rho} = 0$ at $\rho = \rho_0$, $\epsilon = \epsilon_0$ can be solved simultaneously for fixed values of the saturation energy per nucleon ϵ_0 and the saturation density ρ_0 of the cold SNM to obtain the values of β and C. The constants of density dependence β and C, thus obtained, are given by $\beta = \frac{[(1-p)+(q-\frac{3q}{p})]\rho_0^{-n}}{[(3n+1)-(n+1)p+(q-\frac{3q}{p})]}$ where $p{=}\frac{[10m\epsilon_0]}{[\hbar^2 k_{F_0}^2]}$, $q{=}\frac{2\alpha\epsilon_0 J_{00}}{J_{v00}^0}$, $J_{v00}^0{=}J_{v00}(\epsilon_0^{kin})$ implying J_{v00} at $\epsilon^{kin}{=}\epsilon_0^{kin}$, the kinetic energy part of the saturation energy per nucleon of SNM, $k_{F_0}{=}[1.5\pi^2\rho_0]^{1/3}$ and $C = -\frac{[2\hbar^2 k_{F_0}^2]}{5mJ_{v00}^0\rho_0[1-(n+1)\beta\rho_0^n - \frac{q\hbar^2 k_{F_0}^2(1-\beta\rho_0^n)}{10m\epsilon_0}]}$.

The basic equation in neutron star matter research is the shape of the relationship between the pressure and energy density $P = P(\varepsilon)$, usually called the equation of state. At the zero temperature, the state of neutron star matter should be uniquely described by the quantities that are conserved by the process leading to equilibrium. Stable high density nuclear matter must be in chemical equilibrium for all types of reactions including the weak interactions, while the beta decay and orbital electron capture takes place simultaneously. For the β-equilibrated neutron star matter we have free neutron decay $n \rightarrow p + \beta^- + \nu_e$ which are governed by weak interaction and the electron capture process $p+\beta^- \rightarrow n+\underline{\nu_e}$. Both types of reactions determine the proton fraction while neutrinos leave the system. The absence of neutrino implies that $\mu = \mu_n - \mu_p = \mu_e$ where μ_e, μ_n and μ_p are the chemical potentials for electron, neutron and proton, respectively.

The β-equilibrium proton fraction is obtained by solving $\hbar c(3\pi^2\rho x_p)^{1/3} = -\frac{\partial\epsilon(\rho,x_p)}{\partial x_p} = +2\frac{\partial\epsilon}{\partial X} \approx 4E_{sym}(\rho)(1-2x_p)$, where isospin asymmetry $X = 1-2x_p$ and the symmetry energy $E_{sym}(\rho) = \frac{1}{2}\frac{\partial^2\epsilon(\rho,X)}{\partial X^2} \mid_{X=0} \approx \epsilon(\rho,1) - \epsilon(\rho,0)$. The pressure P of pure neutron matter (PNM) and β-equilibrated neutron star matter are plotted in Fig.-1 as functions of ρ/ρ_0. Although, the parameters of the density dependence of DDM3Y interaction have been tuned to reproduce ρ_0 and ϵ_0 which are obtained from finite nuclei, the agreement of the present EoS with the experimental flow data, where the high density behaviour looks phenomenologically confirmed, justifies its extrapolation to high density. The quantity $V_{thermal}$ which determines the thermodynamic instability region of neutron star matter at β-equilibrium is given by [2] $V_{thermal} = -(\frac{\partial P}{\partial v})_\mu = \rho^2\Big[2\rho\frac{\partial\epsilon^b}{\partial\rho} + \rho^2\frac{\partial^2\epsilon^b}{\partial\rho^2} - \rho^2\frac{(\epsilon^b_{\rho x_p})^2}{\epsilon^b_{x_p x_p}}\Big]$. The condition for core-crust transition is obtained by making $V_{thermal} = 0$.

The standard value of n=2/3 used here has a unique importance because then the constant of density dependence β has the dimension of cross section and can be interpreted as the isospin averaged effective nucleon-nucleon interaction cross section in ground state symmetric nuclear medium. The comparison of the theoretical values of symmetric nuclear matter incompressibility and isobaric incompressibility with the recent experimental values for $K_\infty = 250 - 270$ MeV [3, 4] and $K_\tau = -370 \pm 120$ MeV [5] further justifies importance for our choice of n=2/3. It is interesting to mention here that the present

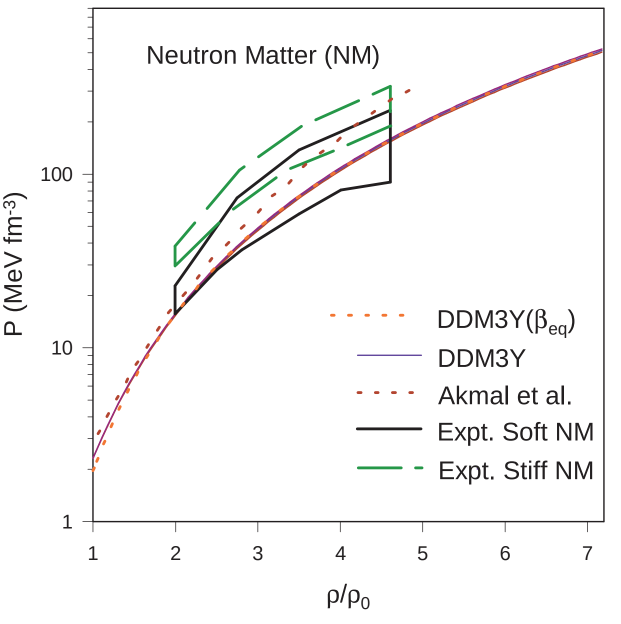

Figure 1: Plots for pressure P of dense nuclear matter as functions of ρ/ρ_0. The continuous line represents the pure neutron matter and the dashed line represents the β-equilibrated neutron star matter. The areas enclosed by the continuous and the dashed lines correspond to the pressure regions for neutron matter consistent with the experimental flow data after inclusion of the pressures from asymmetry terms with weak (soft NM) and strong (stiff NM) density dependences, respectively [6].

EoS for n=2/3, provides the maximum mass for the static case is 1.92 M$_\odot$ with radius ~9.7 km and for the star rotating with Kepler's frequency it is 2.27 M$_\odot$ with equatorial radius ~13.1 km [7]. However, for stars rotating with maximum frequency limited by the r-mode instability, the maximum mass turns out to be 1.95 (1.94) M$_\odot$ corresponding to rotational period of 1.5 (2.0) ms with radius about 9.9 (9.8) kilometers [8] which reconcile with the recent observations of the massive compact stars ~2 M$_\odot$ [9, 10].

The calculations are performed using n=2/3 and saturation density as 0.1533 fm^{-3}. Present calculations for symmetric nuclear matter provide nuclear incompressibility K_∞ = 274.7 ± 7.4, symmetry energy at saturation density $E_{sym}(\rho_0)$ = 30.71 ± 0.26, the slope L = 45.11 ± 0.02 and K_τ = −408.97 ± 3.01 (all in MeV) [11] and for β-equilibrated

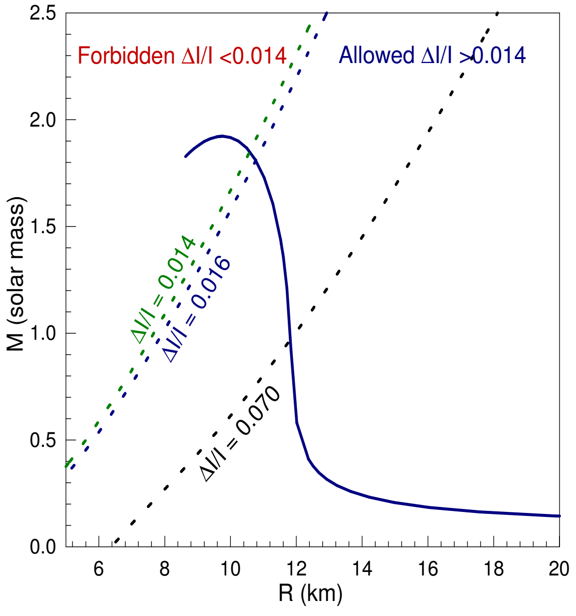

Figure 2: Mass-radius relation of slowly rotating neutron stars for present nuclear EoS. Constraint $\frac{\Delta I}{I}$>1.4% (1.6%, 7%) for Vela pulsar implies that to right of line defined by $\frac{\Delta I}{I}$=0.014(0.016,0.07) (ρ_t=0.0938 fm^{-3}, P$_t$=0.5006 MeV fm^{-3}) allowed masses & radii lie.

neutron star matter at the core-crust transition, the density $\rho_t = 0.0938$ fm^{-3}, pressure P$_t$ = 0.5006 MeV fm^{-3} and proton fraction x$_{p(t)}$ = 0.0308. The mass-radius relation for neutron stars is obtained by solving the Tolman-Oppenheimer-Volkoff Equation (TOV) [12, 13] and then the crustal fraction of moment of inertia is determined using ρ_t and P$_t$ at core-crust transition. Since in the Vela pulsar the angular momentum requirements of glitches indicate that 1.4% of the star's moment of inertia drives these events, the allowed region for masses and radii for Vela pulsar is determined from the condition that the crustal fraction of the total moment of inertia $\frac{\Delta I}{I} > 0.014$ which sets a limit for its radius.

The structure of a spherically symmetric body of isotropic material which is in static gravitational equilibrium is given by the Tolman-Oppenheimer-Volkoff (TOV) equation [12, 13] $\frac{dP(r)}{dr} = -\frac{G}{c^4}\frac{[\varepsilon(r)+P(r)][m(r)c^2+4\pi r^3P(r)]}{r^2[1-\frac{2Gm(r)}{rc^2}]}$ where $\varepsilon(r) = (\epsilon + m_b c^2)\rho(r)$, $m(r)c^2 = \int_0^r \varepsilon(r')d^3r'$ where $\varepsilon(r)$ and $P(r)$ are the energy density and pressure at a radial distance r from the centre whereas $m(r)$ is the mass of the star contained inside radius r. The TOV equation can be easily solved numerically using Runge-Kutta method. The $\varepsilon(r)$ and $P(r)$ are provided by the EoS. The size of the star is determined by the boundary condition $P(r) = 0$ at the surface R of the star and the total mass M of the star integrated up to R is given by $M = m(R)$ [14]. Being the initial value problem, the numerical solution of TOV equation requires single integration constant, the pressure P_c at the center $r = 0$ of the star calculated at a given central density ρ_c. The masses of slowly rotating neutron stars are very close [7, 8, 15] to those obtained by solving TOV equation.

Calculations for masses and radii are performed using EoS covering crustal region of a compact star consisting Feynman-Metropolis-Teller (FMT) [16], Baym-Pethick-Sutherland (BPS) [17] and Baym-Bethe-Pethick (BBP) [18] upto number density of 0.0582 fm^{-3} and β-equilibrated neutron star matter beyond. Once masses and radii are determined, $\frac{\Delta I}{I}$ are obtained from $\frac{28\pi \mathrm{P}_t R^3}{3Mc^2}\left(\frac{1-1.67\xi-0.6\xi^2}{\xi}\right) \times \left(1 + \frac{2\mathrm{P}_t}{\rho_t m_b c^2}\frac{(1+7\xi)(1-2\xi)}{\xi^2}\right)^{-1}$ where $\xi = \frac{GM}{Rc^2}$. The mass-radius relation is obtained for fixed values of $\frac{\Delta I}{I}$, ρ_t and P_t. This is then plotted in the same figure for $\frac{\Delta I}{I} = 0.014$. For Vela pulsar, the constraint $\frac{\Delta I}{I} > 1.4\%$ implies that allowed mass-radius lie to the right of the line defined by $\frac{\Delta I}{I} = 0.014$ (for $\rho_t = 0.0938$ fm^{-3}, $\mathrm{P}_t = 0.5006$ MeV fm^{-3}). This condition is given by $R \geq 4.10 + 3.36M/M_\odot$ km.

Recently, it is conjectured that the observed glitches in the Vela pulsar require an additional storage of angular momentum and to explain the phenomenon [19] the crust may not be enough. Large pulsar frequency glitches can be interpreted as sudden transfers of angular momentum between the neutron superfluid permeating the inner crust and the rest of the star. In spite of the absence of viscous drag, the neutron superfluid is strongly coupled to the crust due to non-dissipative entrainment effects. It is often argued that these effects may put a constraint on the maximum amount of angular momentum that during glitches can possibly be transferred [20]. We find that the present EoS can accommodate large crustal moments of inertia and that large enough transition pressures can be generated to explain the large Vela glitches without invoking an additional angular-

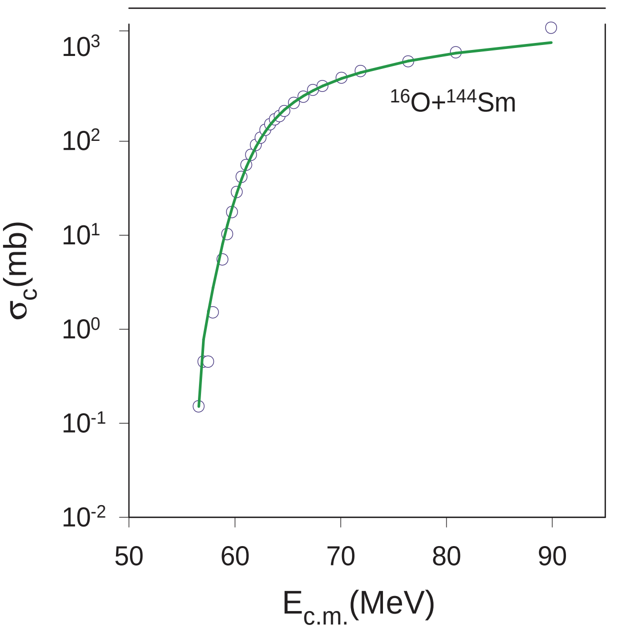

Figure 3: Comparison of the measured capture excitation functions (full circles) for ^{16}O+^{144}Sm with predictions (solid lines) of the diffused barrier formula.

momentum reservoir beyond that confined to the solid crust. Our results suggest that the crust may be enough [21] and $\frac{\Delta I}{I} > 0.014$ for pulsars with masses 1.8 $M_\odot$ or less. However, if the phenomenon of crustal entrainment due to the Bragg reflection of unbound neutrons by the lattice ions is taken into account then [19, 20] a much higher fraction of the moment of inertia (7% instead of 1.4-1.6%) has to be associated to the crust. This causes drastic modification of the moment of inertia of the superfluid component. If $\frac{\Delta I}{I} > 0.07$ is considered, then the corresponding allowed masses and radii will be given by $R \geq 7.60 + 3.71M/M_\odot$ instead of $R \geq 4.10 + 3.36M/M_\odot$ and it would mean maximum mass $\sim 1.M_\odot$ which contradicts the estimated mass of Vela pulsar [22] and suggests that this fraction can be at most 3.6% due to crustal entrainment.

The second part of thesis consists of calculation of fusion cross sections for astrophysical reactions. The aim of the present work is to obtain the fusion cross section for reaction involving medium and heavy nucleus nucleus system. The phenomenological description of fusion excitation functions is achieved by assuming Gaussian barrier

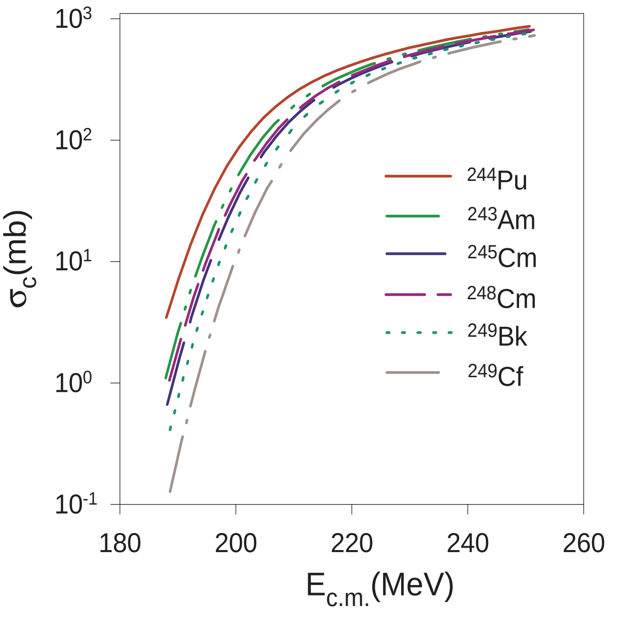

Figure 4: Capture excitation functions for ^{48}Ca+^{244}Pu,^{243}Am,^{245}Cm,^{248}Cm,^{249}Bk,^{249}Cf.

distribution $D(B) = \frac{1}{\sqrt{2\pi}\sigma_B}\exp\Big[-\frac{(B-B_0)^2}{2\sigma_B^2}\Big]$, where the two parameters, the mean barrier B_0 and the distribution width σ_B, to be determined individually for each reaction. Folding this distribution with the classical expression for the fusion cross section given by $\sigma_f(B) = \pi R_B^2\Big[1 - \frac{B}{E}\Big]$ for $B \leq E$ and $= 0$ for $B \geq E$ where R_B denotes the relative distance corresponding to the position of the barrier approximately, which yields $\sigma_c(E) = \pi R_B^2 \frac{\sigma_B}{E\sqrt{2\pi}}\Big[\xi\sqrt{\pi}\Big\{\text{erf}\xi + \text{erf}\xi_0\Big\} + e^{-\xi^2} + e^{-\xi_0^2}\Big]$ where $\xi = \frac{E-B_0}{\sigma_B\sqrt{2}}$, $\xi_0 = \frac{B_0}{\sigma_B\sqrt{2}}$ and erfξ is the Gaussian error integral of argument ξ. The parameters B_0 and σ_B along with R_B is to be determined by fitting this expression to a given fusion excitation function. The same set of target-projectile combinations (along with few others) have been selected for which heavy ion sub-barrier fusion has been recently [23] studied. The values of mean barrier height B_0, width σ_B and the effective radius R_B have been obtained using the least-square fit method. In Fig.-3, the measured fusion excitation functions represented by full circles are compared with the predictions of the diffused barrier formula depicted by the solid lines. The system ^{16}O+^{144}Sm is illustrated in Fig.-3 corresponds to extreme Coulomb parameter (z) value of $\sim$64. It can, therefore, be easily perceived from these figures that precisely measured fusion excitation functions provide systematic information on the essential characteristics of the interaction potential, *viz.* the mean barrier height B_0 and width σ_B of its distribution, for nucleus-nucleus collisions. The fusion cross sections can also be predicted by using $\sigma_c(E)$ and theoretically obtained values of the parameters B_0 and σ_B for planning experiments for synthesizing new super-heavy elements [24].

The nuclear fusion at very low energies (∼1eV to few keV) plays important role in nucleosynthesis of light elements in stellar core. Nuclear fusion reaction in this energy range can be explained successfully by quantum mechanical tunneling through Coulomb barrier of interacting nuclei. In the present work, a complex square-well potential model describes the d+t nuclear fusion reaction where the real part of the potential is derived from the resonance energy while the imaginary part is determined by the Gamow factor at resonance energy. The reduced radial wave function $\zeta(r)$ given by $\Phi(r,t) = \frac{1}{\sqrt{4\pi}r}\zeta(r)\exp(-i\frac{E}{\hbar}t)$ where $\Phi(r,t)$ represents the solution of the Schrödinger equation for the system. The cross section is given by $\sigma = \frac{\pi}{k^2}\left\{-\frac{4W_i}{(1-W_i)^2+W_r^2}\right\} = \left(\frac{\pi}{k^2}\right)\left(\frac{1}{\chi^2}\right)\left\{-\frac{4\bar{\omega}_i}{\bar{\omega}_r^2+(\bar{\omega}_i-\frac{1}{\chi^2})^2}\right\}$; where $\chi^2{=}\left\{\frac{\exp\left(\frac{2\pi}{ka_c}\right)-1}{2\pi}\right\}$ is the Gamow penetration factor. The Astrophysical S-factor $S(E)$ given by $S(E) = \left\{-\frac{4\bar{\omega}_i}{\bar{\omega}_r^2+(\bar{\omega}_i-\frac{1}{\chi^2})^2}\right\}$ is called the astrophysical S-factor, where $\bar{\omega} = \bar{\omega}_r + i\bar{\omega}_i = W/\chi^2 = (W_r + iW_i)/\chi^2$. The boundary condition for the wave function can be expressed by its logarithmic derivative which for the square well is given by $R\frac{[\sin(Kr)]'}{\sin(Kr)}|_{r=R} = KR\cot(KR)$ and in the Coulomb field, it is given by $\frac{R}{a_c}\left\{\frac{1}{\chi^2}\cot(\delta_0) + 2\left[\ln\left(\frac{2R}{a_c}\right) + 2A + y(ka_c)\right]\right\}$; so that $\bar{\omega}_i = W_i/\chi^2 = Im\left[\frac{a_c}{R}(KR)\cot(KR)\right] = \frac{a_c}{R}\left\{\frac{\gamma_i\sin(2\gamma_r)-\gamma_r\sinh(2\gamma_i)}{2[\sin^2(\gamma_r)+\sinh^2(\gamma_i)]}\right\}\bar{\omega}_r = W_r/\chi^2 = \frac{a_c}{R}\left\{\frac{\gamma_r\sin(2\gamma_r)+\gamma_i\sinh(2\gamma_i)}{2[\sin^2(\gamma_r)+\sinh^2(\gamma_i)]}\right\}$, where $K^2{=}\frac{2\mu}{\hbar^2}[E-(V_r+iV_i)]$, $K_i{=}\frac{\mu}{K_r\hbar^2}(-V_i)$, $\gamma{=}(\gamma_r+i\gamma_i) \equiv (K_rR{+}iK_iR)$, $k^2{=}\frac{2\mu E}{\hbar^2}$, $H{=}\left[\ln\left(\frac{2R}{a_c}\right)+2A+y(ka_c)\right]$, $a_c{=}\frac{\hbar^2}{Z_1Z_2\mu e^2}$ and $y(x){=}\frac{1}{x^2}\sum_{j=1}^{\infty}\frac{1}{j(j^2+x^{-2})}$. Here k is the wave number outside the nuclear well, a_c is the Coulomb unit of length, and A=0.577 is Euler's constant, $y(ka_c)$ is related to the logarithmic derivative of Γ function given as y(x). The fusion cross sections and astrophysical S-factors thus calculated show good agreement with the available experimental data.

Bibliography

[1] D. N. Basu, P. Roy Chowdhury and C. Samanta, Nucl. Phys. **A 811**, 140 (2008).

[2] Jun Xu et.al. Phys. Rev. **C 79**, 035802 (2009).

[3] M. M. Sharma, Nucl. Phys. **A 816**, 65 (2009).

[4] J. R. Stone, N. J. Stone and S. A. Moszkowski, Phys. Rev. **C 89**, 044316 (2014).

[5] Lie-Wen Chen et.al. Phys. Rev. **C 80**, 014322 (2009).

[6] P. Danielewicz, R. Lacey and W.G. Lynch, Science **298**, 1592 (2002).

[7] P R Chowdhury, A Bhattacharyya, D N Basu, *Phys. Rev.* **C 81**, 062801(R) (2010).

[8] Abhishek Mishra, P R Chowdhury and D N Basu, *Astropart. Phys.* **36**, 42 (2012).

[9] P. B. Demorest et.al. Nature **467**, 1081 (2010).

[10] J. Antoniadis et al., Science **340**, 1233232 (2013).

[11] D. N. Basu, P. Roy Chowdhury and C. Samanta, Phys. Rev. **C 80**, 057304 (2009).

[12] R C Tolman, *Phys. Rev.* **55**, 364 (1939).

[13] J R Oppenheimer and G. M. Volkoff, *Phys. Rev.* **55**, 374 (1939).

[14] V S Uma Maheswari et.al. *Nucl. Phys.* **A 615**, 516 (1997).

[15] D N Basu et.al. *Eur. Phys. J. Plus* **129**, 62 (2014).

[16] R. P. Feynman, N. Metropolis and E. Teller, Phys. Rev. **75**, 1561 (1949).

[17] G. Baym, C. J. Pethick and P. Sutherland, Astrophys. J. **170**, 299 (1971).

[18] G. Baym, H. A. Bethe and C. J. Pethick, Nucl. Phys. **A 175**, 225 (1971).

[19] N Andersson et.al. *Phys. Rev. Lett.* **109**, 241103 (2012).

[20] N Chamel, *Phys. Rev. Lett.* **110**, 011101 (2013).

[21] J Piekarewicz, F J Fattoyev and C J Horowitz, *Phys. Rev.* **C 90**, 015803 (2014).

[22] G. G. Pavlov et.al. *Astrophys. J.* **552**, L129 (2001).

[23] Roman Wolski, Phys. Rev. **C 88**, 041603(R) (2013).

[24] Debasis Atta, D. N. Basu, Phys. Rev. **C 90**, 064622 (2014).

<u>Publications in Refereed Journal:</u>

a. <u>Published</u>

1) Stability of β- eqilibrated dense matter and core crust transition in neutron stars. **Debasis Atta**, D. N. Basu, **Physical Review C 90, 035802 (2014)**.

2) Fusion cross section for reactions involving medium and heavy nucleus-nucleus system. **Debasis Atta**, D. N. Basu, **Physical Review C 90, 064622 (2014)**.

3) Yields of neutron rich nuclei by actinide photofission in the giant dipole resonance region. Debasis Bhowmick, **Debasis Atta**, D.N. Basu, Alok Chakraborty, **Physical Review C 91, 044611 (2015)**.

4) Energy Dependence of exotic nuclei production cross sections by photofission reaction in GDR range. Debasis Bhowmick, F.A. Khan, **Debasis Atta**, D.N. Basu, Alok Chakraborty, **Can. J. Phys. 94, 243-248 (2016)**.

5) Nuclear constraints on the core-crust transition and crustal fraction of moment of inertia of neutron stars. **Debasis Atta**, S Mukhopadhyay, D.N. Basu , **Ind. J. Phys. 91, 235-242 (2017)**.

6) Landau Quantization and mass-radius relation of magnetized white dwarfs in general relativity. S. Mukhopadhyay, **Debasis Atta**, D.N. Basu, **Rom. Rep. Phys 69, 101 (2017)**.

7) Compact bifluid hybrid stars: hadronic matter mixed with self-interacting fermionic asymmetric dark matter. S. Mukhopadhyay, **Debasis Atta**, K. Imam, D.N. Basu, C. Samanta, **Eur. Phys. J. C. 77, 440 (2017).**

b. <u>Accepted</u>: NA

c. <u>Communicated:</u> NA

<u>Other Publications:</u>

a. <u>Book/Book Chapter</u> NA

b. Conference/Symposium

1) Locating inner edge of neutron star crust from stability of neutron star matter. **Debasis Atta**, D.N. Basu, Proceedings of the DAE Symposium on Nuclear Physics, BHU University, Varanasi, UP, India, 59, 784-785 (2014).

2) Near barrier fusion cross sections for medium-heavy nuclei. **Debasis Atta**, D.N. Basu, Proceedings of the DAE Symposium on Nuclear Physics, BHU University, Varanasi, UP, India, 59, 384-385 (2014).

3) Exotic nuclei production by photofission at many energies. F. A. Khan, Debasis Bhowmick, **Debasis Atta**, D.N. Basu, M. Farooq, Alok Chakraborty, Proceedings of the DAE Symposium on Nuclear Physics, Satya Sai University, Andhra Pradesh, India, 60, 634-635 (2015).

4) Mass radius relation of magnetized white dwarfs. Somnath Mukhopadhyay, **Debasis Atta**, D.N. Basu, Proceedings of the DAE Symposium on Nuclear Physics, Satya Sai University, Andhra Pradesh, India, 60, 838-839 (2015).

5) Crustal fraction of moment of inertia of pulsars. **Debasis Atta**, Somnath Mukhopadhyay, D.N. Basu, Proceedings of the DAE Symposium on Nuclear Physics, Satya Sai University, Andhra Pradesh, India, 60, 854-855 (2015).

6) Interacting & non-interacting fermionic dark matter and quark matter compact stars. **Debasis Atta**, Somnath Mukhopadhyay, D.N. Basu, C. Samanta, Proceedings of the DAE Symposium on Nuclear Physics, Saha Institute of Nuclear Physics, Kolkata, India, 61, 890-891 (2016).

7) Astrophysical S factor for sub-barrier Fusion Reaction. Vinay Singh, **Debasis Atta** , Md. A. Khan, Proceedings of the DAE Symposium on Nuclear Physics.Saha Institute of Nuclear Physics, Kolkata, India, 61, 930-931 (2016).

Signature of Student: Debasis Atta

Date: 01/09/2017

Based on the scientific content of the lecture delivered by the candidate in the seminar, his capability to answer several questions raised in the seminar and his publications in refereed journals, Sri Debasis Atta may be permitted to write his thesis.

<u>Doctoral Committee</u>:

S. No.	Name	Designation	Signature	Date
1.	Prof. S. R. Banerjee	Chairman	S R Banerjee	01/9/2017
2.	Prof. D. N. Basu	Guide/ Convener	D N Basu	01/09/2017
3.		Co-guide (if any)		
4.	Prof. Gargi Chaudhuri	Member	Gargi Chaudhuri	01/09/2017
5.	Prof. Subinit Roy (SINP)	Member	Subinit Roy	01/09/17
6.		Member		

Contents

List of Figures

List of Tables

Chapter 1

INTRODUCTION

The nuclear matter is an idealized system of nucleons (with a fixed ratio of neutrons to protons) interacting without Coulomb forces and is translationally invariant. The aim of nuclear matter theory is to determine an equation of state (EoS) for it employing two-body Nucleon-Nucleon (NN) effective interaction. The nuclear EoS is basically the energy per nucleon E/A= ϵ of nuclear matter expressed as a function of nucleonic density ρ. It can then be used to find out the bulk properties of nuclear matter (NM) such as the nuclear energy density, pressure, incompressibility, velocity of sound in medium, etc. The EoS is also of fundamental importance in the theories of nucleusnucleus collisions at energies where the nuclear incompressibility comes into play as well as in the theories of supernova explosions and neutron stars. The properties of nuclear matter with isospin asymmetry, the symmetry energy of nuclear matter and its dependency on nucleonic density happens to be the principal goal of study [1, 2, 3, 4, 5, 6]. The new experimental facilities can now explore the properties of nuclei and nuclear matter at high isospin asymmetry. Therefore, the essential aim of such a study is to obtain the details about the in-medium effective NN interactions and its isospin dependence and the isospin asymmetric nuclear matter (IANM) EoS. These informations, particularly the latter, is not only important to understand the structure of radioactive nuclei, the liquid-gas phase transition in IANM and the reaction dynamics induced by rare isotopes, but also many important phenomena in nuclear astrophysics [1, 2, 3, 7].

The effective interactions are either of microscopic origin such as M3Y forces [8, 9] or of phenomenological origin such as Seyler-Blanchard [10, 11, 12, 13, 14], Skyrme [15, 16, 17] and simple effective interactions [18, 19, 20]. Based upon the characterization of nuclear matter described by the two-body density dependent M3Y effective interaction [8, 9] (DDM3Y) based on the Brueckner-Goldstone G-matrix elements of the Reid-Elliott NN interaction, a systematic description of the spin and isospin symmetric nuclear matter (SNM) and the dependence of bulk behavior of IANM on isospin have been provided. To be specific, the density dependence of the nuclear symmetry energy (NSE) has been studied and its slope L and curvature K_{sym} and the isospin dependent part K_τ of the isobaric incompressibility have been extracted. These results are then compared with the values of constraints obtained from the analysis of the data of isospin diffusion in heavy ion collision (depending upon the momentum and isospin dependent transport model, IBUU04, with the in-medium NN cross section) [5, 21], the measurement of the isotopic dependency of the giant monopole resonances (GMR) in the tin isotopes [22] with even-A, isoscaling analyses of isotope ratios in intermediate energy heavy-ion collisions [23] and from the neutron skin thickness of nuclei [24].

The study of the neutron star (NS) (made up of β-equilibrated hadronic matter) and compact hybrid star properties have been presented in a systematic manner. The EoS obtained using DDM3Y effective NN interaction for the nuclear matter under β-equilibrium agrees with the constraints from the flow data observation of heavy ion collision. At higher densities, depending upon model, the quark matter energy density may be lower than that of nuclear matter. This would imply the possibility of transition inside the core from the NM to the quark matter (QM). The density at which the transition occurs depends upon the specific model of quark matter used in the calculations. The Einstein's field equations for rotating axisymmetric stars with nuclear matter and with quark core inside have been solved. Highly massive compact stars can be described successfully by this NS matter and with different EoSs for the crust. It was found that the NS matter to the QM deconfinement phase transition inside neutron stars resulted in diminishing of their masses. The recently observed binary millisecond pulsars named J1614-2230 by P. B. Demorest et al. [25] and named PSR J0348+0432 by J. Antoniadis et al. [26] indicate that their masses, respectively, are within (1.97 ± 0.04) $M_\odot$ & (2.01 ± 0.04) $M_\odot$. Here $M_\odot$ stands for the mass of our sun. In compliance with the recent observations, the β-equilibrated NS matter ascertains that maximum mass of the rotating NS is $\sim$1.95 $M_\odot$ with a corresponding radius of $\sim$10 kms for frequencies below the r-mode instability. The compact stars with quark cores can have masses up to $\sim$2 $M_\odot$ rotating with Kepler's frequency. However, the maximum mass can go only up to $\sim$1.7 $M_\odot$ corresponding to the maximum frequency limited by the r-mode instability, which happens to be smaller than the mass of NS, *viz.* (1.97 ± 0.04) $M_\odot$ & (2.01 ± 0.04) $M_\odot$, which are the highest masses measured till now with such accuracy and certainty.

The EoS of nuclear matter under exotic conditions is an indispensable tool for the understanding of the nuclear force and for astrophysical applications. This implies knowledge of EoS at high isospin asymmetries and for a wide density range (both for subsaturation and suprasaturation densities). In order to ascertain our knowledge on the nature of matter under extreme conditions, neutron stars are among the most mysterious objects in the universe that provide natural laboratory. Understanding their structures and properties has long been a very challenging task for both the astrophysics and the nuclear physics communities [27].

One of the most important predictions of an EoS is the location of the inner edge of a neutron star crust. Knowledge of the properties of the crust plays an important role in understanding many astrophysical observations [2, 28, 29, 30, 31, 32, 33, 34, 35, 36, 37, 38, 39]. The inner crust spans the region from the neutron drip point to the inner edge separating the solid crust from the homogeneous liquid core. While the neutron drip density ρ_d is relatively well determined to be about 4.3×10^{11} g cm^{-3} [40], the transition density ρ_t at the inner edge is still largely uncertain mainly because of limited knowledge on EoS, especially the density dependence of the symmetry energy, of neutron-rich nuclear matter [33, 34]. At the inner edge a phase transition occurs from the high-density homogeneous matter to the inhomogeneous one at lower densities. The transition density takes its critical value ρ_t when the uniform neutron-proton-electron matter (npe) becomes unstable with respect to the separation into two coexisting phases (one corresponding to nuclei, the other to a nucleonic sea) [34].

In general, the determination of the transition density ρ_t itself is a very complicated problem because the inner crust may have a very complicated structure. A well established approach is to find the density at which the uniform liquid first becomes unstable against small-amplitude density fluctuations, indicating the formation of nuclear clusters. This approach includes the dynamical method [28, 29, 30, 31, 41, 42, 43, 44, 45], the thermodynamical one [34, 46, 47, 48] and the random phase approximation [49, 50]. It is worthwhile to mention here that both the dynamical and the thermodynamical methods give very similar results with the former giving slightly smaller transition density than the later and this is due to the fact that the former includes the density gradient and Coulomb terms that make the system more stable and lower the transition density. The small difference between the two methods implies that the effects of density gradient terms and the Coulomb term are unimportant in determining the transition density [51].

In the present work, using the EoS for neutron-rich nuclear matter constrained by the recent isospin diffusion data from heavy-ion reactions in the same subsaturation density range as the neutron star crust, the inner edge of neutron star crusts is determined. For the EoS used in the present work, which is obtained from the density dependent M3Y effective nucleon-nucleon interaction (DDM3Y), the incompressibility K_∞ for the symmetric nuclear matter (SNM), nuclear symmetry energy $E_{sym}(\rho_0)$ at saturation density ρ_0, the isospin dependent part K_τ of the isobaric incompressibility and the slope L are all in excellent agreement with the constraints recently extracted from measured isotopic dependence of the giant monopole resonances in even-A Sn isotopes, from the neutron skin thickness of nuclei, and from analyses of experimental data on isospin diffusion and isotopic scaling in intermediate energy heavy-ion collisions [52, 53]. The core-crust transition in neutron stars is determined by analyzing the stability of the β-equilibrated dense nuclear matter with respect to the thermodynamic stability conditions [54].

The pulsar glitches, which are discontinuities in the spin-down of pulsars, involve sudden transfer of angular momentum from an isolated component (consisting of superfluid neutrons in crust) to the entire star through vortex unpinning. The sudden jumps in rotational frequencies ω which may be as large as $\frac{\Delta\omega}{\omega} \sim 10^{-6} - 10^{-9}$ have been observed for many pulsars. The observed glitch frequencies are consistent statistically with the hypothesis that glitches are experienced by all radio pulsars [55]. These glitches are expected to be originated from interactions between rotational vortices in a neutron superfluid and the rigid neutron star crust which is more or less a kilometer thick. The inner part of the crust consists of a crystal nuclear lattice submerged in a superfluid of neutron [35]. Since the pulsar is spinning, this neutron superfluid (both inside the inner crust and deeper within the star) is coupled with a periodic rotational vortices. Becasue of the reason that the spin of the pulsar slows gradually, as the rotational frequency of a superfluid is proportional to the density of vortices, these vortices must also move outwards gradually. These vortices are free to move outwards deep inside the star. However, the vortices are pinned in the crust due to their interaction with the nuclear lattice. Various theoretical models [56, 57, 58, 59, 60] differ in important aspects of the stress release mechanism of glitch which are associated with pinned vortices. The crust may get rearranged due to the breaking of vortices or a cluster of vortices may move macroscopically outward by overcoming the pinning force suddenly. This phenomenon results in a glitch due to sudden decrease in the angular momentum of the superfluid within the crust causing a sudden increase in angular momentum of the rigid crust itself. The common feature of all the models is that they agree that the fundamental requirement is the presence of a rigid structure which impedes the motion of rotational vortices present in a superfluid and which encompasses enough of the volume of the pulsar to contribute significantly to the total moment of inertia.

In the present work, the equation of state (EoS) used is obtained from the density dependent M3Y effective nucleon-nucleon interaction (DDM3Y) for which the incompressibility K_∞ for the symmetric nuclear matter (SNM), nuclear symmetry energy $E_{sym}(\rho_0)$ at saturation density ρ_0, the isospin dependent part K_τ of the isobaric incompressibility and the slope L are in excellent agreement with the constraints recently extracted from measured isotopic dependence of the giant monopole resonances in even-A Sn isotopes, from the neutron skin thickness of nuclei, and from analyses of experimental data on isospin diffusion and isotopic scaling in intermediate energy heavy-ion collisions [52, 53]. The core-crust transition in neutron stars is determined [61] by analyzing the stability of the β-equilibrated dense nuclear matter with respect to the thermodynamic stability conditions [34, 46, 47, 48, 54]. The mass-radius relation for neutron stars is obtained by solving the Tolman-Oppenheimer-Volkoff Equation (TOV) [62, 63] and then the crustal fraction of moment of inertia is determined using pressure and density at core-crust transition. As the angular momentum requirements of glitches in Vela pulsar indicate that 1.4% of the star's moment of inertia drives these events, the allowed region for masses and radii for Vela pulsar is determined from the condition that the crustal fraction of moment of inertia $\frac{\Delta I}{I} > 0.014$ which sets a new limit for its radius [64].

Nuclear fusion reactions are widely used in nuclear physics to produce nuclei far from the β- stability line and superheavy nuclei, to explore the properties of excited nuclear states and the mechanisms of their decay and to study the dynamics of nuclear reactions [65, 66, 67, 68, 69, 70, 71, 72]. The burning of stars is also associated with reactions involving the sub-barrier fusion of nuclei [73]. It is well known that fusion excitation functions cannot be satisfactorily explained assuming penetration through a single, well-defined barrier in the total potential energy of a colliding nucleus-nucleus system. In order to reproduce shapes of the fusion excitation functions, especially at low near-threshold energies, it is necessary to assume coexistence of different barriers, a situation that is naturally accounted for in the description of fusion reactions in terms of coupled channel calculations involving coupling to various collective states. The enhancement of fusion [74, 75, 76] below Coulomb barrier is an important phenomena to investigate the importance of deformation and transfer effects in this complex process [77, 78, 79].

The aim of the present work is to obtain the nuclear fusion cross sections for reactions involving medium and heavy nucleus-nucleus systems. The phenomenological description of the fusion excitation functions is achieved by assuming a Gaussian shape of the barrier distribution treating the mean barrier and its variance as free parameters and folding it with the classical expression for the fusion cross section for a fixed barrier with the distance corresponding to the location of the interaction barrier as another free parameter. The free parameters are then determined individually for each of the reactions by comparing the predicted fusion excitation function with experimental data. The energy dependence of the fusion cross section, thus obtained, provides good description to the existing data on near-barrier fusion and capture excitation functions for medium and heavy nucleus-nucleus systems. The effect two-neutron transfer is also investigated which is due to changes in the mass numbers, the deformation parameters of interacting nuclei and the height and shape of the Coulomb barrier. The predictions of fusion or capture cross sections are especially important for planning experiments aimed at producing new super-heavy elements.

The deep sub-barrier fusion reaction (∼1eV to few keV) cross sections are very important in primordial and stellar nucleosyntheses. These fusion reactions can be estimated reasonably well using quantum tunneling through Coulomb barrier of interacting nuclei. In the present work, a complex square-well potential is used to describe the light nuclei nuclear fusion reactions. The real part of the nuclear potential is primarily derived from the resonance energy whereas the imaginary part is determined by the Gamow factor at resonance energy. The complex potential causes absorption of the projectile into the nuclear well. The resonance state of deuteron-triton fusion is contemplated as a reasonable logic for its rather high cross-section (by a factor of several hundred) compared to that of the fusion of deuteron-deuteron despite both having almost the same Coulomb barrier. The nice agreement between the quantum-mechanical calculations and the experimental data advocates a model of selective resonant tunneling, rather than the traditional compound nucleus (CN) model, because the particle undergoing fusion will retain the memory of the wave function's phase factor. For non-resonant fusion cross section calculations, using the nucleus-nucleus potential and the barrier penetration formalism, the astrophysical S-factor for several fusion reactions involving stable and neutron-rich nuclei are calclated. The results can be easily converted to thermonuclear or pycnonuclear reaction rates to simulate various nuclear burning phenomena, in particular, stellar burning at high temperatures and nucleosynthesis in high density environments.

Chapter 2

EQUATION OF STATE FOR NUCLEAR MATTER

The EoS for nuclear matter is obtained by using the isoscalar and the isovector [68] components of M3Y effective NN interaction along with its density dependence. The nuclear matter calculation is then performed which enables complete determination of this density dependence. The minimization of energy/baryon determines the equilibrium density of the SNM. The dependence of the pseudo-potential having zero range on the energy, over the entire range of the energy/baryon ϵ, is worked out properly by permitting its free variation with ϵ^{kin}, the only kinetic energy part of the ϵ. This treatment is more plausible as well as provides excellent result for the SNM incompressibility K_∞. Moreover, the EoS for SNM is not plagued with the superluminosity problem.

Employing various forms of density dependence [80, 81, 82], the EoS for nuclear matter has also been derived using explicitly the direct and finite range exchange contributions. Moreover, using finite range M3Y interaction, Hartree-Fock approximation has been used to compute properties of nuclear matter and finite nuclei [83, 84, 85]. In the limiting case of constant density, which holds true for infinite nuclear matter, the exchange integral reduces to a constant leading to an 'effective' exchange interaction of $J_{00}(\epsilon)\delta(s)$ type [86], typically the zero range potential used in the present calculations to evaluate the exchange term.

The energy per nucleon ϵ for IANM can be derived within a Fermi gas model of protons and neutrons interacting mutually. It is given by [87]

$$\epsilon(\rho, X) = [\frac{3\hbar^2 k_F^2}{10m}]F(X) + (\frac{\rho J_v C}{2})(1 - \beta\rho^n) \tag{2.1}$$

where the isospin asymmetry parameter $X = \frac{\rho_n - \rho_p}{\rho_n + \rho_p}$, $\rho = \rho_p + \rho_n$ with ρ_p, ρ_n and ρ being the proton number density, neutron number density and the baryon number density, respectively, m is the nucleonic mass, k_F=$(1.5\pi^2\rho)^{\frac{1}{3}}$ = the Fermi momentum of SNM, $\epsilon^{kin} = [\frac{3\hbar^2 k_F^2}{10m}]F(X)$ where $F(X) = [(1{+}X)^{5/3}{+}(1{-}X)^{5/3}]/2$ and J_v=J_{v00}+$X^2 J_{v01}$, J_{v00} represents the volume integral of the isoscalar part and and J_{v01} represents the volume integral of the isovector part of M3Y interaction. The isoscalar and isovector components t_{00}^{M3Y} and t_{01}^{M3Y} of the M3Y effective NN interaction are given by $t_{00}^{M3Y}(s, \epsilon) = 7999\frac{\exp(-4s)}{4s} - 2134\frac{\exp(-2.5s)}{2.5s} + J_{00}(1 - \alpha\epsilon)\delta(s)$ and $t_{01}^{M3Y}(s, \epsilon) = -4886\frac{\exp(-4s)}{4s} + 1176\frac{\exp(-2.5s)}{2.5s} + J_{01}(1 - \alpha\epsilon)\delta(s)$, respectively, with J_{00}=-276 MeV fm^3, J_{01}=228 MeVfm^3, $\alpha = 0.005\text{MeV}^{-1}$. The DDM3Y effective NN interaction is given by $v_{0i}(s, \rho, \epsilon) = t_{0i}^{M3Y}(s, \epsilon)g(\rho)$ where $g(\rho) = C(1 - \beta\rho^n)$ is the density dependence with C and β are the constants of density dependence. This form of density dependence was originally taken by Myers in the single folding calculation [88] and it also has a physical meaning for $n = 2/3$ because then β can be interpreted as the 'in medium' effective NN interaction cross section.

Differentiating Eq.(2.1) with respect to ρ one obtains equation for $X = 0$:

$$\frac{\partial\epsilon}{\partial\rho} = [\frac{\hbar^2 k_F^2}{5m\rho}] + \frac{J_{v00}C}{2}[1 - (n+1)\beta\rho^n] - \alpha J_{00}C[1 - \beta\rho^n][\frac{\hbar^2 k_F^2}{10m}]. \tag{2.2}$$

The saturation condition $\frac{\partial\epsilon}{\partial\rho} = 0$ at $\rho = \rho_0$, $\epsilon = \epsilon_0$, determines the density of the cold

SNM at equilibrium. Then for the fixed values of ρ_0, the saturation density and ϵ_0, the saturation energy per nucleon of the SNM at zero temperature, Eq.(2.1) and Eq.(2.2) can be solved simultaneously along with the saturation condition to obtain the values of β and C which are given by

$$\beta = \frac{[(1-p) + (q - \frac{3q}{p})]\rho_0^{-n}}{[(3n+1) - (n+1)p + (q - \frac{3q}{p})]} \tag{2.3}$$

$$\text{where} \quad p = \frac{[10m\epsilon_0]}{[\hbar^2 k_{F_0}^2]},\ q = \frac{2\alpha\epsilon_0 J_{00}}{J_{v00}^0} \tag{2.4}$$

where $J_{v00}^0 = J_{v00}(\epsilon_0^{kin})$ which implies J_{v00} at $\epsilon^{kin} = \epsilon_0^{kin}$, the kinetic energy part ϵ_0^{kin} of the saturation energy per nucleon ϵ_0 of SNM, $k_{F_0} = [1.5\pi^2\rho_0]^{1/3}$ and

$$C = -\frac{[2\hbar^2 k_{F_0}^2]}{5mJ_{v00}^0\rho_0[1-(n+1)\beta\rho_0^n - \frac{q\hbar^2 k_{F_0}^2(1-\beta\rho_0^n)}{10m\epsilon_0}]}, \tag{2.5}$$

respectively. Obviously, the constants of the density dependence, β and C, determined by this methodology depend upon ϵ_0, ρ_0, the index n and on the ranges and strengths of M3Y effective interaction via J_{v00}^0, the volume integral of its isoscalar part.

The calculations have been carried out by using the values of saturation density $\rho_0 = 0.1533$ fm^{-3} [13] and saturation energy per nucleon $\epsilon_0 = -15.26$ MeV [89] for the SNM. ϵ_0 is the co-efficient a_v of the volume term of Bethe-Weizsäcker mass formula, calculated by fitting the recent experimental and estimated Audi-Wapstra-Thibault atomic mass excesses [90]. This term has been obtained by the mean square deviation minimization technique while including corrections due the electronic binding energies [91]. In an earlier work, in which Wigner term, surface symmetry term, shell correction term and the proton form factor correction to Coulomb energy were included, a_v was extracted as 15.4496 MeV [92] ($a_v = 14.8497$ MeV when $A^{1/3}$ and A^0 terms were also incorporated). Taking the standard values of $\alpha = 0.005$ MeV^{-1} and $n = \frac{2}{3}$, the values deduced for β, C and K_∞

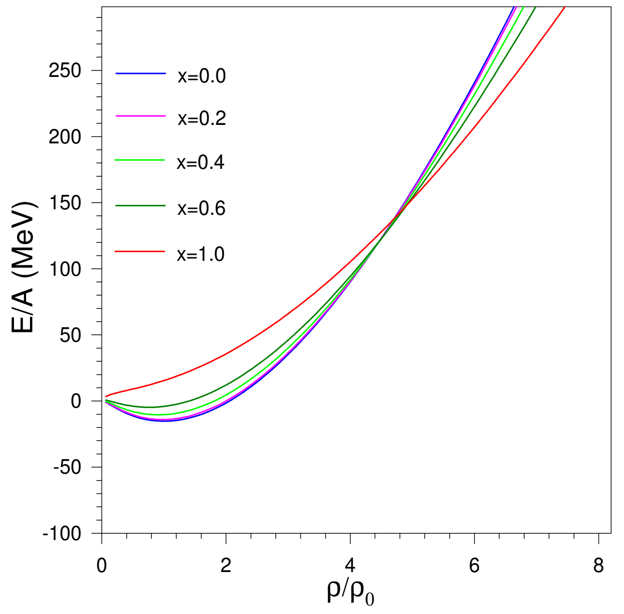

Figure 2.1: Nuclear matter energy per baryon ϵ versus ρ/ρ_0 plots for various isospin asymmetry X.

are 1.5934 fm^2, 2.2497 and 274.7 MeV, respectively. The term ϵ_0 is a_v and its value of -15.26 ± 0.52 MeV encompasses surrounding the complete range of values. For this value of a_v, now the values turn out to be $\beta = 1.5934 \pm 0.0085$ fm^2, $C = 2.2497 \pm 0.0420$ and the incompressibility $K_\infty = 274.7 \pm 7.4$ MeV [87] of SNM.

2.1 The Equation of State

2.1.1 Symmetric and isospin asymmetric nuclear matter

The SNM and the IANM EoSs describe dependence of energy per particle ϵ on the nucleonic density ρ and can be achieved by putting, respectively, the isospin asymmetry $X = 0$ and $X \neq 0$ in Eq.(2.1). For the present calculations, the nuclear matter energy per baryon ϵ versus ρ/ρ_0 is plotted for different X in Fig.-2.1. It can be observed that the energy per nucleon ϵ for SNM is negative (bound) up to nucleonic density of $\sim 2\rho_0$ while for pure neutron matter (PNM) $\epsilon > 0$ and is always unbound by nuclear forces.

The incompressibility of the SNM that measures the curvature of any EoS at saturation density is defined as $k_F^2 \frac{\partial^2 \epsilon}{\partial k_F^2} \mid_{k_F = k_{F_0}}$. This curvature is a measure of the stiffness of an EoS and can be theoretically obtained by using Eq.(2.1) for X=0. The IANM incompressibilities are calculated at saturation densities ρ_s along with the condition of vanishing pressure which is $\frac{\partial \epsilon}{\partial \rho} = 0$. The incompressibility K_s for IANM is therefore expressed as

$$\begin{aligned} K_s = & -\frac{3\hbar^2 k_{F_s}^2}{5m} F(X) - \frac{9 J_v^s C n(n+1)\beta \rho_s^{n+1}}{2} \\ & -9\alpha J C[1-(n+1)\beta\rho_s^n][\frac{\rho_s \hbar^2 k_{F_s}^2}{5m}] F(X) \\ & +[\frac{3\rho_s \alpha J C(1-\beta\rho_s^n)\hbar^2 k_{F_s}^2}{10m}] F(X), \end{aligned} \tag{2.6}$$

where k_{F_s} implies that the k_F is calculated at saturation density ρ_s. The term $J_v^s = J_{v00}^s + X^2 J_{v01}^s$ is J_v at $\epsilon^{kin} = \epsilon_s^{kin}$, the part of the saturation energy per baryon ϵ_s that contains only the contribution from kinetic energy and $J = J_{00} + X^2 J_{01}$.

In Table-2.1, IANM incompressibility K_s as a function of X, for the standard values of the parameter $\alpha = 0.005$ MeV^{-1} of energy dependence and $n = \frac{2}{3}$, is provided. The magnitude of the compression modulus K_s of IANM reduces with isospin asymmetry X because of the decrease in the saturation density ρ_s with the X and reduction in the EoS curvature. At higher values of X, there is no occurrence of a minimum in the IANM which signifies that IANM at such high X values is unbound by the interaction of nuclear force alone. Nevertheless, the β-equilibrated NS matter, a highly neutron rich IANM, does exist inside the NS core as its energy per nucleon is lower than that of SNM at high densities. Although it is unbound by the nuclear interaction alone, the very high gravitational field that can be realized inside neutron stars binds it.

In Fig.-2.2 and Fig.-2.3, the pressure P of SNM and PNM are shown, respectively, as a function of ρ/ρ_0. The continuous lines typify our calculations corresponding to the

Table 2.1: IANM incompressibility at different isospin asymmetry X using the usual values of $n = \frac{2}{3}$ and $\alpha = 0.005$ MeV^{-1}.

X	ρ_s	K_s
	fm^{-3}	MeV
0.0	0.1533	274.69
0.1	0.1525	270.44
0.2	0.1500	257.68
0.3	0.1457	236.64
0.4	0.1392	207.62
0.5	0.1300	171.16
0.6	0.1170	127.84
0.7	0.0980	78.38

SNM and PNM whereas the dash-dotted line of Fig.-2.2 shows the plot of P versus ρ/ρ_0 for SNM corresponding to RMF employing NL3 parameter set [93]. The enclosed region shown by the continuous line depicts the pressure zone which is consistent with the flow data [7] obtained experimentally. It is worthwhile to mention here that the compression modulus of RMF-NL3 for the SNM is 271.76 MeV [94] and is very close to 274.7 ± 7.4 MeV achieved by the present theoretical description. In Fig.-2.3, the regions bounded by the dashed and the continuous lines correlate, respectively, with the areas of pressures for neutron matter compatible with the flow data observed experimentally after including the pressures from asymmetry expressions with the strong (stiff NM) and the weak (soft NM) density dependences [7]. In spite of the fact that the constants of the density dependence, β and C, of the DDM3Y effective interaction have been tuned to reproduce ϵ_0 and ρ_0 of the cold SNM which have been extracted from finite nuclei, the conformity of the present equation of state to the flow data obtained experimentally, where its behavior at high density appears to be phenomenologically firmly established, rationalizes its extrapolation to higher densities.

The SNM incompressibility is experimentally determined from the compression modes isoscalar giant monopole resonance (ISGMR) and isoscalar giant dipole resonance (ISGDR) of nuclei. The violations of self consistency in Hartree-Fock Random Phase Approximation calculations [95] of the strength functions of ISGMR and ISGDR cause shifts in the calculated values of the centroid energies. These shifts can be larger in magnitude compared to the current experimental uncertainties. In fact, due to the use of a not fully self-consistent calculations with Skyrme interactions [95], the low values of the compression modulus K_∞ in the range of $210 - 220$ MeV were predicted. The SLy4 type Skyrme parmetrizations predict the values of K_∞ lying from 230 MeV to 240 MeV [95] when this drawback is corrected. Besides that authentic Skyrme forces can be built such that K_∞ for the SNM is rather in proximity to the relativistic value of $\sim$ 250 MeV to 270 MeV. It

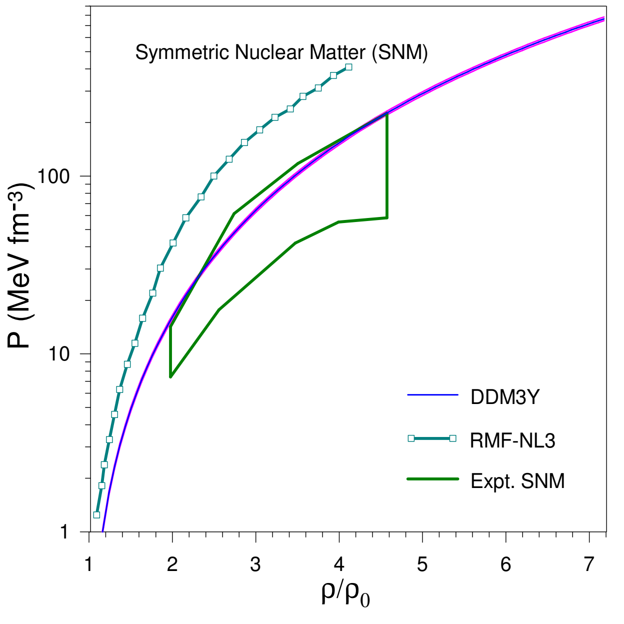

Figure 2.2: Plots of pressure versus ρ/ρ_0 for SNM. Our calculations using $\epsilon_0 = -15.26 \pm 0.52$ MeV are represented by the continuous lines while the RMF calculations with NL3 parameter set [93] are represented by the dash-dotted line. The area of pressures (shown in figure), which is compatible with the flow data obtained experimentally for the SNM [7], is bounded by the continuous line.

may be concluded that from the ISGMR experimental data $K_\infty \approx 240 \pm 20$ MeV.

The lower values [96, 97] for K_∞ are usually predicted by the ISGDR data. However, it is generally agreed upon that the obtaining of K_∞ for these cases is more complicated for diverse causes. Particularly, for the excitation energies [95] higher than 30 MeV for ^{116}Sn and 26 MeV for ^{208}Pb, the largest cross section for the ISGDR at high excitation energies decreases very strongly and can even fall below the range of the present day sensitivity of such experiments. The topmost limit for the compression modulus K_∞ for SNM extracted recently [98] from the experiments is rather close to those obtained with non-relativistic mean field model estimate employing DDM3Y interaction which is also in agreement with the theoretical estimations of the relativistic-mean-field (RMF) model. The Gogny effective interactions [99] that include nuclides in which pairing correlations are

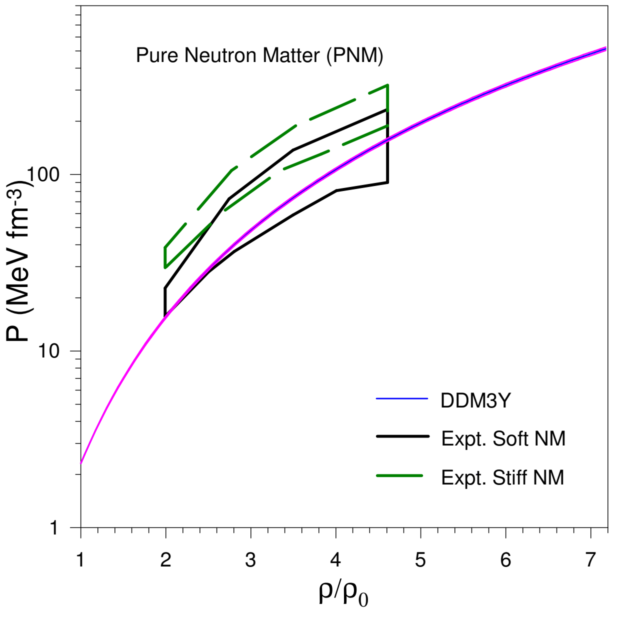

Figure 2.3: Plots of pressure versus ρ/ρ_0 for PNM. Our calculations using $\epsilon_0 = -15.26 \pm 0.52$ MeV are represented by the continuous lines. The pressure regions for PNM which is compatible with the flow data observed experimentally after including pressures from the asymmetry expressions with the strong (stiff NM) and the weak (soft NM) dependences on density [7] are enclosed by the dashed and the continuous lines, respectively.

significant, the results of microscopic calculations replicate the experimentally measured values on heavier nuclei for K_∞ in the gamut of ∼220 MeV [100]. The magnitude of $K_\infty = 274.7 \pm 7.4$ MeV obtained from present calculations is a fine theoretical result and is only little bit high compared to the recent acceptable value [101, 102] of K_∞ for SNM the range of 250-270 MeV.

2.1.2 Nuclear symmetry energy & its slope, incompressibility and isobaric incompressibility

The EOS of IANM, provided by the Eq.(2.1) can be, in general, expanded as

$$\epsilon(\rho, X) = \epsilon(\rho, 0) + E_{sym}(\rho)X^2 + O(X^4) \tag{2.7}$$

where $E_{sym}(\rho) = \frac{1}{2}\frac{\partial^2\epsilon(\rho,X)}{\partial X^2}\mid_{X=0}$ is named as the NSE. The exchange symmetry between protons and neutrons in nuclear matter when one neglects the Coulomb interaction and assumes the charge symmetry of nuclear forces results in the absence of odd-order terms in X in Eq.(2.7). To a good approximation, the NSE $E_{sym}(\rho)$, which is density-dependent, can be obtained using equation [103] given below

$$E_{sym}(\rho) = \epsilon(\rho, 1) - \epsilon(\rho, 0) \tag{2.8}$$

as the higher order terms in X are negligibly small. The value of $E_{sym}(\rho)$ of the above equation can be calculated using Eq.(2.1). It represents a cost imposed on the system as it deviates from the symmetric limit of same number of neutrons and protons. It is, therefore, pertinent to define $E_{sym}(\rho)$ as energy/baryon needed to convert the SNM to the PNM. In Fig.-2.4 the plot of NSE as a function of $\frac{\rho}{\rho_0}$ is shown for this calculation (DDM3Y) and comparisons with those of Akmal-Pandharipande-Ravenhall [104] interaction and MDI interaction [105] have been provided.

The volume symmetry energy coefficient S_v, which can be extracted from atomic mass excesses measured experimentally, provides a constraint for the NSE $E_{sym}(\rho_0)$ at ρ_0. The theoretical estimate of $E_{sym}(\rho_0) = 30.71 \pm 0.26$ MeV for value of the NSE at ρ_0 obtained from these calculations (DDM3Y) is reasonably close to the value of $S_v = 30.048 \pm 0.004$ MeV extricated [106] from the atomic mass excesses measured experimentally for 2228 nuclei. The value of $E_{sym}(\rho_0)$ stays mostly the same which is 30.03 ± 0.26 MeV if one uses the mathematical definition of $E_{sym}(\rho) = \frac{1}{2}\frac{\partial^2\epsilon(\rho,X)}{\partial X^2}\mid_{X=0}$ alternatively. The magnitude of $E_{sym}(\rho_0) \approx 30$ MeV [2, 107, 108] appears empirically well established. The different parameterizations for the RMF models, which fit the observables of isospin symmetric

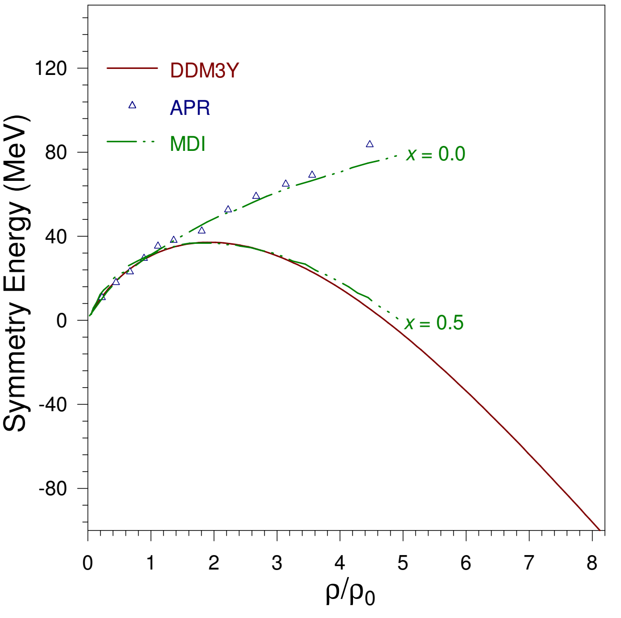

Figure 2.4: Plots of NSE versus ρ/ρ_0 for our calculation (DDM3Y). The same for the interactions of Akmal-Pandharipande-Ravenhall (APR) [104] and MDI with x = 0.00 and 0.50 (described in [105]) are plotted for comparison.

nuclei nicely, steers to a comparatively large range of estimates from $24-40$ MeV for $E_{sym}(\rho_0)$ theoretically. Our present result (DDM3Y) of 30.71 ± 0.26 MeV is reasonably close to that of SkMP (29.9 MeV) Skyrme interaction [109] and the variational calculation Av18+δv+UIX* (30.1 MeV) [104].

The NSE $E_{sym}(\rho)$ can be expanded around the nuclear matter saturation density ρ_0 as

$$E_{sym}(\rho) = E_{sym}(\rho_0) + \frac{L}{3}\Big(\frac{\rho-\rho_0}{\rho_0}\Big) + \frac{K_{sym}}{18}\Big(\frac{\rho-\rho_0}{\rho_0}\Big)^2 \tag{2.9}$$

up to second order in density where L and K_{sym} represent the slope parameter and the curvature parameter of NSE at ρ_0, respectively. Hence, these quantities are defined as $L = 3\rho_0\frac{\partial E_{sym}(\rho)}{\partial\rho}\mid_{\rho=\rho_0}$ and $K_{sym} = 9\rho_0^2\frac{\partial^2 E_{sym}(\rho)}{\partial\rho^2}\mid_{\rho=\rho_0}$. The K_{sym} and L highlights the density dependence of NSE around ρ_0 and carry important information at both high and low densities on the properties of NSE. Particularly, it is found that the slope parameter

L linearly correlates to the thickness of neutron skin in heavy nuclei. It can be obtained from the measurement of the neutron skin thickness of heavy nuclei [4, 5, 6]. Although the experimental measurements are plagued with large uncertainties, this is possible [24] recently.

Differentiating Eq.(2.8) twice successively with respect to the baryonic density ρ while using Eq.(2.1) to provide [110]

$$\begin{aligned}
\frac{\partial E_{sym}}{\partial \rho} &= \frac{2}{5}(2^{2/3}-1)\frac{E_F^0}{\rho}(\frac{\rho}{\rho_0})^{2/3} + \frac{C}{2}[1-(n+1)\beta\rho^n] \\
&\times J_{v01}(\epsilon^{kin}_{X=1}) - \frac{\alpha J_{01} C}{5} E_F^0(\frac{\rho}{\rho_0})^{2/3}[1-\beta\rho^n]F(1) \\
&-(2^{2/3}-1)\frac{\alpha J_{00} C}{5} E_F^0(\frac{\rho}{\rho_0})^{2/3}[1-\beta\rho^n] \\
&-\frac{3}{10}(2^{2/3}-1)\alpha J_{00} C E_F^0(\frac{\rho}{\rho_0})^{2/3}[1-(n+1)\beta\rho^n]
\end{aligned} \tag{2.10}$$

$$\begin{aligned}
\frac{\partial^2 E_{sym}}{\partial \rho^2} &= -\frac{2}{15}(2^{2/3}-1)\frac{E_F^0}{\rho^2}(\frac{\rho}{\rho_0})^{2/3} - \frac{C}{2}n(n+1)\beta\rho^{n-1} \\
&\times J_{v01}(\epsilon^{kin}_{X=1}) - \frac{2\alpha J_{01} C}{5}\frac{E_F^0}{\rho}(\frac{\rho}{\rho_0})^{2/3}[1-(n+1)\beta\rho^n]F(1) \\
&+\frac{\alpha J_{01} C}{15}\frac{E_F^0}{\rho}(\frac{\rho}{\rho_0})^{2/3}[1-\beta\rho^n]F(1) \\
&+(2^{2/3}-1)\frac{\alpha J_{00} C}{15}\frac{E_F^0}{\rho}(\frac{\rho}{\rho_0})^{2/3}[1-\beta\rho^n] \\
&-\frac{2}{5}(2^{2/3}-1)\alpha J_{00} C\frac{E_F^0}{\rho}(\frac{\rho}{\rho_0})^{2/3}[1-(n+1)\beta\rho^n] \\
&+\frac{3}{10}(2^{2/3}-1)\alpha J_{00} C E_F^0(\frac{\rho}{\rho_0})^{2/3} n(n+1)\beta\rho^{n-1}.
\end{aligned} \tag{2.11}$$

Here the Fermi energy $E_F^0 = \frac{\hbar^2 k_{F_0}^2}{2m}$ for the ground state of SNM and to evaluate the values of L and K_{sym} Eqs.(10,11) at ρ=ρ_0 have been used.

The isobaric incompressibility $K_\infty(X)$ for infinite IANM can be expanded in a power series of X. Writing explicitly, it is $K_\infty(X) = K_\infty + K_\tau X^2 + K_4 X^4 + O(X^6)$. Compared to K_τ [52] the magnitude of the higher order K_4 parameter is rather small in general. The former characterizes essentially the isospin dependence of the compression modulus at ρ_0 and is given by $K_\tau = K_{sym} - 6L - \frac{Q_0}{K_\infty}L = K_{asy} - \frac{Q_0}{K_\infty}L$ where the third order derivative Q_0 of SNM at $\rho = \rho_0$ is given by

$$Q_0 = 27\rho_0^3 \frac{\partial^3 \epsilon(\rho, 0)}{\partial \rho^3} \mid_{\rho=\rho_0} . \tag{2.12}$$

One obtains, using Eq.(2.1), the following

$$\begin{aligned}
&\frac{\partial^3 \epsilon(\rho, X)}{\partial \rho^3} = -\frac{CJ_v(\epsilon^{kin})n(n+1)(n-1)\beta\rho^{n-2}}{2} \\
&+\frac{8}{45}\frac{E_F^0}{\rho^3}F(X)(\frac{\rho}{\rho_0})^{\frac{2}{3}} + \frac{3\alpha JC}{5}n(n+1)\beta\rho^{n-1}\frac{E_F^0}{\rho} \\
&\times F(X)(\frac{\rho}{\rho_0})^{\frac{2}{3}} + \frac{\alpha JC}{5}[1-(n+1)\beta\rho^n]\frac{E_F^0}{\rho^2}F(X)(\frac{\rho}{\rho_0})^{\frac{2}{3}} \\
&-\frac{4\alpha JC}{45}[1-\beta\rho^n]\frac{E_F^0}{\rho^2}F(X)(\frac{\rho}{\rho_0})^{\frac{2}{3}}
\end{aligned} \tag{2.13}$$

where the Fermi energy $E_F^0 = \frac{\hbar^2 k_{F_0}^2}{2m}$ for ground state of the SNM, $k_{F_0} = (1.5\pi^2\rho_0)^{\frac{1}{3}}$ and $J = J_{00} + X^2 J_{01}$. Thus

$$\begin{aligned}
&\frac{\partial^3 \epsilon(\rho, 0)}{\partial \rho^3} \mid_{\rho=\rho_0} = -\frac{CJ_{v00}(\epsilon_0^{kin})n(n+1)(n-1)\beta\rho_0^{n-2}}{2} \\
&+\frac{8}{45}\frac{E_F^0}{\rho_0^3} + \frac{3\alpha J_{00}C}{5}n(n+1)\beta\rho_0^{n-1}\frac{E_F^0}{\rho_0} + \frac{\alpha J_{00}C}{5} \\
&\times[1-(n+1)\beta\rho_0^n]\frac{E_F^0}{\rho_0^2} - \frac{4\alpha J_{00}C}{45}[1-\beta\rho_0^n]\frac{E_F^0}{\rho_0^2}
\end{aligned} \tag{2.14}$$

where the kinetic energy part of ϵ_0 is expressed as ϵ_0^{kin}. For the calculations of SNM, the values of ρ_0=0.1533 fm^{-3}, $\epsilon_0 = -15.26 \pm 0.52$ MeV and $n = \frac{2}{3}$ [111] are used. The liquid drop model energy coefficient a_v for the volume term can be identified as the saturation energy per baryon ϵ_0. The magnitude of $a_v = -15.26 \pm 0.52$ MeV roughly covers the full range of its variation. Using this range of values for ϵ_0, one obtains $C = 2.2497 \pm 0.0420$, $\beta = 1.5934 \pm 0.0085$ fm^2 and the compression modulus $K_\infty = 274.7 \pm 7.4$

MeV [87] for SNM. Using the improved quantum molecular dynamics transport model, the collisions involving ^{112}Sn and ^{124}Sn nuclei, from two different observables, can be simulated to regenerate the isospin diffusion data and the ratios of proton and neutron spectra. At subnormal density, the constraints on the density dependence of the NSE can be established [112] by comparison of these data with calculations done over a wide range of NSEs at ρ_0 and various descriptions of the dependence of NSE on the density. The results for K_∞, L, $E_{sym}(\rho_0)$ and density dependence of $E_{sym}(\rho)$ [111] of the present calculations are compatible with these constraints [112]. In Table-2.2, the values of K_∞, $E_{sym}(\rho_0)$, L, K_{sym} and K_τ are tabulated and compared with the corresponding quantities obtained from the RMF models [113]. The range of values of the ten constraints (experimental and empirical) provided in Table-I of Ref.[114] compare well with the theoretical values listed in Table-2.2, Fig.-2.2 and Fig.-2.3 except incompressibility which is only slightly overestimated.

What value of incompressibility [95] would be rational, remains controversial. In what follows next we present our results in the backdrop of others, without justifying any specific value of K_∞, but for an factual overview of the present situation which, we emphasize, is nonetheless progressing. In Fig.-2.5, the plot of K_τ versus K_∞ for our calculation using DDM3Y effective interaction has been compared with the predictions of SkI3, SkI4, SLy4, SkM, SkM*, FSUGold, NL3, Hybrid [113], DDME1, DDME2, NLSH, TM1 and TM2, as tabulated in Table-I of Ref.[115]. The current values of K_∞ ranges from 250 MeV to 270 MeV [102] and that of K_τ is -370 ± 120 MeV [52]. These ranges of values are enclosed by the dotted rectangular area. Though both SkI3 and DDM3Y lie within the same region, the L value (unlike DDM3Y) for SkI3 is 100.49 MeV and is far above the limit of acceptability which is 58.9 ± 16 MeV [116, 117, 118, 119]. Another recent review [120] also finds that $E_{sym}(\rho_0) = 31.7 \pm 3.2$ MeV and $L = 58.7 \pm 28.1$ MeV with an error for L that is considerably larger than that for $E_{sym}(\rho_0)$. However, DDME2 is considerably close to

Table 2.2: Comparison of the present results obtained using DDM3Y effective interaction with those of RMF models [113] for SNM incompressibility K_∞, NSE at saturation density $E_{sym}(\rho_0)$, slope L and the curvature K_{sym} parameters of NSE, K_{asy} and isobaric incompressibility K_τ of IANM (all in MeV).

Model	K_∞	$E_{sym}(\rho_0)$	L	K_{sym}	K_{asy}
This work	274.7 ± 7.4	30.71 ± 0.26	45.11 ± 0.02	-183.7 ± 3.6 $Q_0 = -276.5 \pm 10.5$	-454.4 ± 3.5 $K_\tau = -408.97 \pm 3.01$
FSUGold	230.0	32.59	60.5	-51.3 $Q_0 = -523.4$	-414.3 $K_\tau = -276.77$
NL3	271.5	37.29	118.2	+100.9 $Q_0 = +204.2$	-608.3 $K_\tau = -697.36$
Hybrid	230.0	37.30	118.6	+110.9 $Q_0 = -71.5$	-600.7 $K_\tau = -563.86$

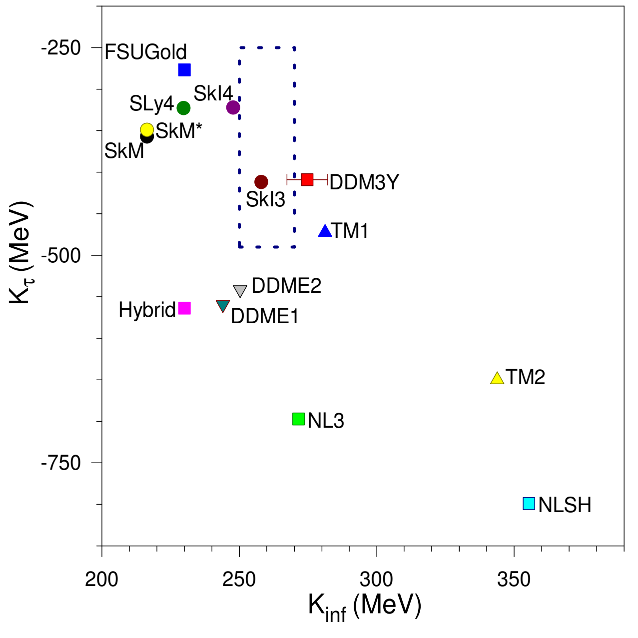

Figure 2.5: The plots of K_τ versus K_∞ (K_{inf}). Other predictions (tabulated in Refs. [113, 115]) are compared with our calculation (DDM3Y). The dotted region enclosed by the rectangular area encompasses the range of values for $K_\infty = 250 - 270$ MeV [102] and $K_\tau = -370 \pm 120$ MeV [52].

the rectangular region which has $L = 51$ MeV. It is noteworthy that the DDM3Y effective interaction with identical strengths, ranges and the dependence on nuclear density that provides $L = 45.11 \pm 0.02$, allows rather excellent descriptions of radioactivity via proton emission [87] and α particle emission radioactivity of the superheavy nuclei [121, 122] and elastic and inelastic scattering. The present NSE grows in magnitude with nucleonic density initially up to $\sim 2\rho_0$ and thereafter slides down continuously (hence 'soft') and at higher densities ($\sim 4.7\rho_0$) [87, 111] it goes negative (hence 'super-soft'). It is compatible with the present-day corroboration of a soft NSE at supra-saturation densities [105]. Moreover, the experimental data from FOPI of GSI on the ratio of $\frac{\pi^+}{\pi^-}$ in the relativistic collisions of heavy ions favor a super-soft NSE. This behavior of NSE can also provide stable neutron star configurations if the non-Newtonian gravity suggested in the GUT is considered [123].

Chapter 3

MASSES & RADII OF NEUTRON STARS: A REVIEW

3.1 Modeling of the Neutron Stars

The rapidly rotating, non-axisymmetric, compact stars would certainly release gravitational waves of extremely short duration and would come down to configurations which are axisymmetric. This implies that one has to solve, in the framework of general relativity, the rotating and axisymmetric configurations. While solving, it is assumed that the spacetime and the matter distribution are axisymmetric and are in a stationary state, the only movement of the matter is in a circular motion (assumption of no meridional motions) which is described by an angular velocity, as observed by an observer at a distance and at rest, the angular velocity is constant and a perfect fluid description for the matter is considered. The perfect fluid is described by $T^{\mu\nu}$, the energy-momentum tensor, which is given by

$$T^{\mu\nu} = (\varepsilon + P)u^{\mu}u^{\nu} - g^{\mu\nu}P \tag{3.1}$$

in case of a perfect fluid, where ε is the energy density, P is the pressure, u^μ are the four velocity and $g^{\mu\nu}$ is the metric tensor. The metric used for studying the rotating stars is given by

$$\begin{aligned} ds^2 = -e^{(\gamma+\rho)}dt^2 + e^{2\alpha}(dr^2 + r^2 d\theta^2) \\ +e^{(\gamma-\rho)}r^2 \sin^2\theta(d\phi - \omega dt)^2 \end{aligned} \tag{3.2}$$

where the gravitational potentials γ, ρ, α and ω are functions of polar coordinates r and θ only. For the three potentials γ, ρ and α, the Einstein's field equations can be solved using the Green's-function technique [124] and from other potentials the fourth potential ω can be determined. Then using these potentials all the other physical quantities can be obtained. It is quite obvious that the formalism used here provides results for the solution to the Tolman-Oppenheimer-Volkoff (TOV) equation [125] corresponding to the static solutions of the Einstein's field equations for spheres of fluid in case of the zero frequency limit. The 'rns' code [126] has been used for computing the properties of compact stars. The code requires pressure as a function of energy density as well as corresponding number density of baryons and enthalpy. As various EoSs for different regions have been used, these EoSs are evenly connected.

The different EoSs govern the various portions of a compact star. Broadly these regions can be divided into two parts, *viz.* a crust and a core. Although the crustal thickness depends on the mass, for maximum mass star the crust accounts for nearly 5% of the radius and less than 1% of the mass of a neutron star while the core accounts for the remaining radius and mass of the neutron star. The outer layers of about 1 km thickness are a solid crust. Barring the outer crust of few meter thickness, the rest of the crust contains a lattice of bare nuclides submerged in a gas of degenerate electrons. Inside the deeper part of the crust, because of the rising electron Fermi energy, the nuclear species become progressively more neutron rich, beginning (ideally) as ^{56}Fe through ^{118}Kr at mass density $\approx 4.3\times10^{11}$ g cm^{-3}. This density is called the 'neutron drip' point and beyond this the lattice of neutron-rich nuclei becomes permeated by a sea of neutrons. This happens because the neutron richness of the nuclei so that neutron states in the continuum starts getting filled with increasing density.

The crustal region of a compact can be described well by the EoSs of FMT (Feynman-Metropolis-Teller) [127], BPS (Baym-Pethick-Sutherland) [28] and BBP (Baym-Bethe-Pethick) [29], respectively. At the endpoint of thermonuclear burning, energetically ^{56}Fe is the most favored nucleus at low densities. The outermost layer of crust, which essentially contains the iron nuclei and a fraction of electrons which are bound to these nuclei, is well described by the EoS of FMT. It is, in fact, the high pressure matter EoS, derivation of which is based upon the model of Thomas-Fermi. The calculation of the electronic energy is a more difficult task in the derivation of this EoS. The EoS of BPS is applicable at subnuclear densities from $\sim 10^4$ g cm^{-3} up to the neutron drip density 4.3×10^{11} g cm^{-3}. It incorporates the effects of the Coulomb lattice energy on the equilibrium of nuclei. The EoS of BBP is applicable in the realm of neutron drip density to the nuclear density of about 2.5×10^{14} g cm^{-3}. This region comprises of electrons, nuclei and free neutrons and the derivation of this EoS is based upon a compressible liquid drop model of nuclei appertaining to the constraints that free neutron gas should be in equilibrium with the neutrons in nuclides that must be stable against beta-decay.

3.2 The Neutron and Hybrid stars and their Masses and Radii

The masses and radii of rotating compact stars have been calculated using the EoS for crust comprising of FMT, BPS and BBP up to the number density 0.0458 fm^{-3} of baryons followed by the β-equilibrated NS matter at higher densities. It is important here to state that due to the r-mode instability, a compact star may not acquire the maximum permissible limit of Keplerian frequency. It has been suggested that the time period may be limited to 1.5 ms [128] due to the r-mode instability. Nevertheless, a faster rotating pulsar (e.g., PSR J17482446ad) than the r-mode limit has hitherto been observed [129]. The variation of the NS mass with the central density has been calculated for static and rotating NSs up to r-mode frequency limit as well as at the Keplerian limit with β-equilibrated NS matter inside [110]. The mass-radius relationship has been obtained for static and rotating NSs up to r-mode frequency limit as well as at the Keplerian limit with the β-equilibrated NS matter inside. It has been found that NSs containing the β-equilibrated NS matter, the maximum mass calculated for the static star is 1.92 $M_\odot$ with corresponding radius of about 9.7 km and for the NS rotating with Keplerian frequency it turns out to be 2.27 $M_\odot$ with corresponding equatorial radius of about 13.1 km [130]. However, for NSs rotating up to the r-mode frequency limit, the maximum mass emerges to be 1.94 [1.95] $M_\odot$ for the time period of 2.0 [1.5] ms of rotation with radius $\sim$9.8 [9.9] kilometers.

The perturbative EoS [131] with a running coupling constant and one massive and two massless quark flavors, has been used to describe dense and cold quark (QCD) matter. The constant B, which allows to take into account non-perturbative effects not captured by the weak coupling expansion, is regarded as a free parameter. Employing the number density of free quarks, in fact, the pressure expression in the original MIT bag model [132] can be recovered with B taking the role of the bag constant. However, the allowed values of B are usually rather quantized due to physics criteria that require a positive energy density and allow to make statements quantitative in nature that were not feasible in the actual bag model of MIT.

At number densities beyond 0.405 fm^{-3}, the energy density of our DDM3Y EoS for the charge neutral β-equilibrated NS matter is greater than that of the quark matter (QM) EoS for the bag constant $B^{\frac{1}{4}} = 110$ MeV [131] that signals the appearance of the quark matter at the core. The β-equilibrated NS matter EoS energy density and the QM EoS energy density for the bag constant $B^{\frac{1}{4}} = 110$ MeV intersects at 0.405 fm^{-3}. On the contrary, the β-equilibrated NS matter EoS energy density produces a cross over with the QM EoS energy density at higher density of $\sim$1.2 fm^{-3} corresponding to the lower values, such as $B^{\frac{1}{4}}$=89 MeV, of the bag constant which causes very small amount of QM at the core and thus estimating almost the identical results as that for the β-equilibrated NS matter EoS inside. Hence $B^{\frac{1}{4}}$=110 MeV has been chosen for representative calculations (rather arbitrarily) to permit a phase transition at those densities which are realizable in the core of hybrid stars. Because the NS matter energy density is given by $\varepsilon = \rho(\epsilon + mc^2)$, one can readily obtain $\frac{d\varepsilon}{d\rho} = \epsilon + mc^2 + \rho\frac{d\epsilon}{d\rho}$ which can be rearranged as $\varepsilon = \rho\frac{d\varepsilon}{d\rho} - P$. Thus the pressure $P = \rho^2\frac{d\epsilon}{d\rho}$ at a point is the negative intercept of the tangent (with slope $\frac{d\varepsilon}{d\rho}$) drawn at that point to the energy density versus number density plot. The common tangent has been drawn to these plots for quark and nuclear matter. The phase co-existence region (which is too small for the case considered here) is depicted by the portion of the common tangent between the two contact points on the two plots [133] which implies a constant pressure exists during the phase transition. This procedure, therefore, is analoguous to the Maxwell's construction.

The mass variation of NS with its central density has been calculated for the static NS and rotating NS up to the r-mode frequency limit and also at the Keplerian limit with the β-equilibrated NS matter and quark matter inside [110]. The mass-radius relationship has been obtained for static and rotating neutron stars up to r-mode frequency limit and at the Keplerian limit with the β-equilibrated NS matter and quark matter inside. It shows that the inclusion of quark core reduces the maximum mass corresponding to the static NS to 1.68 $M_\odot$ with a radius of about 10.4 km while that for the NS rotating with Keplerian frequency it reduces to 2.02 $M_\odot$ with an equatorial radius of about 14.3 km. In a study alike, it has been conjectured that the compact star masses with a QM inside and an outer core of hadronic matter always stay below those of the pure quark stars or the pure hadronic stars [134]. The two different sets of parameters *viz.* TM1 and NL3 [134] of RMF were used to investigate the effects of the hadronic contribution to the EoS. It is worthwhile to mention here that the high density behavior of these two EoSs do not satisfy the benchmark set by the flow data [7] obtained experimentally. For our representative case, the stars rotating up to r-mode frequency limit, the maximum mass emerges to be 1.71 [1.72] $M_\odot$ for a time period of 2.0 [1.5] ms of rotation with a corresponding radius about 10.6 [10.7] kilometers [135].

Chapter 4

STABILITY OF β-EQUILIBRATED DENSE MATTER AND CORE CRUST TRANSITION

4.1 Intrinsic stability of a single phase under beta-equilibrium and core crust transition

The basic equation in neutron star matter research is the shape of the relationship between the pressure and energy density $P = P(\varepsilon)$, usually called the equation of state. At the zero temperature, the state of neutron star matter should be uniquely described by the quantities that are conserved by the process leading to equilibrium. Stable high density nuclear matter must be in chemical equilibrium for all types of reactions including the weak interactions, while the beta decay and orbital electron capture takes place simultaneously. For the β-equilibrated neutron star matter we have free neutron decay $n \to p + \beta^- + \overline{\nu_e}$ which are governed by weak interaction and the electron capture process $p + \beta^- \to n + \nu_e$. Both types of reactions change the electron fraction and thus affect the EoS. Here we assume that neutrinos generated in these reactions leave the system. The absence of neutrino has a dramatic effect on the equation of state and mainly induces a significant change on the values of proton fraction x_p. The absence of neutrino implies that

$$\mu = \mu_n - \mu_p = \mu_e \tag{4.1}$$

where μ_e, μ_n and μ_p are the chemical potentials for electron, neutron and proton, respectively.

The baryon number B is conserved by this type of reaction so the energy density ε and pressure P should be function of baryon number density ρ. We assume that the matter is electrically neutral and spatially homogeneous. The star as a whole is electrically neutral but the matter does not need to be locally neutral. So the thermodynamic state of a given phase is described by two quantities: baryon number B and charge Q where Q is the sum of all charges. The total energy U then becomes a function of U(V,B,Q). To consider stability of a single phase one need to introduce local quantities $\epsilon = \frac{U}{B}$. The energy per particle ϵ then becomes a function of other local quantities taken per baryon number $v = \frac{V}{B}$ and $x_p = \frac{Q}{B}$. The first principle of thermodynamics takes the following form:

$$d\epsilon = -Pdv - \mu dx_p \tag{4.2}$$

where P is the pressure and μ is the chemical potential of an electric charge. The stability of any single phase, also called intrinsic stability, is ensured by convexity of $\epsilon(v, x_p)$. The thermodynamical inequalities allow us to express the requirement in terms of following inequalities:

$$-(\frac{\partial P}{\partial v})_{x_p} > 0, \qquad -(\frac{\partial \mu}{\partial x_p})_P > 0 \tag{4.3}$$

One may find another pair of inequalities that are equivalent to above equations:

$$-(\frac{\partial P}{\partial v})_\mu > 0, \qquad -(\frac{\partial \mu}{\partial x_p})_v > 0 \tag{4.4}$$

The intrinsic stability condition are equivalent to requiring the convexity of the energy per particle in the single phase [34, 46, 47] by ignoring the finite size effects due to surface and Coulomb energies as shown in following. Here the $P = P^b + P^e$ is the total pressure of the npe system with the contributions P^b and P^e from baryons and electrons, respectively. The proton fraction $x_p = \frac{Q}{B} = \frac{\rho_p}{\rho}$ where $\rho = \rho_n + \rho_p$ and the asymmetry parameter $X = \frac{\rho_n - \rho_p}{\rho_n + \rho_p}$. Total energy $\epsilon = \epsilon_b(x_p) + \epsilon_e(\mu)$.

$$P = -\frac{\partial \epsilon}{\partial v} = \rho^2 \frac{\partial \epsilon}{\partial \rho} \tag{4.5}$$

$$(\frac{\partial P}{\partial v})_\mu = \frac{\partial P^b(\rho, x_p)}{\partial v} + \frac{\partial P^e(\mu)}{\partial v} \tag{4.6}$$

Here $\frac{\partial P^e(\mu)}{\partial v} = 0$ because if β-equilibrium is satisfied then $\mu = \mu_n - \mu_p = \mu_e$ and the electron contribution to P^e is only a function of the chemical potential μ and in that case $(\frac{\partial P^e(\mu)}{\partial v}) = 0$. Eventually $-(\frac{\partial P}{\partial v})_\mu > 0$ can be written as $-(\frac{\partial P^b}{\partial v})_\mu > 0$.

$$\begin{aligned}(\frac{\partial P}{\partial v})_\mu &= \frac{\partial P^b}{\partial \rho}\frac{\partial \rho}{\partial v} + \frac{\partial P^b}{\partial x_p}\frac{\partial x_p}{\partial v} \\ &= -\rho^2 \frac{\partial P^b}{\partial \rho} - \rho^2 \frac{\partial P^b}{\partial x_p}\frac{\partial x_p}{\partial \rho}\end{aligned} \tag{4.7}$$

$$-(\frac{\partial P}{\partial v})_\mu = \rho^2 (\frac{\partial P^b}{\partial \rho} + \frac{\partial P^b}{\partial x_p}\frac{\partial x_p}{\partial \rho}) \tag{4.8}$$

$$\mu = \mu_n - \mu_p = -(\frac{\partial \epsilon^b}{\partial x^p})_\rho = -\frac{\partial \epsilon^b(\rho, x_p)}{\partial x_p} \tag{4.9}$$

Differentiating above equation with respect to x_p we get

$$\frac{\partial \mu}{\partial x_p} = -\frac{\partial^2 \epsilon^b}{\partial x_p^2} \tag{4.10}$$

From Eq.(4.5) we get

$$P^b = \rho^2 \frac{\partial \epsilon^b}{\partial \rho} \tag{4.11}$$

and differentiating above with respect to x_p one obtains

$$(\frac{\partial P^b}{\partial x_p}) = \rho^2 \frac{\partial^2 \epsilon^b}{\partial x_p \partial \rho} = \rho^2 \epsilon^b_{\rho x_p} \tag{4.12}$$

By Maxwell's relation

$$(\frac{\partial x_p}{\partial \rho})_\mu = -v^2 (\frac{\partial x_p}{\partial v})_\mu = v^2 (\frac{\partial P^b}{\partial \mu})_{s,v} \tag{4.13}$$

$$\frac{\partial P^b}{\partial \mu} = \frac{\frac{\partial P^b}{\partial x_p}}{\frac{\partial \mu}{\partial x_p}} = \frac{\rho^2 \frac{\partial^2 \epsilon^b}{\partial \rho \partial x_p}}{\frac{\partial \mu}{\partial x_p}} = -\frac{\rho^2 \frac{\partial^2 \epsilon^b}{\partial \rho \partial x_p}}{\frac{\partial^2 \epsilon^b}{\partial x_p^2}} \tag{4.14}$$

Using Eq.(4.13) and Eq.(4.14) we get

$$(\frac{\partial x_p}{\partial \rho}) = -v^2 \rho^2 \frac{\frac{\partial^2 \epsilon^b}{\partial \rho \partial x_p}}{\frac{\partial^2 \epsilon^b}{\partial x_p^2}} = -\frac{\frac{\partial^2 \epsilon^b}{\partial \rho \partial x_p}}{\frac{\partial^2 \epsilon^b}{\partial x_p^2}} \tag{4.15}$$

From Eq.(4.11)

$$\frac{\partial P^b}{\partial \rho} = 2\rho \frac{\partial \epsilon^b}{\partial \rho} + \rho^2 \frac{\partial^2 \epsilon^b}{\partial \rho^2} \tag{4.16}$$

Using Eq.(4.12), Eq.(4.15) and Eq.(4.16) in Eq.(4.8) we get

$$-(\frac{\partial P^b}{\partial v})_\mu = \rho^2(2\rho\frac{\partial\epsilon^b}{\partial\rho} + \rho^2\frac{\partial^2\epsilon^b}{\partial\rho^2} - \rho^2\frac{\epsilon^b_{\rho x_p}\epsilon^b_{\rho x_p}}{\epsilon_{x_p x_p}}) \tag{4.17}$$

The quantity $V_{thermal}$ which determines the thermodynamic instability region of neutron star matter at β-equilibrium is given by $V_{thermal} = -(\frac{\partial P}{\partial v})_\mu$. Hence

$$V_{thermal} = \rho^2(2\rho\frac{\partial\epsilon^b}{\partial\rho} + \rho^2\frac{\partial^2\epsilon^b}{\partial\rho^2} - \rho^2\frac{\epsilon^{b2}_{\rho x_p}}{\epsilon_{x_p x_p}}) \tag{4.18}$$

The condition for core-crust transition is obtained by making $V_{thermal} = 0$. In the following we drop the superscript b and use ϵ for ϵ^b and P for P^b.

4.2 Theoretical Calculation

The β-equilibrated nuclear matter EoS is obtained by evaluating the asymmetric nuclear matter EoS at the isospin asymmetry X determined from the β-equilibrium proton fraction x_p $[= \frac{\rho_p}{\rho}]$, obtained approximately by solving

$$\hbar c(3\pi^2\rho x_p)^{1/3} = 4E_{sym}(\rho)(1-2x_p), \tag{4.19}$$

where $E_{sym}(\rho)$ is the nuclear symmetry energy. In general $E_{sym}(\rho)$ is defined as $\frac{1}{2}\frac{\partial^2\epsilon(\rho,X)}{\partial X^2}\mid_{X=0}$. The higher-order terms in X are negligible and to a good approximation, $E_{sym}(\rho)$=$\epsilon(\rho,1)-\epsilon(\rho,0)$ [103] which represents a penalty levied on the system as it departs from the symmetric limit of equal number of protons and neutrons and can be defined as the energy required per nucleon to change the SNM to PNM.

The exact way of obtaining β-equilibrium proton fraction is by solving

$$\hbar c(3\pi^2\rho x_p)^{1/3} = -\frac{\partial\epsilon(\rho,x_p)}{\partial x_p} = +2\frac{\partial\epsilon}{\partial X}, \tag{4.20}$$

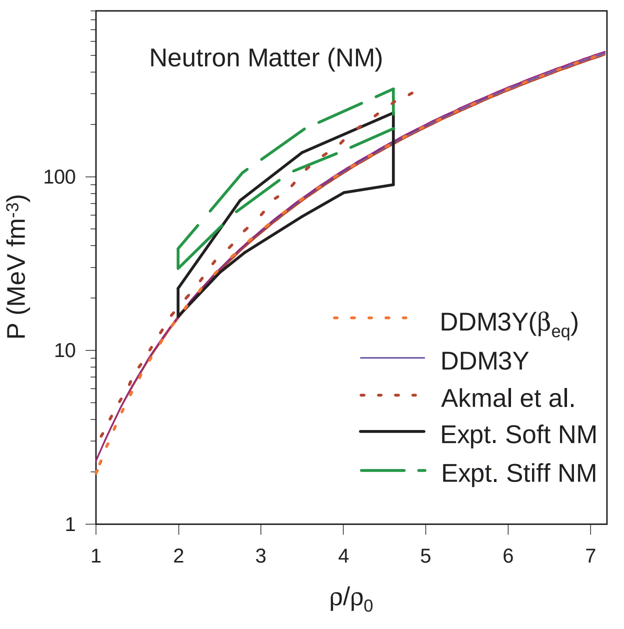

Figure 4.1: Plots for pressure P of dense nuclear matter as functions of ρ/ρ_0. The continuous line represents the pure neutron matter and the dashed line represents the β-equilibrated neutron star matter. The dotted line represents the same for A18 model using variational chain summation (VCS) of Akmal et al. [104]. The areas enclosed by the continuous and the dashed lines correspond to the pressure regions for neutron matter consistent with the experimental flow data after inclusion of the pressures from asymmetry terms with weak (soft NM) and strong (stiff NM) density dependences, respectively [7].

where isospin asymmetry $X = 1 - 2x_p$.

The pressure P of pure neutron matter (PNM) and β-equilibrated neutron star matter are plotted in Fig.-4.1 as functions of ρ/ρ_0. The continuous line represents the PNM and the dashed line (almost merges with the continuous line) represents the β-equilibrated neutron star matter (present calculations) whereas the dotted line represents the same using the A18 model using variational chain summation (VCS) of Akmal et al. [104] for the PNM. The areas enclosed by the continuous and the dashed lines in Fig.-4.1 correspond to the pressure regions for neutron matter consistent with the experimental

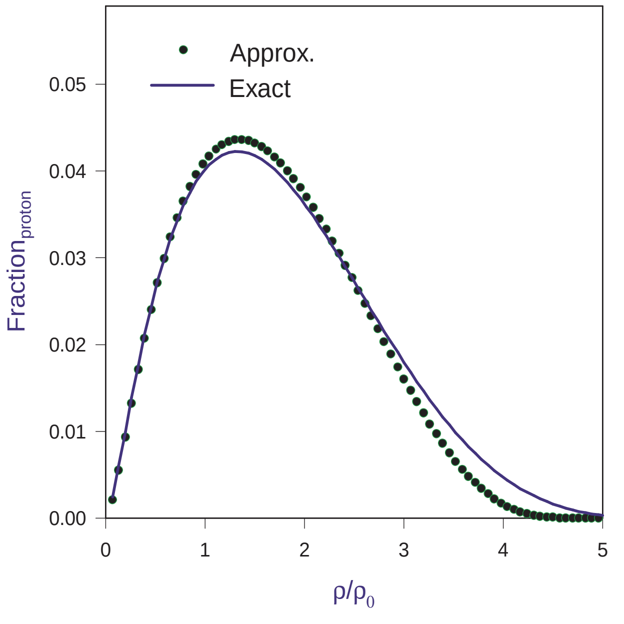

Figure 4.2: The β equilibrium proton fraction obtained from nuclear symmetry energy (approx.) and from exact calculations using DDM3Y interaction are plotted as functions of ρ/ρ_0.

flow data after including pressures from asymmetry expressions with the strong (stiff NM) and the weak (soft NM) dependences on density [7]. In spite of the fact that the β and C of the density dependent M3Y effective interaction have been attuned to replicate ρ_0 and ϵ_0 which were procured from the nuclei of finite sizes, the compatibility of nuclear EoS of the present work with the flow data obtained experimentally, where the behavior at high density appears to be confirmed phenomenologically, rationalizes its high density extrapolation. Interestingly, the RMF-NL3 value of the incompressibility is 271.76 MeV [93, 94] for SNM which is rather very close to 274.7 ± 7.4 MeV obtained from the present calculation but the plot of P versus ρ/ρ_0 for PNM of RMF using NL3 parameter set [93] does not pass through the pressure regions for neutron matter consistent with the experimental flow data [7].

In Fig.-4.2 it can be seen that the maximum of the β-equilibrium proton fraction $x_p \sim 0.0436$ calculated using the symmetry energy (approximate calculation) occurs at

$\rho \sim 1.35\rho_0$ whereas the exact calculation yields a maximum of $x_p \sim 0.0422$ around the same density [61]. Since the equilibrium proton fraction is always less than 1/9 [136] calculated value of x_p forbids the direct URCA process. This feature is consistent with the fact that there are no strong indications [137, 138] that fast cooling occurs. It was also concluded theoretically that an acceptable EoS of asymmetric nuclear matter shall not allow the direct URCA process to occur in neutron stars with masses below 1.5 solar masses [103]. Even recent experimental observations that suggest high heat conductivity and enhanced core cooling process indicating the enhanced level of neutrino emission, were not attributed to the direct URCA process but were proposed to be due breaking and formation of neutron Cooper pairs [139, 140, 141, 142].

The intrinsic stability condition of a single phase for locally neutral matter under β-equilibrium is determined, thermodynamically, by the positivity of the $V_{thermal}$, under constant chemical potential which is generally valid in our case. However, the limiting density that breaks these conditions will correspond to the core-crust (liquid-solid) phase transition. Thus transition density ρ_t (with corresponding pressure P_t and proton fraction $\mathrm{x}_{p(t)}$) is determined at which $V_{thermal}$ becomes zero and goes to negative with decreasing density.

4.3 Results

In Table-4.1, the number density ρ, energy density ε and pressure P for FMT, BBP and BPS, respectively, are presented. In Table-4.2, the number density ρ, energy density ε and pressure P are presented for β equilibrated neutron star matter using DDM3Y effective interaction with $n = 2/3$. The stability of the β-equilibrated dense matter in neutron stars is investigated and the location of the inner edge of their crusts and core-crust transition density and pressure are determined using the DDM3Y effective nucleon-nucleon interaction. The results for the transition density, pressure and proton fraction at the inner edge separating the liquid core from the solid crust of neutron stars are calculated [61] and presented in Table-4.3 for $n = 2/3$. The symmetric nuclear matter incompressibility K_∞, nuclear symmetry energy at saturation density $E_{sym}(\rho_0)$, the slope L and isospin dependent part K_τ of the isobaric incompressibility are also tabulated since these are all in excellent agreement with the constraints recently extracted from measured isotopic dependence of the giant monopole resonances in even-A Sn isotopes, from the neutron skin thickness of nuclei, and from analyses of experimental data on isospin diffusion and isotopic scaling in intermediate energy heavy-ion collisions.

It is recently conjectured that there may be a good correlation between the core-crust transition density and the symmetry energy slope L and it is predicted that this behaviour should not depend on the relation between L and K_τ [143]. On the contrary, no correlation of the transition pressure with L was obtained [143]. In Table-4.4, variations of different quantities with parameter n which controls the nuclear matter incompressibility are listed. It is worthwhile to mention here that the incompressibility increases with n. The standard value of n=2/3 used here has a unique importance because then the constant of density dependence β has the dimension of cross section and can be interpreted as the isospin averaged effective nucleon-nucleon interaction cross section for the symmetric

Table 4.1: Number density ρ, Energy density ε and Pressure P for Feynman-Metropolis-Teller, Baym-Pethick-Sutherland and Baym-Bethe-Pethick EoSs.

ρ	ε	P	ρ	ε	P
fm^{-3}	$\mathrm{MeV.fm}^{-3}$	$\mathrm{MeV.fm}^{-3}$	fm^{-3}	$\mathrm{MeV.fm}^{-3}$	$\mathrm{MeV.fm}^{-3}$
.476000E-14	.443820E-11	.630462E-23	.491000E-14	.457865E-11	.630462E-22
.699000E-14	.651685E-11	.755306E-21	.990000E-14	.921348E-11	.873908E-20
.272000E-13	.253371E-10	.106117E-18	.127000E-12	.119101E-09	.363296E-17
.693000E-12	.646067E-09	.118602E-15	.629500E-11	.586517E-08	.608240E-14
.158100E-10	.147303E-07	.310112E-13	.397200E-10	.370056E-07	.151748E-12
.997600E-10	.929213E-07	.718477E-12	.250600E-09	.233483E-06	.328714E-11
.629400E-09	.586517E-06	.144694E-10	.158100E-08	.147303E-05	.608926E-10
.397200E-08	.370112E-05	.244132E-09	.500000E-08	.465899E-05	.328277E-09
.997600E-08	.929775E-05	.895755E-09	.199000E-07	.185506E-04	.239263E-08
.397200E-07	.370169E-04	.627965E-08	.792400E-07	.738764E-04	.162547E-07
.158100E-06	.147416E-03	.416729E-07	.199000E-06	.185618E-03	.545443E-07
.315500E-06	.294213E-03	.101685E-06	.500000E-06	.466348E-03	.189076E-06
.629400E-06	.587079E-03	.257740E-06	.792400E-06	.739326E-03	.314357E-06
.997600E-06	.930899E-03	.428215E-06	.158100E-05	.147528E-02	.794007E-06
.250600E-05	.233933E-02	.147066E-05	.397200E-05	.370843E-02	.272285E-05
.500000E-05	.466966E-02	.353433E-05	.629400E-05	.587640E-02	.480774E-05
.792400E-05	.740449E-02	.654182E-05	.997600E-05	.932022E-02	.889513E-05
.125600E-04	.117416E-01	.120974E-04	.158100E-04	.147809E-01	.156242E-04
.199000E-04	.186124E-01	.212484E-04	.250600E-04	.234382E-01	.288889E-04

ρ	ε	P	ρ	ε	P
fm^{-3}	$MeV.fm^{-3}$	$MeV.fm^{-3}$	fm^{-3}	$MeV.fm^{-3}$	$MeV.fm^{-3}$
.315500E-04	.295169E-01	.371348E-04	.397200E-04	.371742E-01	.504931E-04
.500000E-04	.468090E-01	.686642E-04	.629400E-04	.584270E-01	.933208E-04
.792400E-04	.742697E-01	.126904E-03	.997600E-04	.934831E-01	.162110E-03
.110500E-03	.103596E+00	.180524E-03	.125600E-03	.117753E+00	.205368E-03
.158100E-03	.148315E+00	.279213E-03	.199000E-03	.186798E+00	.363046E-03
.250600E-03	.235281E+00	.470537E-03	.257200E-03	.241517E+00	.487203E-03
.267000E-03	.250562E+00	.492509E-03	.312600E-03	.293708E+00	.521348E-03
.395100E-03	.371348E+00	.567915E-03	.475900E-03	.447416E+00	.613670E-03
.581200E-03	.546517E+00	.676030E-03	.714300E-03	.671910E+00	.760300E-03
.878600E-03	.826404E+00	.873283E-03	.107700E-02	.101404E+01	.102247E-02
.131400E-02	.123708E+01	.121723E-02	.174800E-02	.164607E+01	.161798E-02
.228700E-02	.215337E+01	.218851E-02	.294200E-02	.277135E+01	.297815E-02
.372600E-02	.351011E+01	.404557E-02	.465000E-02	.438258E+01	.546067E-02
.572800E-02	.539944E+01	.730337E-02	.742400E-02	.700000E+01	.105805E-01
.890700E-02	.840449E+01	.137890E-01	.105900E-01	.998876E+01	.177778E-01
.131500E-01	.124157E+02	.245381E-01	.177700E-01	.167865E+02	.385643E-01
.223900E-01	.211629E+02	.547690E-01	.301700E-01	.285449E+02	.865169E-01
.367500E-01	.347921E+02	.117478E+00	.458500E-01	.434382E+02	.166167E+00
.582100E-01	.552022E+02	.243258E+00			

Table 4.2: Number density ρ, Energy density ε and Pressure P for β equilibrated neutron star matter using DDM3Y effective interaction with n=2/3.

ρ	ε	P	ρ	ε	P
fm^{-3}	$MeV.fm^{-3}$	$MeV.fm^{-3}$	fm^{-3}	$MeV.fm^{-3}$	$MeV.fm^{-3}$
.06	.5672E+02	.1915E+00	.07	.6620E+02	.2576E+00
.08	.7568E+02	.3432E+00	.09	.8517E+02	.4524E+00
.10	.9467E+02	.5896E+00	.11	.1042E+03	.7591E+00
.12	.1137E+03	.9650E+00	.13	.1233E+03	.1211E+01
.14	.1328E+03	.1502E+01	.15	.1424E+03	.1841E+01
.16	.1520E+03	.2231E+01	.17	.1617E+03	.2675E+01
.18	.1713E+03	.3178E+01	.19	.1810E+03	.3742E+01
.20	.1908E+03	.4369E+01	.21	.2006E+03	.5063E+01
.22	.2104E+03	.5826E+01	.23	.2202E+03	.6659E+01
.24	.2301E+03	.7566E+01	.25	.2401E+03	.8547E+01
.26	.2500E+03	.9606E+01	.27	.2601E+03	.1074E+02
.28	.2702E+03	.1196E+02	.29	.2803E+03	.1326E+02
.30	.2905E+03	.1464E+02	.31	.3007E+03	.1611E+02
.32	.3110E+03	.1767E+02	.33	.3214E+03	.1931E+02
.34	.3318E+03	.2104E+02	.35	.3422E+03	.2285E+02
.36	.3527E+03	.2476E+02	.37	.3633E+03	.2676E+02
.38	.3739E+03	.2886E+02	.39	.3846E+03	.3104E+02
.40	.3954E+03	.3333E+02	.41	.4062E+03	.3570E+02
.42	.4171E+03	.3818E+02	.43	.4280E+03	.4075E+02
.44	.4390E+03	.4343E+02	.45	.4501E+03	.4621E+02

ρ	ε	P	ρ	ε	P
fm^{-3}	$\mathrm{MeV.fm}^{-3}$	$\mathrm{MeV.fm}^{-3}$	fm^{-3}	$\mathrm{MeV.fm}^{-3}$	$\mathrm{MeV.fm}^{-3}$
.46	.4612E+03	.4908E+02	.47	.4724E+03	.5207E+02
.48	.4837E+03	.5516E+02	.49	.4950E+03	.5835E+02
.50	.5064E+03	.6166E+02	.51	.5178E+03	.6507E+02
.52	.5293E+03	.6860E+02	.53	.5409E+03	.7225E+02
.54	.5526E+03	.7600E+02	.55	.5643E+03	.7988E+02
.56	.5761E+03	.8387E+02	.57	.5880E+03	.8799E+02
.58	.5999E+03	.9223E+02	.59	.6119E+03	.9659E+02
.60	.6240E+03	.1011E+03	.61	.6361E+03	.1057E+03
.62	.6484E+03	.1104E+03	.63	.6607E+03	.1153E+03
.64	.6730E+03	.1203E+03	.65	.6855E+03	.1255E+03
.66	.6980E+03	.1308E+03	.67	.7107E+03	.1362E+03
.68	.7233E+03	.1417E+03	.69	.7361E+03	.1474E+03
.70	.7490E+03	.1533E+03	.71	.7619E+03	.1593E+03
.72	.7749E+03	.1654E+03	.73	.7881E+03	.1717E+03
.74	.8013E+03	.1781E+03	.75	.8145E+03	.1846E+03
.76	.8279E+03	.1914E+03	.77	.8414E+03	.1982E+03
.78	.8549E+03	.2053E+03	.79	.8686E+03	.2124E+03
.80	.8823E+03	.2197E+03	.81	.8961E+03	.2272E+03
.82	.9100E+03	.2349E+03	.83	.9240E+03	.2426E+03
.84	.9381E+03	.2506E+03	.85	.9523E+03	.2587E+03

ρ	ε	P	ρ	ε	P
fm^{-3}	$MeV.fm^{-3}$	$MeV.fm^{-3}$	fm^{-3}	$MeV.fm^{-3}$	$MeV.fm^{-3}$
.86	.9666E+03	.2669E+03	.87	.9810E+03	.2754E+03
.88	.9955E+03	.2839E+03	.89	.1010E+04	.2927E+03
.90	.1025E+04	.3015E+03	.91	.1040E+04	.3106E+03
.92	.1054E+04	.3198E+03	.93	.1069E+04	.3292E+03
.94	.1085E+04	.3387E+03	.95	.1100E+04	.3484E+03
.96	.1115E+04	.3583E+03	.97	.1130E+04	.3683E+03
.98	.1146E+04	.3785E+03	.99	.1162E+04	.3889E+03
1.00	.1177E+04	.3994E+03	1.01	.1193E+04	.4101E+03
1.02	.1209E+04	.4210E+03	1.03	.1225E+04	.4320E+03
1.04	.1241E+04	.4432E+03	1.05	.1257E+04	.4546E+03
1.06	.1274E+04	.4661E+03	1.07	.1290E+04	.4779E+03
1.08	.1307E+04	.4898E+03	1.09	.1324E+04	.5018E+03
1.10	.1340E+04	.5141E+03	1.11	.1357E+04	.5265E+03
1.12	.1374E+04	.5391E+03	1.13	.1391E+04	.5519E+03
1.14	.1409E+04	.5648E+03	1.15	.1426E+04	.5779E+03
1.16	.1444E+04	.5912E+03	1.17	.1461E+04	.6047E+03
1.18	.1479E+04	.6184E+03	1.19	.1497E+04	.6322E+03
1.20	.1515E+04	.6462E+03	1.21	.1533E+04	.6604E+03
1.22	.1551E+04	.6748E+03	1.23	.1569E+04	.6894E+03
1.24	.1588E+04	.7041E+03	1.25	.1606E+04	.7191E+03

ρ	ε	P	ρ	ε	P
fm^{-3}	MeV.fm^{-3}	MeV.fm^{-3}	fm^{-3}	MeV.fm^{-3}	MeV.fm^{-3}
1.26	.1625E+04	.7342E+03	1.27	.1644E+04	.7495E+03
1.28	.1662E+04	.7649E+03	1.29	.1681E+04	.7806E+03
1.30	.1701E+04	.7965E+03	1.31	.1720E+04	.8125E+03
1.32	.1739E+04	.8287E+03	1.33	.1759E+04	.8451E+03
1.34	.1778E+04	.8617E+03	1.35	.1798E+04	.8785E+03
1.36	.1818E+04	.8955E+03	1.37	.1838E+04	.9126E+03
1.38	.1858E+04	.9300E+03	1.39	.1879E+04	.9475E+03
1.40	.1899E+04	.9652E+03	1.41	.1919E+04	.9832E+03
1.42	.1940E+04	.1001E+04	1.43	.1961E+04	.1020E+04
1.44	.1982E+04	.1038E+04	1.45	.2003E+04	.1057E+04
1.46	.2024E+04	.1076E+04	1.47	.2045E+04	.1095E+04
1.48	.2067E+04	.1114E+04	1.49	.2088E+04	.1133E+04
1.50	.2110E+04	.1153E+04	1.51	.2132E+04	.1173E+04
1.52	.2154E+04	.1193E+04	1.53	.2176E+04	.1213E+04
1.54	.2198E+04	.1233E+04	1.55	.2220E+04	.1254E+04
1.56	.2243E+04	.1275E+04	1.57	.2265E+04	.1296E+04
1.58	.2288E+04	.1317E+04	1.59	.2311E+04	.1338E+04
1.60	.2334E+04	.1360E+04	1.61	.2357E+04	.1382E+04
1.62	.2381E+04	.1404E+04	1.63	.2404E+04	.1426E+04
1.64	.2428E+04	.1448E+04	1.65	.2451E+04	.1471E+04

ρ	ε	P	ρ	ε	P
fm^{-3}	$MeV.fm^{-3}$	$MeV.fm^{-3}$	fm^{-3}	$MeV.fm^{-3}$	$MeV.fm^{-3}$
1.66	.2475E+04	.1494E+04	1.67	.2499E+04	.1517E+04
1.68	.2523E+04	.1540E+04	1.69	.2547E+04	.1563E+04
1.70	.2572E+04	.1587E+04	1.71	.2596E+04	.1610E+04
1.72	.2621E+04	.1634E+04	1.73	.2646E+04	.1659E+04
1.74	.2671E+04	.1683E+04	1.75	.2696E+04	.1707E+04
1.76	.2721E+04	.1732E+04	1.77	.2747E+04	.1757E+04
1.78	.2772E+04	.1782E+04	1.79	.2798E+04	.1808E+04
1.80	.2823E+04	.1833E+04	1.81	.2849E+04	.1859E+04
1.82	.2876E+04	.1885E+04	1.83	.2902E+04	.1911E+04
1.84	.2928E+04	.1937E+04	1.85	.2955E+04	.1964E+04
1.86	.2981E+04	.1991E+04	1.87	.3008E+04	.2018E+04
1.88	.3035E+04	.2045E+04	1.89	.3062E+04	.2072E+04
1.90	.3089E+04	.2100E+04	1.91	.3117E+04	.2127E+04
1.92	.3144E+04	.2155E+04	1.93	.3172E+04	.2183E+04
1.94	.3200E+04	.2212E+04	1.95	.3228E+04	.2240E+04
1.96	.3256E+04	.2269E+04	1.97	.3284E+04	.2298E+04
1.98	.3313E+04	.2327E+04	1.99	.3341E+04	.2356E+04
2.00	.3370E+04	.2386E+04			

Table 4.3: Results of the present calculations (DDM3Y) of symmetric nuclear matter incompressibility K_∞, nuclear symmetry energy at saturation density $E_{sym}(\rho_0)$, the slope L and isospin dependent part K_τ of the isobaric incompressibility (all in MeV) [53] are tabulated along with the saturation density and the density, pressure and proton fraction at the core-crust transition for β-equilibrated neutron star matter.

K_∞	$E_{sym}(\rho_0)$	L	K_τ
274.7 ± 7.4	30.71 ± 0.26	45.11 ± 0.02	-408.97 ± 3.01
ρ_0	ρ_t	P_t	$\mathrm{x}_{p(t)}$
0.1533 fm^{-3}	0.0938 fm^{-3}	0.5006 MeV fm^{-3}	0.0308

Table 4.4: Variations of the core-crust transition density, pressure and proton fraction for β-equilibrated neutron star matter, symmetric nuclear matter incompressibility K_∞ and isospin dependent part K_τ of isobaric incompressibility with parameter n.

n	ρ_t	P_t	$\mathrm{x}_{p(t)}$	K_∞	K_τ
1/6	0.0797 fm^{-3}	0.4134 MeV fm^{-3}	0.0288	182.13 MeV	-293.42 MeV
1/3	0.0855 fm^{-3}	0.4520 MeV fm^{-3}	0.0296	212.98 MeV	-332.16 MeV
1/2	0.0901 fm^{-3}	0.4801 MeV fm^{-3}	0.0303	243.84 MeV	-370.65MeV
2/3	0.0938 fm^{-3}	0.5006 MeV fm^{-3}	0.0308	274.69 MeV	-408.97 MeV
1	0.0995 fm^{-3}	0.5264 MeV fm^{-3}	0.0316	336.40 MeV	-485.28 MeV

nuclear medium in its ground state. The values of $k_F \approx 1.3$ fm^{-1} and $q_0 \sim \hbar k_F c \approx 260$ MeV for a nucleon in the ground state of the nuclear matter and the present result for the 'in medium' effective cross section is reasonably close to the value obtained from a rigorous Dirac-Brueckner-Hartree-Fock [144] calculations corresponding to such k_F and q_0 values which is $\approx$ 12 mb. Using the value of β=1.5934 fm^2 along with the nucleonic density 0.1533 fm^{-3}, the value obtained for the nuclear mean free path λ is about 4 fm which is in excellent agreement with that obtained using another method [145]. Moreover, comparison of the theoretical values of symmetric nuclear matter incompressibility and isobaric incompressibility with the recent experimental values for $K_\infty = 250 - 270$ MeV [102, 146] and $K_\tau = -370 \pm 120$ MeV [147] further justifies importance for our choice of n=2/3. It is interesting to mention here that the present EoS for n=2/3, provides the maximum mass for the static case is 1.92 M$_\odot$ with radius ~9.7 km and for the star rotating with Kepler's frequency it is 2.27 M$_\odot$ with equatorial radius ~13.1 km [130]. However, for stars rotating with maximum frequency limited by the r-mode instability, the maximum mass turns out to be 1.95 (1.94) M$_\odot$ corresponding to rotational period of 1.5 (2.0) ms with radius about 9.9 (9.8) kilometers [135] which reconcile with the recent observations of the massive compact stars ~2 M$_\odot$ [25, 26].

Chapter 5

CRUSTAL FRACTION OF MOMENT OF INERTIA OF PULSARS

5.1 Crustal fraction of moment of inertia in neutron stars

The crustal fraction of the moment of inertia $\frac{\Delta I}{I}$ can be expressed as a function of M (gravitational mass of the star) and R (radius of the star) with the only dependence on the equation of state arising from the values of transition density ρ_t and pressure P_t. Actually, the major dependence is on the value of P_t, since ρ_t enters only as a correction in the following approximate formula [35]

$$\frac{\Delta I}{I} \approx \frac{28\pi \mathrm{P}_t R^3}{3Mc^2}\left(\frac{1-1.67\xi-0.6\xi^2}{\xi}\right) \times \left(1+\frac{2\mathrm{P}_t}{\rho_t m_b c^2}\frac{(1+7\xi)(1-2\xi)}{\xi^2}\right)^{-1} \tag{5.1}$$

where $\xi = \frac{GM}{Rc^2}$. The fraction of the moment of inertia attributed to the crust is of particular importance. This crustal fraction can be deduced from the observations of pulsar glitches. The glitches are the intermittent disturbance of the otherwise exceptionally regular pulses of electromagnetic wave originated from magnetized, rotating neutron stars [45] with magnetic axis different from the axis of rotation. In Ref.[35] it was shown that the glitches depict a self-regulating instability during which the star arranges itself over a waiting time. The requirement of the angular momentum for glitches in the Vela pulsar indicates that these events are driven by the moment of inertia greater than 1.4%. Therefore, if the glitches originate in the inner crustal liquid would imply that $\frac{\Delta I}{I} > 0.014$.

5.2 Tolman-Oppenheimer-Volkoff Equation and mass-radius relation

In astrophysics, the Tolman-Oppenheimer-Volkoff (TOV) equation [62, 63] constrains the structure of a spherically symmetric body of isotropic material which is in static gravitational equilibrium, as modelled by general relativity and is given by

$$\frac{dP(r)}{dr} = -\frac{G}{c^4}\frac{[\varepsilon(r) + P(r)][m(r)c^2 + 4\pi r^3 P(r)]}{r^2[1 - \frac{2Gm(r)}{rc^2}]} \tag{5.2}$$
$$\text{where } \varepsilon(r) = (\epsilon + m_b c^2)\rho(r), \;\; m(r)c^2 = \int_0^r \varepsilon(r')d^3r'$$

which can be readily solved for masses and radii numerically employing the Runge-Kutta (RK4) method. The quantities $P(r)$ and $\varepsilon(r)$ are the pressure and the energy density, respectively, at a radial distance r from the center of the compact star, and are obtained from the equation of state. The quantity $m(r)$ represents the mass of the compact star

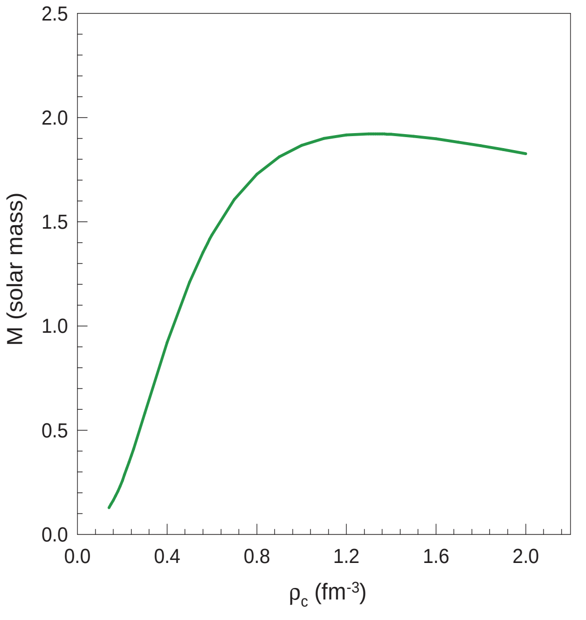

Figure 5.1: Variation of mass with central density for slowly rotating neutron stars for the present nuclear EoS.

accommodated within a radius of r. It is now obvious that the boundary condition $P(r) = 0$ determines the size of the compact star and the total mass M of the compact star is given by $M = m(R)$ [148] obtained by integrating up to the surface R. The only integration constant needed is P_c, the pressure at the center of the star calculated at a given central density ρ_c, to solve the TOV equation. The masses of slowly rotating neutron stars are very close [110, 130, 135] to those obtained by solving TOV equation.

The moment of inertia of neutron stars is calculated by assuming the star to be rotating slowly with a uniform angular velocity Ω [149]. The angular velocity $\bar{\omega}(r)$ of a point in the star measured with respect to the angular velocity of the local inertial frame is determined by the equation

$$\frac{1}{r^4}\frac{d}{dr}\left[r^4 j \frac{d\bar{\omega}}{dr}\right] + \frac{4}{r}\frac{dj}{dr}\bar{\omega} = 0 \tag{5.3}$$

where

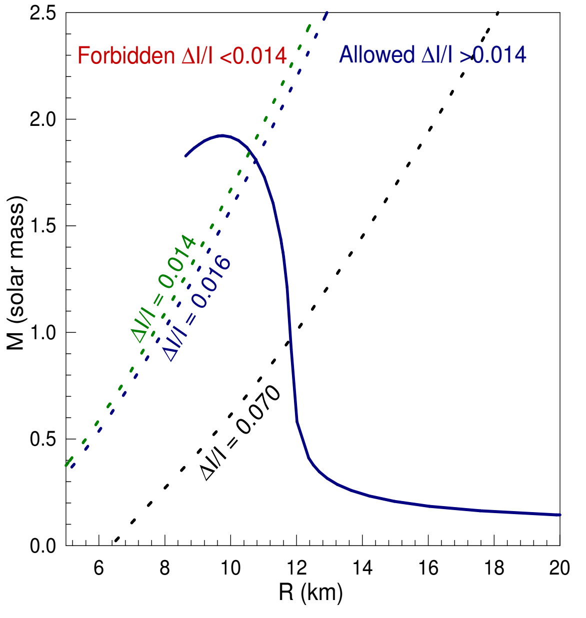

Figure 5.2: The mass-radius relation of slowly rotating neutron stars for the present nuclear EoS. For the Vela pulsar, the constraint of $\frac{\Delta I}{I} > 1.4\%$ implies that allowed masses and radii lie to the right of the line defined by $\frac{\Delta I}{I} = 0.014$ (for $\rho_t = 0.0938$ fm^{-3}, P$_t$ = 0.5006 MeV fm^{-3}).

$$j(r) = e^{-\phi(r)}\sqrt{1 - \frac{2Gm(r)}{rc^2}}. \tag{5.4}$$

The function $\phi(r)$ is constrained by the condition

$$e^{\phi(r)}\mu(r) = \text{constant} = \mu(R)\sqrt{1 - \frac{2GM}{Rc^2}} \tag{5.5}$$

where the chemical potential $\mu(r)$ is defined as

$$\mu(r) = \frac{\varepsilon(r) + P(r)}{\rho(r)}. \tag{5.6}$$

Using these relations, Eq.(5.3) can be solved subject to the boundary conditions that $\bar{\omega}(r)$ is regular as $r \to 0$ and $\bar{\omega}(r) \to \Omega$ as $r \to \infty$. Then moment of inertia of the star can be calculated using the definition $I = J/\Omega$, where the total angular momentum J is given as

$$J = \frac{c^2}{6G} R^4 \frac{d\bar{\omega}}{dr}\Big|_{r=R}. \tag{5.7}$$

Table 5.1: Results of present calculations for $n=\frac{2}{3}$ of symmetric nuclear matter incompressibility K_∞, nuclear symmetry energy at saturation density $E_{sym}(\rho_0)$, the slope L and isospin dependent part K_τ of the isobaric incompressibility (all in MeV) [53] are tabulated along with the density, pressure and proton fraction at the core-crust transition for β-equilibrated neutron star matter and corresponding Vela pulsar constraint.

K_∞	$E_{sym}(\rho_0)$	L	K_τ
274.7 ± 7.4	30.71 ± 0.26	45.11 ± 0.02	-408.97 ± 3.01
$\rho_t(\mathrm{fm}^{-3})$	$\mathrm{P}_t(\mathrm{MeVfm}^{-3})$	$x_{p(t)}$	Vela pulsar R(km)
0.0938	0.5006	0.0308	$R \geq 4.10 + 3.36 M/M_\odot$

5.3 Theoretical Calculation and Results

The calculations have been performed using the values of C=2.2497, β=1.5934 fm^2, the saturation density ρ_0=0.1533 fm^{-3} [13] and the saturation energy per baryon ϵ_0=-15.26 MeV [89] as described in Chapter 2. The stability of the β-equilibrated dense matter in neutron stars is investigated and the location of the inner edge of their crusts and core-crust transition density and pressure are determined using the DDM3Y effective nucleon-nucleon interaction. The results for the transition density, pressure and proton fraction at the inner edge separating the liquid core from the solid crust of neutron stars are calculated and presented in Table-5.1 for $n = \frac{2}{3}$. The symmetric nuclear matter incompressibility K_∞, nuclear symmetry energy at saturation density $E_{sym}(\rho_0)$, the slope L and isospin dependent part K_τ of the isobaric incompressibility are also tabulated since these are all in excellent agreement with the constraints recently extracted from measured isotopic dependence of the giant monopole resonances in even-A Sn isotopes, from the neutron skin thickness of nuclei, and from analyses of experimental data on isospin diffusion and isotopic scaling in intermediate energy heavy-ion collisions.

The calculations for masses and radii are performed using the EoS covering the crustal region of a compact star which are Feynman-Metropolis-Teller (FMT) [127], Baym-Pethick-Sutherland (BPS) [28] and Baym-Bethe-Pethick (BBP) [29] up to number density of 0.0582 fm^{-3} and the present β-equilibrated neutron star matter beyond. The values of I obtained by solving Eq.(5.3) subject to the boundary conditions stated earlier are listed in Table-5.2 along with masses M, radii R and crustal thickness ΔR of neutron stars for $n = \frac{2}{3}$. Once masses and radii are determined, $\frac{\Delta I}{I}$ are obtained from Eq.(5.1) and listed in Table-5.2. In Fig.-5.1, variation of mass with central density is plotted for slowly rotating neutron stars for the present nuclear EoS for $n = \frac{2}{3}$. In Fig.-5.2, the mass-radius relation of slowly rotating neutron stars is shown for $n = \frac{2}{3}$. Using Eq.(5.1) again the mass-radius

Table 5.2: Radii, masses, total & crustal fraction of moment of inertia and crustal thickness as functions of central density ρ_c.

ρ_c	R	M	I	$\frac{\Delta I}{I}$	ΔR
fm^{-3}	km	$M_\odot$	$M_\odot \mathrm{km}^2$	fraction	km
2.00	8.6349	1.8277	70.88	0.0055	0.2462
1.90	8.7598	1.8467	73.83	0.0057	0.2523
1.80	8.8957	1.8651	77.00	0.0060	0.2598
1.70	9.0444	1.8824	80.38	0.0063	0.2696
1.60	9.2052	1.8980	83.97	0.0067	0.2806
1.50	9.3810	1.9109	87.70	0.0072	0.2951
1.40	9.5710	1.9197	91.52	0.0079	0.3121
1.39	9.5911	1.9203	91.91	0.0080	0.3144
1.38	9.6109	1.9208	92.29	0.0080	0.3161
1.37	9.6314	1.9213	92.67	0.0081	0.3185
1.36	9.6514	1.9217	93.05	0.0082	0.3203
1.35	9.6718	1.9220	93.43	0.0083	0.3222
1.34	9.6928	1.9223	93.81	0.0084	0.3248
1.33	9.7141	1.9225	94.18	0.0085	0.3275
1.32	9.7349	1.9226	94.55	0.0085	0.3296
1.31	9.7559	1.9227	94.93	0.0086	0.3318
1.30	9.7770	1.9226	95.30	0.0087	0.3340
1.20	9.9995	1.9173	98.85	0.0098	0.3620
1.10	10.2371	1.9004	101.88	0.0112	0.3970
1.00	10.4902	1.8675	103.94	0.0132	0.4441
0.90	10.7544	1.8127	104.42	0.0158	0.5066
0.80	11.0239	1.7285	102.47	0.0197	0.5929

ρ_c	R	M	I	$\frac{\Delta I}{I}$	ΔR
fm^{-3}	km	$M_\odot$	$M_\odot$km^2	fraction	km
0.70	11.2865	1.6064	97.04	0.0255	0.7148
0.60	11.5245	1.4369	87.06	0.0344	0.8952
0.59	11.5456	1.4170	85.78	0.0356	0.9175
0.58	11.5666	1.3965	84.44	0.0368	0.9411
0.57	11.5874	1.3753	83.04	0.0381	0.9663
0.56	11.6073	1.3536	81.58	0.0394	0.9924
0.55	11.6262	1.3313	80.07	0.0408	1.0193
0.50	11.7135	1.2104	71.65	0.0492	1.1792
0.45	11.7830	1.0734	61.88	0.0602	1.3897
0.40	11.8388	0.9206	51.00	0.0752	1.6801
0.30	12.0129	0.5808	28.54	0.1249	2.7618
0.25	12.3703	0.4103	19.24	0.1686	3.9149
0.24	12.5113	0.3779	17.73	0.1805	4.2542
0.23	12.6944	0.3464	16.35	0.1942	4.6511
0.22	12.9314	0.3159	15.14	0.2103	5.1189
0.21	13.2434	0.2867	14.12	0.2296	5.6802
0.20	13.6576	0.2587	13.31	0.2537	6.3643
0.19	14.2131	0.2323	12.74	0.2847	7.2125
0.18	14.9725	0.2075	12.47	0.3265	8.2904
0.17	16.0398	0.1845	12.59	0.3863	9.7057
0.16	17.5771	0.1634	13.25	0.4767	11.6254
0.15	19.8913	0.1445	14.77	0.6254	14.3634
0.14	23.5740	0.1278	17.88	0.8972	18.5215

Table 5.3: Variations of the core-crust transition density, pressure and proton fraction for β-equilibrated neutron star matter, symmetric nuclear matter incompressibility K_∞ and isospin dependent part K_τ of isobaric incompressibility with parameter n.

n	ρ_t	P_t	$x_{p(t)}$	K_∞	K_τ	Maximum Mass	Radius	Crustal Thickness
	fm^{-3}	$MeVfm^{-3}$		MeV	MeV	$M_\odot$	km	km
Expt.	values	- - $\rightarrow$	$\rightarrow$	250-270	-370±120	1.97±0.04		
1/6	0.0797	0.4134	0.0288	182.13	-293.42	1.4336	8.5671	0.4009
				R(km) $\geq$	4.48 +	$3.37M/M_\odot$		
1/3	0.0855	0.4520	0.0296	212.98	-332.16	1.6002	8.9572	0.3743
				R(km) $\geq$	4.31 +	$3.36M/M_\odot$		
1/2	0.0901	0.4801	0.0303	243.84	-370.65	1.7634	9.3561	0.3515
				R(km) $\geq$	4.19 +	$3.36M/M_\odot$		
2/3	0.0938	0.5006	0.0308	274.69	-408.97	1.9227	9.7559	0.3318
				R(km) $\geq$	4.10 +	$3.36M/M_\odot$		
1	0.0995	0.5264	0.0316	336.40	-485.28	2.2335	10.6408	0.3088
				R(km) $\geq$	3.99 +	$3.36M/M_\odot$		

relation is obtained for fixed values of $\frac{\Delta I}{I}$, ρ_t and P_t. This is then plotted in the same figure for $\frac{\Delta I}{I}$ equal to 0.014. For Vela pulsar, the constraint $\frac{\Delta I}{I} > 1.4\%$ implies that allowed mass-radius lie to the right of the line defined by $\frac{\Delta I}{I} = 0.014$ (for $\rho_t = 0.0938$ fm^{-3}, $\mathrm{P}_t =$ 0.5006 MeV fm^{-3}). This condition is given by the inequality $R \geq 4.10 + 3.36M/M_\odot$ kms [64].

The calculations are performed for five different n values that correspond to SNM incompressibility ranging from ∼180-330 MeV. For each case, the constants C and β obtained by reproducing the ground state properties of SNM become different leading to five different sets of these three parameters. We certainly can not change strengths and ranges of the M3Y interaction. In Table-5.3, the variations of the core-crust transition density, pressure and proton fraction for β-equilibrated neutron star matter, symmetric nuclear matter incompressibility K_∞, isospin dependent part K_τ of isobaric incompressibility, neutron star's maximum mass with corresponding radius and crustal thickness with parameter n are listed along with corresponding Vela pulsar constraints. It is important to mention here that recent observations of the binary millisecond pulsar J1614-2230 by P. B. Demorest et al. [25] suggest that the masses lie within 1.97 ± 0.04 M$_\odot$ where M$_\odot$ is the solar mass. Recently the radio timing measurements of the pulsar PSR J0348 + 0432 and its white dwarf companion have confirmed the mass of the pulsar to be in the range 1.97-2.05 M$_\odot$ at 68.27% or 1.90-2.18 M$_\odot$ at 99.73% confidence [26]. The observed 1.97 ± 0.04 M$_\odot$ neutron star rotates with 3.1 ms and results quoted in Table-5.2 are for non-rotating case. For rotating stars [110] present EoS predict masses higher than the lower limit of 1.93 M$_\odot$ for maximum mass of neutron stars. We used the same value of $\rho_0 = 0.1533$ fm^{-3} since we wanted to keep consistency with all our previous works on nuclear matter. We would like to mention that if instead we would have used the value of 0.16 fm^{-3} for ρ_0, the value of K_∞ would have been slightly higher by ∼2 MeV and correspondingly maximum mass of neutron stars by ~ 0.01 M$_\odot$.

Recently, it is conjectured that the glitches observed in the Vela pulsar require an additional reservoir of angular momentum and the crust may not be enough to explain the phenomenon [150]. Large pulsar frequency glitches can be interpreted as sudden transfers of angular momentum between the neutron superfluid permeating the inner crust and the rest of the star. In spite of the absence of viscous drag, the neutron superfluid is strongly coupled to the crust due to non-dissipative entrainment effects. It is often argued that these effects may limit the maximum amount of angular momentum that can possibly be transferred during glitches [151]. We find that the present EoS can accommodate large crustal moments of inertia and that large enough transition pressures can be generated to explain the large Vela glitches without invoking an additional angular-momentum reservoir beyond that confined to the solid crust. Our results suggest that the crust may be enough [152] which can be substantiated from Table-5.2 that $\frac{\Delta I}{I} > 0.014$ for pulsars with masses 1.8 $M_\odot$ or less.

The results listed in Table-5.3 suggest that SNM incompressibility do have some effect, albeit small, in determining the crustal fraction of moment of inertia and on the Vela Pulsar Radius Constraint like some other recent studies [153]. But the incompressibility values of about 15 MeV window around 274.7 MeV corresponding to $n = \frac{2}{3}$ is experimentally supported. The current status of the determination of the compression modulus of the SNM experimentally from the ISGMR compression modes and from the ISGDR of finite nuclei concludes [95] that due to the self-consistency violations of the Hartree-Fock Random Phase Approximation calculations of the giant resonance strength functions causes shifts in the calculated values of the centroid energies. These shifts may rather be greater in magnitudes than the recent uncertainties in the experimental measurements. Actually, the compression modulus K_∞ predictions lying in the 210 MeV to 220 MeV range were because of the fact that not a completely self-consistent Skyrme calculations [95] were used. Rectifying for this shortcoming, Skyrme parmetrizations of SLy4 type can be build for which K_∞ values lie between 230 MeV to 240 MeV [95]. Furthermore, it is quite feasible to construct authentic Skyrme interactions such that the compression modulus of SNM is in the vicinity of the relativistic value, *viz.* 250 MeV to 270 MeV. Hence, it may be concluded from the ISGMR data that magnitude of K_∞ is about 240 ± 20 MeV.

The newer observational data [154] on Vela pulsar claims slightly higher estimate for $\frac{\Delta I}{I} > 1.6\%$ based on glitch activity. This minute change neither affects the conclusions nor warrants any new idea of the neutron superfluidity extending partially into the core. However, if the phenomenon of crustal entrainment due to the Bragg reflection of unbound neutrons by the lattice ions is taken into account then [150, 151] a much higher fraction of the moment of inertia (7% instead of 1.4-1.6%) has to be associated to the crust. This causes drastic modification of the moment of inertia of the superfluid component. If $\frac{\Delta I}{I} > 0.07$ is considered, then the corresponding allowed masses and radii will be given by $R \geq 7.60 + 3.71 M/M_\odot$ instead of $R \geq 4.10 + 3.36 M/M_\odot$ which is shown in Fig.-5.2 [64]. But from Table-5.2 this would mean that the maximum mass is less than $\sim 1.M_\odot$ which contradicts the mass of Vela pulsar. The mass of Vela pulsar was fixed to the canonical value of $\sim 1.4 M_\odot$ for simplicity, to fit the X-ray spectrum in Ref.[155]. This is by no means a mass measurement. The mass of Vela is unknown till date. The only reasonable constraint is that it should exceed about one solar mass according to core-collapse supernova simulations. Therefore, the present calculations suggest that without entrainment, the crust is enough to explain the Vela glitch data and with entrainment, the crust is not enough since the mass of Vela pulsar would be below $1.M_\odot$ (table 2 and Fig.-5.2), in accordance with other studies [150, 151, 156, 157, 158].

The rigorous way of dealing with core-crust transition is producing a unified EoS and evaluating the density where the clustered phase becomes energetically disfavored with respect to the homogeneous solution [159]. It should be clarified here that the crustal region of the compact star in the present work consists of FMT+BPS+BBP up to number density of 0.0582 fm^{-3} and β-equilibrated neutron star matter up to core-crust transition number density of 0.0938 fm^{-3} which is far beyond 0.0582 fm^{-3}, otherwise we would have taken a unified EoS. The three different methods to calculate the transition density are the thermodynamical spinodal (the method used in this work), the dynamical spinodal within the Vlasov formalism and the relativistic random phase approximation. It was shown that the last two methods [160] give similar results, confirming previous studies [161, 162]. The thermodynamical method also gives a good estimate of the transition density [160, 163] and involves simpler calculations.

Chapter 6

FUSION CROSS SECTION FOR REACTIONS INVOLVING MEDIUM AND HEAVY NUCLEUS-NUCLEUS SYSTEM

6.1 Fusion barrier distribution

It is well known that the energy dependence of the fusion cross sections can not be well estimated assuming simply the penetration through a well-defined barrier in one-dimensional potential of a colliding nucleus-nucleus system. The heavy-ion fusion cross sections require interpretation [71] in terms of a distribution of potential barriers. The smoothening due to the quantal barrier penetration replaces set of discrete barriers by an effective continuous distribution. In order to reproduce shapes of experimentally observed fusion excitation functions, particularly at low, near-threshold energies, it is necessary to assume a distribution of the fusion barrier heights, the effect that results from the coupling to other than relative distance degrees of freedom. This is naturally achieved in coupled-channel calculations, involving the coupling to the lowest collective states in both colliding nuclei. The structure effects in the barrier distributions are neglected in the present work and for the distribution of the fusion barrier heights, a Gaussian shape for the barrier distribution $D(B)$ is assumed [164]. The barrier distribution is, therefore, given by

$$D(B) = \frac{1}{\sqrt{2\pi}\sigma_B} \exp\Big[-\frac{(B-B_0)^2}{2\sigma_B^2}\Big] \tag{6.1}$$

where the two parameters, the mean barrier B_0 and the distribution width σ_B, to be determined individually for each reaction.

6.2 The fusion cross section

In order to provide a systematic analysis of the data on the fusion excitation functions, a simple formula for the cross section for overcoming the potential energy barrier is derived. The energy dependence of the fusion cross section is obtained by folding the barrier distribution [164, 165] provided by Eq.(6.1), with the classical expression for the fusion cross section given by

$$\begin{aligned} \sigma_f(B) = & \quad \pi R_B^2\Big[1-\frac{B}{E_{c.m.}}\Big] & \text{for} \quad B \leq E_{c.m.} \\ = & \quad 0 & \text{for} \quad B \geq E_{c.m.} \end{aligned} \tag{6.2}$$

where $E_{c.m.}$ is the energy in centre-of-mass system of colliding nuclei and R_B denotes the relative distance corresponding to the position of the barrier approximately, which yields

$$\sigma_c(E_{c.m.}) = \int_0^\infty \sigma_f(B)D(B)dB$$

$$= \int_0^{B_0} \sigma_f(B)D(B)dB + \int_{B_0}^{E_{c.m.}} \sigma_f(B)D(B)dB \tag{6.3}$$
$$= \pi R_B^2 \frac{\sigma_B}{E_{c.m.}\sqrt{2\pi}} \Big[\xi\sqrt{\pi}\Big\{\mathrm{erf}\xi + \mathrm{erf}\xi_0\Big\} + e^{-\xi^2} + e^{-\xi_0^2}\Big]$$

where

$$\xi = \frac{E_{c.m.} - B_0}{\sigma_B\sqrt{2}}$$
$$\xi_0 = \frac{B_0}{\sigma_B\sqrt{2}} \tag{6.4}$$

and erfξ is the Gaussian error integral of argument ξ. The parameters B_0 and σ_B along with R_B is to be determined by fitting Eq.(6.3) along with Eq.(6.4) to a given fusion excitation function. In the derivation of formula Eq.(6.3), the quantum effect of sub-barrier tunneling is not accounted for explicitly. However, the influence of the tunneling on shape of a given fusion excitation function is effectively included in the width parameter σ_B.

The fusion cross section formula of the Eq.(6.3) obtained by using the diffused-barrier, is a very elegant parametrization of the cross section for a process of overcoming the potential-energy barrier. Hence, it can be successfully used for analysis and predictions of the fusion excitation functions of light, medium and moderately heavy systems, especially in the range of near-barrier energies.

In case of light and medium systems, surmounting the barrier automatically guarantees fusion of the colliding nuclei leading to formation of the compound nucleus. The term 'capture' is used to refer the process of overcoming the interaction barrier in a nucleus-nucleus collision, followed by formation of a composite system. In general, the composite system undergoes fusion only in a fraction f of the capture events. For light and medium systems, $f \approx 1$, and almost all the 'capture' events lead to fusion resulting fusion cross sections to be practically identical with the capture cross sections. However, for very heavy systems, only a small fraction ($f < 1$) of 'capture' events ultimately lead to fusion while for the remaining part of the events, the system re-separates prior to equilibration and clear distinction between fusion and capture cross sections then becomes necessary. Therefore, for very heavy systems, when the overcoming the barrier does not guarantee fusion, predictions based on Eq.(6.3) provide the capture cross section.

6.3 Calculation and results

6.3.1 Calculation of fusion excitation functions

The near-barrier (above barrier) fusion excitation functions of medium and heavy nucleus-nucleus systems have been analyzed using a simple diffused barrier formula (given by Eq.(6.1)) derived by folding the Gaussian barrier distribution with the classical expression for the fusion cross section for a fixed barrier. The same set of target-projectile combinations (along with few others) have been selected for which heavy ion sub-barrier fusion has been recently [166] studied. The values of mean barrier height B_0, width σ_B and the effective radius R_B have been obtained using the least-square fit method. These values are listed in Table-6.1 and arranged in order of the increasing value of the Coulomb parameter z. Since the number of data points for ^{48}Ca+^{124}Sn is too low compared to other systems, the error bars for B_0 (111.93 ± 0.44), σ_B (1.28 ± 0.83) and R_B (8.24 ± 0.09) are rather large.

In Figs.-6.1 & 6.2, the measured fusion excitation functions represented by full circles are compared with the predictions of the diffused barrier formula depicted by the solid lines. The two systems of ^{16}O+^{144}Sm and ^{40}Ca+^{124}Sn illustrated in Figs.-6.1 & 6.2 correspond to two extreme Coulomb parameter (z) values of ~ 64 and ~ 119, respectively. In Fig.-6.3, the measured fusion excitation functions (full circles) for ^{36}S+^{90,96}Zr for with predictions (solid lines) of the diffused barrier formula are presented to highlight the effects of isotopic dependence. It can, therefore, be easily perceived from these figures that precisely measured fusion excitation functions provide systematic information on the essential characteristics of the interaction potential, *viz.* the mean barrier height B_0 and width σ_B of its distribution, for nucleus-nucleus collisions. The fusion or capture cross sections can also be predicted by using Eq.(6.3) and theoretically obtained values of the parameters B_0 and σ_B for planning experiments for synthesizing new super-heavy elements.

As seen in the Figs.-6.1-6.3, the present theoretical description provides excellent fits to the experimental data. This implies that for the chosen set of nuclei almost all the capture events lead to fusion resulting fusion cross sections to be practically identical with the capture cross sections. Moreover, the Gaussian form for the barrier distribution describes near barrier fusion cross sections quite well justifying the beyond single barrier model arising out of tunneling, deformation and vibration of nuclei. Although theoretically the concept of a barrier distribution is valid under certain approximations, the good fits to the experimental data shown certainly imply that in reactions involving medium & heavy nucleus-nucleus systems, barrier distribution remains a meaningful concept. The slight mismatch with experimental data at low energies is inherent to the theoretical formalism which starts deviating at energies much below Coulomb barrier. Therefore, for deep sub-barrier fusion cross section calculations altogether different theoretical approach has been adopted which is described in Chapter 7 in detail.

6.3.2 Determination of the parameters of the barrier distribution

The task of estimating $\sigma_c(E)$ rests on predicting B_0, σ_B and R_B values for a particular reaction. Since B_0 is essentially the mean height of the Coulomb barrier, it must be a function of Coulomb parameter $z = Z_1Z_2/(A_1^{1/3} + A_2^{1/3})$ in the vicinity of the barrier and to a crudest approximation it is just ze^2/r_{0c} where e and r_{0c} are the elementary charge and the Coulomb radius parameter, respectively. Thus a fair extrapolation formula for mean barrier height B_0 can be expressed by

$$B_0 = a_1 z + a_2 z^2 + a_3 z^3 \tag{6.5}$$

where the coefficients a_1, a_2 and a_3 are to be fixed from fitting the data for a large number a reacting pair of nuclei and expecting a_1 to be $\sim e^2/r_{0c}$ while a_2 and a_3 to be orders of magnitude smaller.

The second quantity, the effective barrier radius R_B, quite obviously, should have a form of $r_0(A_1^{1/3} + A_2^{1/3})$, where r_0 can be fixed from fitting the data for a large number of colliding pair of nuclei.

The extrapolation of the trend of σ_B is more difficult which primarily arises out of nuclear deformation, nuclear vibrations and quantal barrier penetrability. Assuming all possible orientations of a nucleus i with a static deformation $\beta_2(i)$, one obtains the variation of the effective radius R_i with the standard deviation [167]

$$\Delta R_i = \frac{\beta_2(i) R_i}{\sqrt{4\pi}} \tag{6.6}$$

and multipolarities higher than the quadrupole are disregarded. Thus distribution of the resulting surface-surface distance, for a fixed distance between centers of mass of the two nuclei, leads to the standard deviation σ_i of the barrier height distribution given by

$$\sigma_i = |\frac{\partial V}{\partial r}|_{r=R_B}\Delta R_i = \frac{Z_1 Z_2 e^2}{R_B}\frac{\beta_2(i)}{\sqrt{4\pi}}\frac{R_i}{R_B}\Big[1-\frac{3R_i}{5R_B}\Big] \tag{6.7}$$

Now the σ_B can be given by

$$\sigma_B = \sqrt{\sigma_1^2+\sigma_2^2+\sigma_0^2} \tag{6.8}$$

where $R_B = R_1 + R_2 = r_0[A_1^{1/3} + A_2^{1/3}]$, ΔR_1 and ΔR_2 are the standard deviations of the radius vectors specifying the surfaces of the projectile and target, whose mean radii are R_1 and R_2 and whose quadrupole deformation parameters are $\beta_2(1)$ and $\beta_2(2)$, respectively. The quantity σ_0 in the above Eq.(6.8) is an adjustable parameter that accounts for, at least roughly, nuclear vibrations and quantal barrier penetrability. Obviously, for magic and semi-magic nuclei, $\sigma_1 = \sigma_2 = 0$ and then $\sigma_B = \sigma_0$.

In order to predict the parameters of the barrier distribution, extracted values of mean barrier height B_0, width σ_B and the effective radius R_B are chosen for a set of fiftyone colliding pair of nuclei comprising of all the sets of the above Table-6.1 and that of Ref.[164]. The nonlinear least square fits yield values for Eq.(6.8), $a_1 = 0.912025$ MeV, $a_2 = 0.600849 \times 10^{-4}$ MeV and $a_3 = 0.315525 \times 10^{-5}$ MeV and for R_B, $r_0 = 1.126 \pm 0.029$ fm. Once these values are fixed, the value of σ_0 is extracted from Eq.(6.7) using the quadrupole deformation parameters from Ref.[168] and $r_0 = 1.15$ fm (which gives better fit than its mean value of 1.126 fm) which yielded $\sigma_0 = 1.346 \pm 0.397$ MeV.

Comparing reactions ^{40}Ca+^{90}Zr and ^{48}Ca+^{90}Zr, the extracted values of σ_0 are 1.610 MeV and 2.065 MeV, respectively, showing that the average value of σ_0 is close to 1.346 ± 0.397 MeV obtained above. For both the reactions, the Q-values for neutron transfer are negative and, therefore, the transfer channels are closed (no transfer effect).

For reactions ^{48}Ca+^{90}Zr ($Q < 0$ for fusion) and ^{48}Ca+^{96}Zr ($Q < 0$ for fusion), the Q-values for neutron transfer are negative. By employing σ_0 from ^{48}Ca+^{90}Zr, the extracted

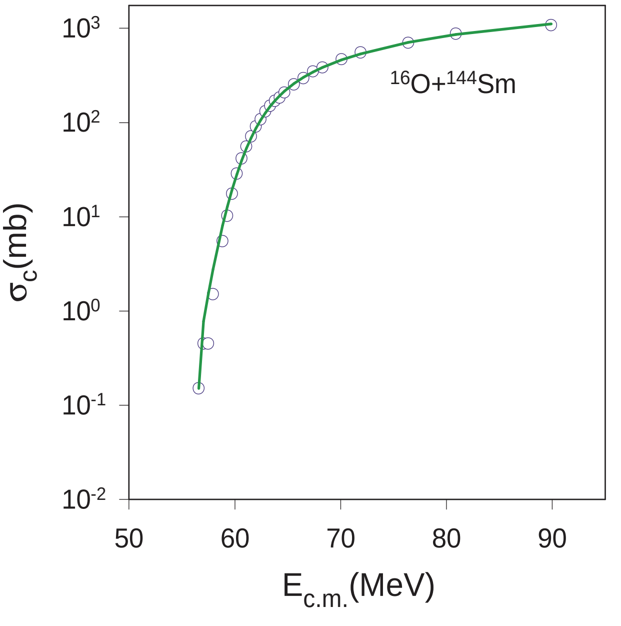

Figure 6.1: Comparison of the measured capture excitation functions (full circles) for ^{16}O+^{144}Sm with predictions (solid lines) of the diffused barrier formula.

value of $\sigma_2(^{96}\mathrm{Zr})$ is 1.816 and, correspondingly, value of $\beta_2(^{96}\mathrm{Zr})$ turns out to be 0.147 whereas its experimental and theoretical values are 0.080(17) [169] and 0.217 [168], respectively. Similarly, by employing σ_0 from ^{16}O+^{144}Sm, the extracted values of ground state (g.s.) $\beta_2(^{148}\mathrm{Sm})$ and $\beta_2(^{154}\mathrm{Sm})$ are 0.177 and 0.194, respectively, whereas the corresponding experimental (2^+ excited state) [theoretical (g.s.)] values are 0.1423(36) [0.161] and 0.3410(20) [0.270]. For these reactions also neutron transfer channels are almost closed.

It is interesting to note that for reaction ^{32}S+^{110}Pd for which neutron transfer $Q > 0$ [thus mixture of transfer and deformation effects] and therefore $\sigma_B = 3.10$ MeV is much larger than $\sigma_B = 1.92$ MeV for the reaction ^{36}S+^{110}Pd for which neutron transfer $Q < 0$ [the pure deformation effect due to the deformed Pd].

The sub-barrier capture (fusion) depends on the two-neutron transfer with the positive Q-value [170, 171, 172]. Before the projectile is captured by target-nucleus, the two-neutron transfer occurs at larger separations that lead to the population of the first 2^+

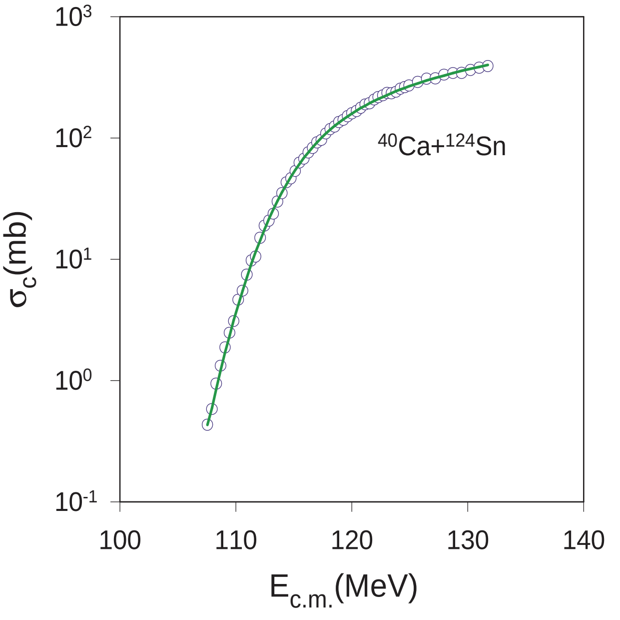

Figure 6.2: Comparison of the measured capture excitation functions (full circles) for ^{40}Ca+^{124}Sn for with predictions (solid lines) of the diffused barrier formula.

state in the recipient nucleus (the donor nucleus remains in the ground state). Since after two-neutron transfer the mass numbers, the deformation parameters of interacting nuclei, and, respectively, the height and shape of the Coulomb barrier are changed, one can expect the enhancement or suppression of the capture. Hence, the transfer effect is an indirect deformation effect.

Although ^{40}Ca+^{90}Zr and ^{40}Ca+^{96}Zr have negative Q-values for fusion reactions, the reaction ^{40}Ca+^{96}Zr has positive Q-values for neutron transfer. After the neutron transfer, the deformation of the nuclei increases and the mass asymmetry of the system decreases, and, thus, the value of the Coulomb barrier decreases and the capture cross section becomes larger. With the strong fusion enhancement, the increase of σ_B(^{40}Ca+^{96}Zr) [with respect to σ_B(^{40}Ca+^{90}Zr)] due to the neutron transfer can be extracted as: $\sigma_{transfer} = \Big([\sigma_B(^{40}\mathrm{Ca}+^{96}\mathrm{Zr})]^2\text{-}[\sigma_B(^{40}\mathrm{Ca}+^{90}\mathrm{Zr})]^2\Big)^{1/2} = 2.5998$, which is mainly related with the deformation of ^{42}Ca in the first 2^+ state enabling one to extract β_2(^{42}Ca) from the $\sigma_{transfer}$ as 0.183 whereas the experimental value is 0.247(9) [169] for the 2^+ excited state. The

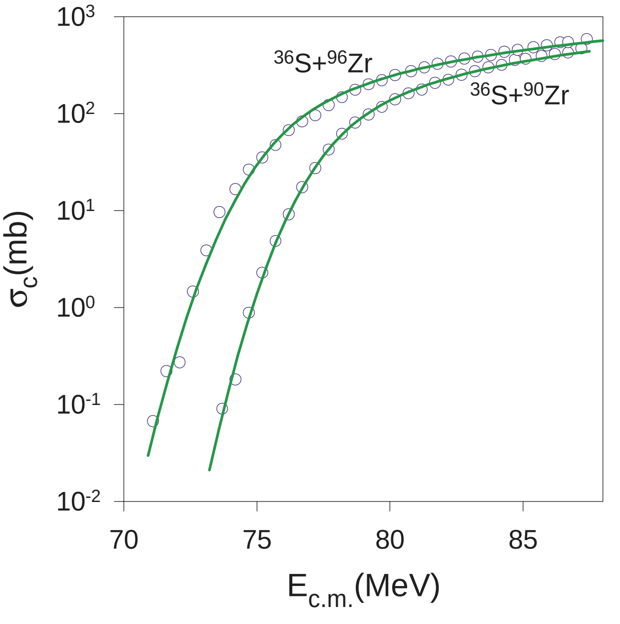

Figure 6.3: Comparison of the measured capture excitation functions (full circles) for $^{36}S+^{90,96}Zr$ for with predictions (solid lines) of the diffused barrier formula.

reactions $^{40}Ca+^{124}Sn$ (two neutron transfer $Q < 0$) and $^{48}Ca+^{124}Sn$ (two neutron transfer $Q > 0$) yields $\sigma_{transfer} = 2.3773$ MeV providing $\beta_2(^{42}Ca)$ as 0.151 for the 2^+ excited state. Similar study for reactions $^{32}S+^{90}Zr$ (two neutron transfer $Q < 0$) and $^{32}S+^{96}Zr$ (two neutron transfer $Q > 0$) yields $\sigma_{transfer} = 2.4495$ MeV which in turn provides $\beta_2(^{34}S)$ as 0.213 for the 2^+ excited state whereas the experimental value is 0.252(7) [169] for the 2^+ excited state.

By employing σ_0 from $^{36}S+^{90}Zr$, the extracted value of $\sigma_2(^{96}Zr)$ is 0.594 MeV and, correspondingly, value of $\beta_2(^{96}Zr)$ turns out to be 0.061 whereas its experimental and theoretical values are 0.080(17) [169] and 0.217 [168], respectively.

The predictions of the present calculations for 250 MeV ^{48}Ca incident beam on few target nuclei that are especially important for planning experiments for synthesizing new super-heavy elements are provided in Table-6.2. It is important to mention here that for such heavy systems, overcoming the barrier does not guarantee fusion and the predictions for σ_c listed in the table provide the capture cross section. Only a small fraction of

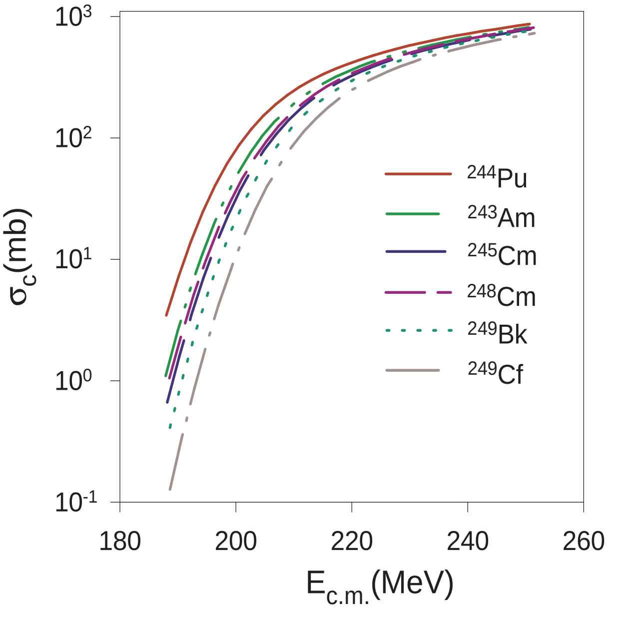

Figure 6.4: Calculated capture excitation functions for ^{48}Ca + ^{244}Pu, ^{243}Am, ^{245}Cm, ^{248}Cm, ^{249}Bk, ^{249}Cf.

capture events ultimately lead to fusion while for the remaining part of the events, the system re-separates prior to equilibration. In Fig.-6.4, calculated excitation functions for ^{48}Ca+^{244}Pu,^{243}Am,^{245}Cm,^{248}Cm,^{249}Bk,^{249}Cf are presented.

In summary, the fusion reaction cross sections have been calculated for above barrier energies over a wide energy range. A set of precisely measured fusion excitation functions has been studied in order to learn about the conditions of overcoming the potential energy barrier in nucleus-nucleus collisions and to obtain systematic information on the essential characteristics of the interaction potential, *viz.* the mean barrier height B_0 and width σ_B of its distribution, between the two colliding nuclei. For the analysis of the experimental data a simple diffused-barrier formula is derived assuming Gaussian shape for the barrier distribution. Using the least-square fit method, precisely determined values of the mean barrier height B_0, the width σ_B and the effective radius R_B have been obtained. The theoretical model for estimating the parameters of the barrier distribution is described and their values are estimated. The observed enhancement of the sub-barrier capture (fusion) cross sections is correlated to the neutron transfer with positive Q-values. The change of the capture cross section after the neutron transfer is due to the change of the deformations of nuclei. Obviously, Eq.(6.8) implies that after the neutron transfer, if the deformations of nuclei do not change or decrease (increase), the neutron transfer weakly influences or suppresses (enhances) the capture process.

To calculate the overcoming-the-barrier cross section for a given projectile-target combination one can use the present fusion cross section formula and apply theoretical values of the parameters B_0 and σ_B to predict cross sections for overcoming the barrier in collisions of very heavy systems. Prediction of the energy dependence of the cross section for capture or sticking can be used as one of three basic ingredients in the sticking-diffusion-survival model [173] for calculating the production cross sections of superheavy nuclei. The reasonably good fit of the present theoretical description to the experimental data implies two important facts that for the investigated set of nuclei almost all the capture events ultimately lead to fusion and the idea of the Gaussian distribution of barrier provides good description of near barrier fusion cross sections.

Table 6.1: The extracted values of the mean barrier height B_0, the width of the barrier height distribution σ_B and the effective radius R_B, deduced from the analysis of the measured fusion excitation functions.

Reaction	z	Refs.	B_0 [MeV]	σ_B [MeV]	R_B [fm]
$^{16}O+^{154}Sm$	62.94	[174]	58.80	2.43	10.04
$^{17}O+^{144}Sm$	63.49	[174]	60.28	1.75	10.46
$^{16}O+^{148}Sm$	63.51	[174]	59.88	2.31	10.61
$^{16}O+^{144}Sm$	63.91	[174]	60.65	1.76	10.46
$^{36}S+^{110}Pd$	90.94	[175]	85.51	1.92	8.20
$^{32}S+^{110}Pd$	92.39	[175]	86.04	3.10	8.45
$^{48}Ca+^{96}Zr$	97.41	[176]	93.76	2.75	10.07
$^{48}Ca+^{90}Zr$	98.58	[176]	94.94	2.11	10.01
$^{40}Ca+^{96}Zr$	100.01	[76]	94.30	3.09	9.71
$^{40}Ca+^{90}Zr$	101.25	[76]	96.26	1.67	10.07
$^{48}Ca+^{124}Sn$	116.00	[177]	111.93	1.28	8.24
$^{40}Ca+^{124}Sn$	118.95	[178]	113.36	2.70	9.57
$^{36}S+^{96}Zr$	81.21	[179]	74.90	1.34	11.00
$^{36}S+^{90}Zr$	82.23	[179]	77.01	1.25	10.81
$^{32}S+^{96}Zr$	82.54	[180]	79.40	3.50	10.26
$^{32}S+^{90}Zr$	83.59	[180]	80.00	2.50	10.60

Table 6.2: Theoretical values of the mean barrier height B_0, the width of the barrier height distribution σ_B and the effective radius R_B and cross section σ_c for 250 MeV ^{48}Ca incident beam on different target nuclei.

Target Nuclei	B_0 [MeV]	σ_B [MeV]	R_B [fm]	σ_c [mb]
^{244}Pu	197.38	6.06	11.37	225.10
^{243}Am	200.19	6.12	11.36	170.73
^{245}Cm	202.37	6.44	11.38	139.56
^{248}Cm	201.72	6.45	11.40	157.97
^{249}Bk	204.12	6.51	11.41	121.18
^{249}Cf	206.74	6.58	11.41	83.89

Chapter 7

ASTROPHYSICAL FUSION REACTIONS AT DEEP SUB-BARRIER ENERGIES

One of the main aim of Nuclear Astrophysics is to study nuclear reactions which cause synthesis of nuclei (nucleosynthesis) inside stars (stellar nucleosynthesis) and during the Big-Bang that occurred in early universe (primordial nucleosynthesis). This area of research had emerged from the early work of Burbidge, Burbidge, Fowler and Hoyle [181] which hypothesized a series of energy generating mechanisms in stars. As the stellar models have become more realistic, this field has become the object of intense theoretical and experimental research. Additional motivation also generated from projects of energy generation through nuclear fusion, which involve many of the nuclear reactions that take place in stellar nucleosynthesis. The nuclear fusion at very low energies plays an important role in nucleosynthesis. Nuclear fusion reaction in this energy range can be explained successfully by the phenomenon of quantum mechanical tunneling through Coulomb barrier of interacting nuclide.

7.1 Astrophysical S-factor for deep sub-barrier resonant fusion reactions

The nuclear reactions play a major role [181, 182, 183] in determining the structure of main-sequence stars, giant stars, supergiants, pre-supernovae and compact stars like white dwarfs and neutron stars and their evolution and nucleosynthesis they undergo as well as in various observational manifestations. Depending upon the density and temperature along with other parameters, stellar burning is likely to involve many reactions of different kind and involving nuclei from light to heavy and from stable to unstable neutron or proton rich. The rates of these reactions can be calculated from the reaction cross sections σ by averaging over a Maxwell-Boltzmann energy distribution. Thus, the thermonuclear reaction rate $< \sigma v >$ at some temperature T is the Maxwellian-averaged cross-section and is given by the following integral [184]:

$$< \sigma v >= \Big[\frac{8}{\pi\mu(k_BT)^3}\Big]^{1/2} \int \sigma(E)E\exp(-E/k_BT)dE, \tag{7.1}$$

where E is the energy in centre-of-mass system of colliding nuclei, v and μ are their relative velocity reduced mass respectively. At energies far below Coulomb barrier, the penetrability can be approximated by $\exp(-2\pi\zeta)$ since the classical turning point is much larger than the nuclear radius. Therefore, the charge induced cross section can be decomposed into

$$\sigma(E) = \frac{S(E)\exp(-2\pi\zeta)}{E} \tag{7.2}$$

where $\zeta = \frac{Z_1Z_2e^2}{\hbar v}$ is the Sommerfeld parameter with Z_1 and Z_2 being the charges of the reacting nuclei in units of elementary charge e and $S(E)$ is the astrophysical S-factor. Besides narrow resonances, $S(E)$ behaves as a smooth function of energy and hence convenient for extrapolating measured cross sections down to astrophysical energies. The resonant cross section is generally approximated by a Breit-Wigner expression in the case of a narrow resonances. The neutron induced reaction cross sections at low energies, however, is given by $\sigma(E) = \frac{R(E)}{v}$ [185]. This form facilitates extrapolation of the measured cross sections down to astrophysical energies, where $R(E)$ is also a smoothly varying energy functional [186] similar to the S-factor.

The nuclear fusion reactions at very low energies plays important role in nucleosynthesis of light elements in big bang nucleosynthesis as well as inside the stellar core. The fusion cross section is also one of the most important physical quantity required for both design and research in fusion engineering. Nuclear fusion reaction in the energy range of $\sim$1eV to few keV can be explained successfully by the phenomenon of quantum mechanical tunneling through Coulomb barrier of interacting nuclei. In the present work, a simple square-well potential model with an imaginary part has been used to describe the nuclear fusion reaction of light nuclei where the real part of the nuclear potential is primarily obtained from the resonance energy while the imaginary part is determined by the Gamow factor at resonance energy. This complex square-well nuclear potential describes the absorption within the nuclear potential well. The energy dependence of the cross sections and astrophysical S-factors for the deep sub-barrier fusion reactions of light nuclei have been calculated using this model.

7.1.1 Theoretical framework

In case of the fusion of light nuclei, treating the resonant tunneling through the Coulomb barrier as a two-step process which means first tunneling and then decay, fails to provide an adequate description. Such a oversimplified one-dimensional model [187], based on the assumption of decay being independent of tunneling, does not depict the true picture of the physical process. In fact, when the wave function of the system of two colliding nuclei penetrates the barrier, inside the nuclear potential well it reflects back and forth. These reflections inside the nuclear potential well is completely discounted in one dimensional model where the wave suffers no reflection while penetrating the barrier. For α-decay case as well, the outgoing α-particle encounters no reflection after penetrating the barrier in a three dimensional model [188]. However, reflection is indeed essential for the resonant penetration through the barrier into the centre of nuclear well. While the decay of the penetrating nuclei terminates the bouncing motion inside the nuclear well, if nuclear reaction happens quick enough the wave function will have no time to execute this bouncing motion. In other words, the short lifetime of the penetrating wave may forbid resonant tunneling. This is because of the fact that there will be not enough bouncing motion to built up, inside the nuclear well, the wave function in terms of constructive interference. The tunneling and decay can no longer be independent in light nuclear fusion process and need to be combined as a selective process.

The lifetime effect on the resonant tunneling can be best achieved by introducing an imaginary part into the nuclear interaction potential. The complex nuclear potential has been shown to describe successfully the resonant tunneling effects in deep sub-barrier fusion using a three dimensional model for wide range of energies [189, 190, 191]. It is precisely, maximizing a damp matching resonant tunneling and thus overcoming of the insufficiencies of Gamow tunneling. When a light nucleus is injected into another, the reduced radial wave function $\psi(r)$ describing the relative motion can be related to the full wave function $\Phi(r,t) = \frac{1}{\sqrt{4\pi}r}\psi(r)\exp(-i\frac{E}{\hbar}t)$. The full wave function $\Phi(r,t)$ represents the solution of the general Schrödinger equation for the system. The reaction cross section in terms of the phase shift δ_0 due to the nuclear potential (in low energy limit only s-wave contributes) is given by $\sigma = \frac{\pi}{k^2}[1-|\eta|^2]$ where $\eta = e^{2i\delta_0}$ and $k = \sqrt{\frac{2\mu E}{\hbar^2}}$ = the relative motion wave number between the reacting nuclei. In the three dimensional calculation, nuclear potential being complex, the corresponding phase shift δ_0 is complex and is given by [191]

$$cot(\delta_0) = W_r + iW_i \tag{7.3}$$

where a new set of two parameters, W_r and W_i, the real and the imaginary parts of the cotangent of the conventional phase shift δ_0 have been introduced. Consequently, the reaction cross section for the s-wave given by $\sigma = \frac{\pi}{k^2}\left(1 - |e^{2i\delta_0}|^2\right)$ can be rewritten as

$$\begin{aligned} \sigma &= \frac{\pi}{k^2}\left\{-\frac{4W_i}{(1-W_i)^2 + W_r^2}\right\} \\ &= \left(\frac{\pi}{k^2}\right)\left(\frac{1}{\chi^2}\right)\left\{-\frac{4\omega_i}{\omega_r^2 + (\omega_i - \frac{1}{\chi^2})^2}\right\} \end{aligned} \tag{7.4}$$

where χ^2=$\left\{\frac{\exp\left(\frac{2\pi}{ka_c}\right)-1}{2\pi}\right\}$ and $1/\chi^2$ is the Gamow penetration factor and $a_c = \hbar^2/\mu Z_1 Z_2 e^2$ is the length of Coulomb unit. It is evident that the cross section attains maximum for the condition: $W_r = 0$ and $W_i = -1$ and $W_r = 0$ corresponding to the resonance condition. Thus the condition for resonance is $\mathrm{Re}(\delta_0) = (2n+1)\pi/2$ where n is an integer. The dimensionless quantity $S_r(E)$ given by

$$S_r(E) = \left\{-\frac{4\omega_i}{\omega_r^2 + (\omega_i - \frac{1}{\chi^2})^2}\right\} \tag{7.5}$$

provides an alternative expression for a dimensionless astrophysical S-function, where $\omega = \omega_r + i\omega_i = W/\chi^2 = (W_r + iW_i)/\chi^2$. The real part V_r and the imaginary part V_i of the nuclear potential determines the wave function within the nuclear potential well while the two other parameters, *viz.* the real and the imaginary part of the complex phase shift $(\delta_0)_r$ and $(\delta_0)_i$ determine the Coulomb wave function outside the nuclear well. The parameters, W_r and W_i, have been introduced for convenience to make a connection between the nuclear well and the cross section. It is, then, easier to discuss the resonance and the selective damping. The boundary condition for the wave function can be demonstrated by its logarithmic derivative, which for the square well is given by

$$R\frac{[\sin(Kr)]'}{\sin(Kr)}|_{r=R} = KR\cot(KR) \tag{7.6}$$

and in the Coulomb field, it is given by

$$\frac{R}{a_c}\left\{\frac{1}{\chi^2}\cot(\delta_0) + 2\left[\ln\left(\frac{2R}{a_c}\right) + 2A + y(ka_c)\right]\right\} \tag{7.7}$$

so that

$$\begin{aligned} \omega_i &= W_i/\chi^2 = \mathrm{Im}\left[\frac{a_c}{R}(KR)\cot(KR)\right] \\ &= \frac{a_c}{R}\left\{\frac{\gamma_i\sin(2\gamma_r) - \gamma_r\sinh(2\gamma_i)}{2[\sin^2(\gamma_r) + \sinh^2(\gamma_i)]}\right\} \end{aligned} \tag{7.8}$$

$$\begin{aligned} \omega_r &= W_r/\chi^2 = \frac{a_c}{R}\left\{\frac{\gamma_r\sin(2\gamma_r) + \gamma_i\sinh(2\gamma_i)}{2[\sin^2(\gamma_r) + \sinh^2(\gamma_i)]}\right\} \\ &\quad - 2H \end{aligned} \tag{7.9}$$

where $K^2 = \frac{2\mu}{\hbar^2}[E - (V_r + iV_i)]$, the real part K_r of K and its imaginary part K_i are related by the equation $K_i = \frac{\mu}{K_r\hbar^2}(-V_i)$, $\gamma = (\gamma_r + i\gamma_i) \equiv (K_rR + iK_iR)$, $H = \left[\ln\left(\frac{2R}{a_c}\right) + 2A + y(ka_c)\right]$, radius of the nuclear well $R = r_0(A_1^{1/3} + A_2^{1/3})$, r_0 is the radius parameter, A_1 and A_2 are the mass numbers of the reacting nuclei, Euler's constant $A = 0.5772156649$ and and $y(ka_c)$ is connected to the logarithmic derivative of the Γ function given as $y(x) = \frac{1}{x^2}\sum_{j=1}^{\infty}\frac{1}{j(j^2+x^{-2})} - A + \ln(x)$. In the above relations $k = \sqrt{\frac{2\mu E}{\hbar^2}} =$ the wave number outside the nuclear potential well.

7.1.2 Calculations and results

There are only two adjustable parameters, V_r and V_i, in the selective resonant tunneling model. These are adjusted to meet the resonance peak and then it reproduces the data

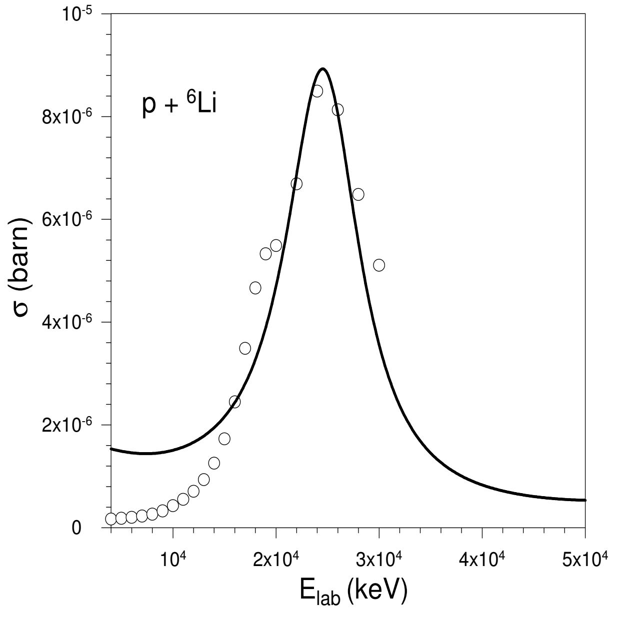

Figure 7.1: Plots of cross-section as a function of lab energy for p+^{6}Li fusion reaction. The continuous line represents the theoretical calculations while the hollow circles represent the experimental data points.

points covering the entire range of energy. The radius parameter r_0 may be kept fixed or adjusted to fine tune the calculations. In the present calculations, it is slightly varied from one system to the other in order to obtain better theoretical estimates. The fusion cross sections and the dimensionless astrophysical S-functions are calculated using Eq.(7.4) and Eq.(7.5), respectively whereas the astrophysical S-factors (in units of keV-barn) are calculated using Eq.(7.4) in Eq.(7.2).

The present formalism has been used to calculate the fusion cross-sections for d+d, d+t, d+^{3}He, p+^{6}Li, p+^{7}Li and p+^{11}B. While the first three [189, 190, 191, 192, 193] of these fusion reactions have been done in past with a completely different motive of fusion power production, the rest have been explored in the present work with an intention to use all these six reactions for astrophysical purposes. For the d+d, d+t and d+^{3}He, we use the same V_r, V_i and R from Refs.[193], [193] and [192], respectively. For the rest of the fusion reactions, V_r and V_i are adjusted to meet the position and magnitude of the

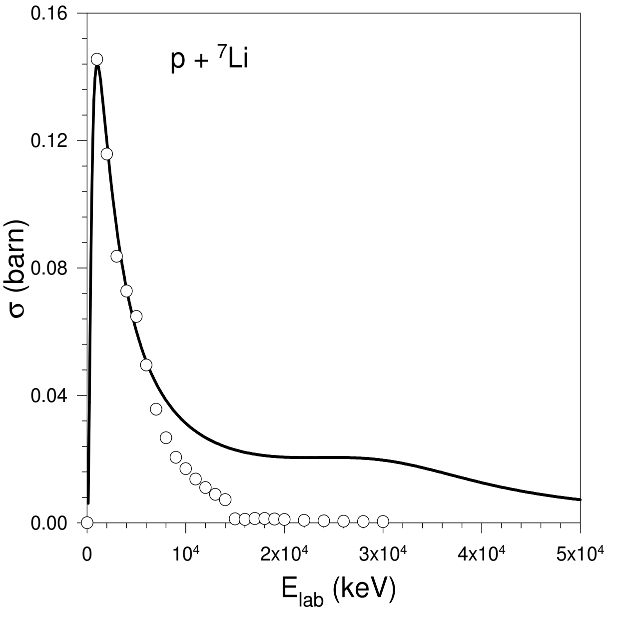

Figure 7.2: Plots of cross-section as a function of lab energy for p+^{7}Li fusion reaction. The continuous line represents the theoretical calculations while the hollow circles represent the experimental data points.

resonance peak in the fusion cross-section. The radius parameter r_0 (or equivalently the radius of the nuclear well R defined after Eq.(7.9)) has been further adjusted to fine tune so that the calculations reproduces the experimental data points covering the entire range of energy.

The results of the present calculation for cross sections of for d+d, d+t, d+^{3}He fusion reactions have been shown to compare well [194] with experimental data as well as those calculated using the three and five parameter fitting formulas of Ref.[193]. The results of the cross-section calculations for d+d, d+t, d+^{3}He fusion reactions are available in Ref.[193], Ref.[193] and Ref.[192], respectively and the magnitudes of V_r, V_i and r_0 for these three cases are, respectively, -48.52 MeV, -263.27 keV, 2.778 fm, -40.69 MeV, -109.18 keV, 1.887 fm and -11.859 MeV, -259.02 keV, 3.331 fm. The results of the cross-section calculations for p+^{6}Li, p+^{7}Li and p+^{11}B fusion reactions are shown in Figs.7.1-7.3, and the magnitudes of V_r, V_i and r_0 for these three cases are, respectively, -85

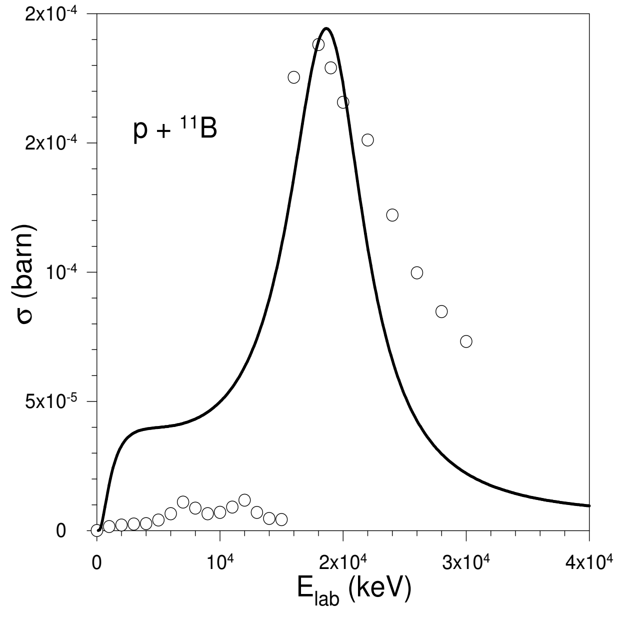

Figure 7.3: Plots of cross-section as a function of lab energy for p+^{11}B fusion reaction. The continuous line represents the theoretical calculations while the hollow circles represent the experimental data points.

MeV, −0.24 keV, 2.871 fm, −6.4 MeV, −3.12 MeV, 1.170 fm and −7.2 MeV, −4.57 keV, 1.180 fm. The experimental data [195] and the quantum-mechanical calculations show reasonable agreement. The results of present calculations for dimensionless S-functions, given by Eq.(7.5), are shown in Figs.-7.4-7.5. Somewhat, mismatch with experimental data in case of p+^{11}B fusion reaction may be due to lack of experimental data points and any conclusion at this stage regarding drawback of resonance tunneling model in case of heavier nuclei would be improper. The not so good agreement for other cases between theory and experiment is due to the fact that the energies involved are mostly above Coulomb barrier, while the theory as it is developed should work well at low energies. We have seen that the present formulation works exceedingly well for the same pair of fusing nuclei at low energies [196]. However, calculations of fusion cross sections for reactions involving medium and heavy nucleus-nucleus systems do need, altogether, a completely different approach [197].

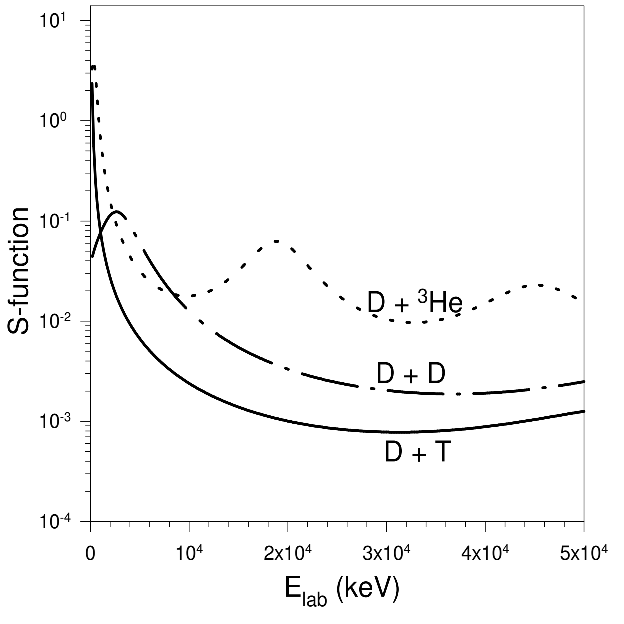

Figure 7.4: Plots of S-function as a function of lab energy for d+d, d+t, d+^{3}He fusion reactions.

In the deep sub-barrier fusion of light nuclei, the nuclear resonance chooses not merely the energy level or frequency but the damping as well that causes reaction between colliding nuclei. When the resonance occurs, the selectivity goes very sharp. In this type of selectivity in resonant tunneling processes, the neutron-emission reaction is suppressed. The compound nuclear picture fails to describe the process of fusion of light nuclides at energies too low, since the fusing nuclei may yet remember the phase factor of wave function describing the system while in the compound nuclear model, it is assumed that the fusing particles forget its past history [69]. In this model of compound nucleus, the reaction is assumed to proceed in two steps: first fusing to form the compound nucleus followed by its decay. In the present calculations that deals with selective resonant tunneling, the process is completely different where the tunneling probability itself depends upon the decay lifetime and is a single step process. The agreement with the experimental data for the deep sub-barrier fusion of light nuclei also suggests that the tunneling proceeds in a single step. The recent findings of halo nuclei [198] further strengthens the fact that

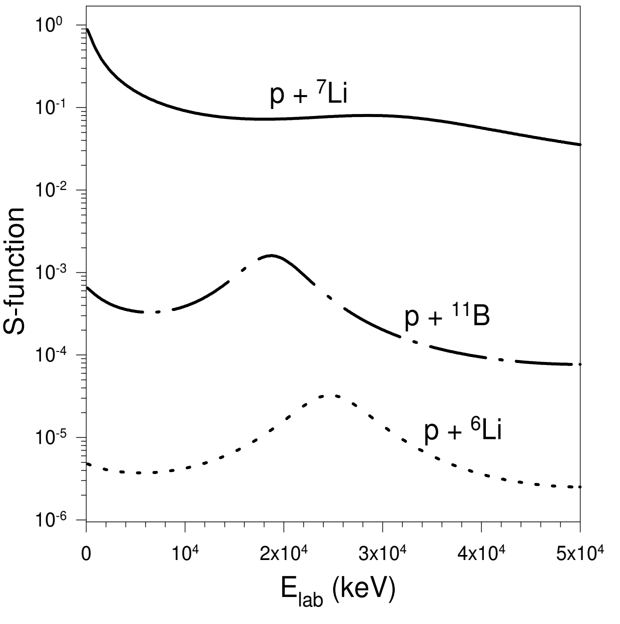

Figure 7.5: Plots of S-function as a function of lab energy for p+^{6}Li, p+^{7}Li and p+^{11}B fusion reactions.

the nucleons can keep their features without the memory loss for the wave function while inside the well of the strongly interacting nuclear region.

The complex potential causes absorption of the projectile into the nuclear well. For over last six decades intense research on controlled nuclear fusion has been focused much on the d-t fusion because of their large cross-section compared to that of d-d fusion by a factor of several hundred in spite of both having almost the same Coulomb barrier. The resonance near 100 keV of the d-t state is deemed as the reason for such a large cross section. A simple square-well potential model with an imaginary part can be used to describe the d+t nuclear fusion as well as other very light nuclei fusion reactions. The p+^{6}Li, p+^{7}Li and p+^{11}B fusion reactions are of astrophysical importance. It is worthwhile to note that whereas the real part of the nuclear potential well is primarily obtained from the energy at resonance, the imaginary part of the nuclear potential is obtained from the Gamow factor at resonance energy. The reasonably good accord between the theoretical (quantum-mechanical) calculation and the experimental data advocates a selective resonant tunneling model, rather than the traditional compound nuclear model, because of the fact that the fusing nuclei will retain the memory of phase factor of its wave function. The consequence of this selectivity in resonant tunneling can be explored further for fusion of other light nuclei.

Chapter 8

CONCLUDING REMARKS

In summary, we find that the EoS obtained using the density dependent M3Y effective interaction provides an excellent description of nuclear matter properties and the β-equilibrated neutron star matter which is stiff enough at high densities to reconcile with the recent observations of the massive compact stars. The stability of the β-equilibrated dense nuclear matter is analyzed with respect to the thermodynamic stability conditions. The proton fraction obtained using nuclear symmetry energy does not affect seriously the results of an exact calculation. Since the higher-order symmetry-energy coefficients are needed to describe reasonably well the proton fraction of the β-stable matter at high nuclear densities and the core-crust transition density, exact calculations are performed using the density dependent M3Y effective nucleon-nucleon interaction for investigating the proton fraction in neutron stars and the location of the inner edge of their crusts and their core-crust transition density and pressure. The nucleon-nucleon effective interaction used in the present work, which is found to provide a unified description of elastic and inelastic scattering, various radioactivities, and nuclear matter properties, also provides an excellent description of the β-equilibrated neutron star matter which is stiff enough at high densities to reconcile with the recent observations of the massive compact stars while the corresponding symmetry energy is supersoft as preferred by the FOPI/GSI experimental data. The density, the pressure, and the proton fraction at the inner edge separating the liquid core from the solid crust of the neutron stars determined to be $\rho_t = 0.0938$ fm^{-3}, $P_t = 0.5006$ MeV fm^{-3} and $x_{p(t)} = 0.0308$, respectively, are also in close agreement with other theoretical calculations corresponding to high nuclear incompressibility and with those obtained using the SLy4 interaction. The neutron star core-crust transition density, pressure and proton fraction determined from the thermodynamic stability condition along with observed minimum crustal fraction of the total moment of inertia of the Vela pulsar provide a limit for its radius. It is somewhat different from the other estimates and imposes a constraint $R \geq 4.10 + 3.36M/M_{\odot}$ km for the mass-radius relation of Vela pulsar like neutron stars.

In the deep sub-barrier fusion of light nuclei, the nuclear resonance selects not only the frequency or the energy level but also the damping that causes nuclear reaction. When the resonance occurs, the selectivity becomes very sharp. In such selective resonant tunneling processes the neutron-emission reaction is suppressed. The compound nuclear picture fails to describe the process of fusion of light nuclei at very low energies, since the fusing nuclei may still remember phase factor of the wave function describing the system while in the compound nuclear model, it is assumed that the fusing particle loses memory of its history. In the compound nuclear model, reaction is assumed to proceed in two steps: first fusing to form the compound nucleus followed by its decay. In the present calculations that deals with selective resonant tunneling, the process is completely different where the tunneling probability itself depends upon the decay lifetime and is a single step process. The agreement with the experimental data for the deep sub-barrier fusion of light nuclei also suggests that the tunneling proceeds in a single step. The recent findings of halo nuclei further strengthens the fact that the nucleons can keep their features without losing memory of the wave function while inside the well of the strongly interacting nuclear region. The complex potential causes absorption of the projectile into the nuclear well. For over last six decades, the research the controlled fusion reactions has been focused mostly on DT fusion for the reason that their cross-section is large compared to that of DD fusion by a few hundred times in spite of both having almost the same Coulomb barrier. The resonance of the d+t state near 100 keV is considered as the reason for such a large cross section. A simple square-well potential model with an imaginary part can be used to describe the d+t nuclear fusion as well as other very light nuclei fusion reactions. The d+d, d+t, d+^{3}He, p+^{6}Li, p+^{7}Li and p+^{11}B fusion reactions are of astrophysical importance. It is important to mention here that although the real part of the nuclear potential is primarily obtained from the energy at the resonance peak, the nuclear potential's imaginary part is obtained by the Gamow factor at resonance energy. Reasonably good agreement between the results of the quantum-mechanical calculations and the experimental data advocates a selective resonant tunneling model, rather than the model of a conventional compound nucleus. It is because of the fact that the penetrating nucleus keeps the memory of its wave functional phase factor. The consequences of this type of model of selective resonant tunneling can be explored further for other fusion reactions between two colliding light nuclei.

The fusion reaction cross sections have been calculated for above-barrier energies over a wide energy range. A set of precisely measured fusion excitation functions has been studied in order to learn about the conditions of overcoming the potential-energy barrier in nucleus-nucleus collisions and to obtain systematic information on the essential characteristics of the interaction potential, viz., the mean barrier height B_0 and width σ_B of its distribution, between the two colliding nuclei. For the analysis of the experimental data, a simple diffused-barrier formula is derived by assuming a Gaussian shape for the barrier distribution. Using the least squares fit method, precisely determined values of the mean barrier height B_0, the width σ_B, and the effective radius RB have been obtained.

The theoretical model for estimating the parameters of the barrier distribution described and their values are estimated. The observed enhancement of the sub-barrier capture (fusion) cross sections is correlated to the neutron transfer with positive Q values. The change of the capture cross section after the neutron transfer is due to the change of the deformations of nuclei. Obviously, it implies that, after the neutron transfer, if the deformations of nuclei do not change or decrease (increase), the neutron transfer weakly influences or suppresses (enhances) the capture process. To calculate the cross section required to overcome the barrier for a given projectile-target combination, one can use the present fusion-cross-section formula and apply theoretical values of the parameters B_0 and σ_B to predict cross sections for overcoming the barrier in collisions of very heavy systems. Prediction of the energy dependence of the cross section for capture or sticking can be used as one of three basic ingredients in the sticking-diffusion-survival model for calculating the production cross sections of superheavy nuclei. The reasonably good fit of the present theoretical description to the experimental data implies two important facts: (i) for the investigated set of nuclei almost all the capture events ultimately lead to fusion and (ii) the idea of the Gaussian distribution of the barrier provides a good description of near-barrier fusion cross sections.

As a future study the r-mode instability windows and the gravitational wave signatures of neutron stars in the slow rotation approximation using the equation of state obtained from the density dependent M3Y effective interaction can be performed. The fiducial gravitational and viscous timescales, the critical frequencies and the time evolutions of the frequencies and the rates of frequency change can be calculated for a range of neutron star masses to study the young and hot rotating neutron stars lie in the r-mode instability region. We anticipate that if the dominant dissipative mechanism of the r-mode is the shear viscosity along the boundary layer of the crust-core interface, then the neutron stars with low L value would lie in the r-mode instability region and would hence emit gravitational radiation. A detailed study in this direction would be of interest.

Bibliography

[1] B. A. Li, L. W. Chen, and C. M. Ko, Phys. Rep. **464**, 113 (2008).

[2] A. W. Steiner, M. Prakash, J. M. Lattimer and P. J. Ellis, Phys. Rep. **411**, 325 (2005).

[3] V. Baran, M. Colonna, V. Greco, and M. Di Toro, Phys. Rep. **410**, 335 (2005).

[4] C. J. Horowitz and J. Piekarewicz, Phys. Rev. Lett. **86**, 5647 (2001); B. G. Todd-Rutel and J. Piekarewicz, Phys. Rev. Lett. **95**, 122501 (2005).

[5] L. W. Chen, C. M. Ko, and B. A. Li, Phys. Rev. Lett. **94**, 032701 (2005); Phys. Rev. **C 72**, 064309 (2005).

[6] A. W. Steiner and B. A. Li, Phys. Rev. **C 72**, 041601(R) (2005).

[7] P. Danielewicz, R. Lacey and W.G. Lynch, Science **298**, 1592 (2002).

[8] G.Bertsch, J.Borysowicz, H.McManus, W.G.Love, Nucl. Phys. **A 284**, 399 (1977).

[9] G. R. Satchler and W. G. Love, Phys. Reports **55**, 183 (1979).

[10] R. G. Seyler and C. H. Blanchard, Phys. Rev. **124**, 227 (1961).

[11] R. G. Seyler and C. H. Blanchard, Phys. Rev. **131**, 355 (1963).

[12] D. Bandyopadhyay and S. K. Samaddar, Nucl. Phys. **A 484**, 315 (1988).

[13] C. Samanta, D. Bandyopadhyay and J. N. De, Phys. Lett. **B 217**, 381 (1989).

[14] D. Bandyopadhyay, C. Samanta, S. K. Samaddar and J. N. De, Nucl. Phys. **A 511**, 1 (1990).

[15] D. Vautherin and D.M. Brink, Phys. Rev. **C 5**, 626 (1972).

[16] Y.M. Engel, D.M. Brink, K. Goeke, S.J. Krieger and D. Vautherin, Nucl. Phys. **A 249**, 215 (1975).

[17] P. Bonche and D. Vautherin, Nucl. Phys. **A 372**, 496 (1981).

[18] B. Behera, T. R. Routray and R. K. Satpathy, J. Phys. **G 24**, 2073 (1998).

[19] B. Behera, T. R. Routray, B. Sahoo and R. K. Satpathy, Nucl. Phys. **A 699**, 770 (2002).

[20] T. R. Routray, X. Viñas, D. N. Basu, S. P. Pattnaik, M. Centelles, L. M. Robledo and B. Behera, J. Phys. **G 43**, 105101 (2016).

[21] B. A. Li and L. W. Chen, Phys. Rev. **C 72**, 064611 (2005).

[22] T. Li, U. Garg, Y. Liu et al., Phys. Rev. Lett. **99**, 162503 (2007).

[23] D. V. Shetty, S. J. Yennello, and G. A. Souliotis, Phys. Rev. **C 75**, 034602 (2007).

[24] M. Centelles, X. Roca-Maza, X. Viñas and M. Warda, Phys. Rev. Lett. **102**, 122502 (2009).

[25] P. B. Demorest, T. Pennucci, S. M. Ransom, M. S. E. Roberts and J. W. T. Hessels, Nature **467**, 1081 (2010).

[26] J. Antoniadis et al., Science **340**, 1233232 (2013).

[27] J. M. Lattimer and M. Prakash Science **304**, 536 (2004).

[28] G. Baym, C. J. Pethick and P. Sutherland, Astrophys. J. **170**, 299 (1971).

[29] G. Baym, H. A. Bethe and C. J. Pethick, Nucl. Phys. **A 175**, 225 (1971).

[30] C. J. Pethick and D. G. Ravenhall, Annu. Rev. Nucl. Part. Sci. **45**, 429 (1995).

[31] C. J. Pethick, D. G. Ravenhall and C. P. Lorenz, Nucl. Phys. **A 584**, 675 (1995).

[32] J. M. Lattimer and M. Prakash, Phys. Rep. **333**, 121 (2000).

[33] J. M. Lattimer and M. Prakash, Astrophys. J. **550**, 426 (2001).

[34] J. M. Lattimer and M. Prakash, Phys. Rep. **442**, 109 (2007).

[35] B. Link, R. I. Epstein and J. M. Lattimer, Phys. Rev. Lett. **83**,3362 (1999).

[36] C. J. Horowitz, M. A. Perez-Garcia and J. Piekarewicz, Phys. Rev. **C 69**, 045804 (2004).

[37] C. J. Horowitz, M. A. Perez-Garcia,J. Carriere, D. K. Berry and J. Piekarewicz, Phys. Rev. **C 70**, 065806 (2004).

[38] A. Burrows, S. Reddy and T. A. Thompson, Nucl. Phys. **A 777**, 356 (2006).

[39] B. J. Owen, Phys. Rev. Lett. **95**, 211101 (2005).

[40] S. B. Ruster, M. Hempel and J. Schaffner-Bielich, Phys. Rev. **C 73**, 035804 (2006).

[41] F. Douchin and P. Haensel, Phys. Let. **B 485**, 107 (2000).

[42] K. Oyamatsu and K. Iida, Phys. Rev. **C 75**, 015801 (2007).

[43] C. Ducoin, Ph. Chomaz and F. Gulminelli, Nucl. Phys. **A 789**, 403 (2007).

[44] Jun Xu, Lie-Wen Chen, Bao-An Li and Hong-Ru Ma, Phys. Rev. **C 79**, 035802 (2009).

[45] J. Xu, L. W. Chen, B. A. Li and H. R. Ma, Astrophys. J. **697**, 1549 (2009).

[46] S. Kubis, Phys. Rev. **C 70**, 065804 (2004).

[47] S. Kubis, Phys. Rev. **C 76**, 025801 (2007).

[48] A. Worley, P. G. Krastev and B. A. Li, Astrophys. J. **685**, 390 (2008).

[49] C. J. Horowitz and J. Piekarewicz, Phys. Rev. Lett. **86**, 5647 (2001).

[50] J. Carriere, C. J. Horowitz and J. Piekarewicz, Astrophys. J. **593**, 463 (2003).

[51] Jun Xu, Lie-Wen Chen, Bao-An Li and Hong-Ru Ma, Phys. Rev. **C 79**, 035802 (2009).

[52] P. Roy Chowdhury, D. N. Basu and C. Samanta, Phys. Rev. **C 80**, 011305(R) (2009).

[53] D. N. Basu, P. Roy Chowdhury and C. Samanta, Phys. Rev. **C 80**, 057304 (2009).

[54] H. B. Callen, Thermodynamics and An Introduction to Thermostatistics, 2nd edition, John Wiley & Sons, New York (1985).

[55] A G Lyne in *Pulsars: Problems and Progress*, S. Johnston, M. A. Walker and M. Bailes, eds., 73 (ASP, 1996).

[56] R I Epstein and G Baym, Astrophys. J. **387**, 276 (1992).

[57] M A Alpar, H F Chau, K S Cheng and D Pines, Astrophys. J. **409**, 345 (1993).

[58] B Link and R I Epstein, Astrophys. J. **457**, 844 (1996).

[59] M Ruderman, T Zhu, and K Chen, Astrophys. J. **492**, 267 (1998).

[60] A Sedrakian and J M Cordes, Mon. Not. R. Astron. Soc. **307**, 365 (1999).

[61] Debasis Atta and D N Basu, Phys. Rev. **C 90**, 035802 (2014).

[62] R. C. Tolman, Phys. Rev. **55**, 364 (1939).

[63] J. R. Oppenheimer and G. M. Volkoff, Phys. Rev. **55**, 374 (1939).

[64] D. Atta, S. Mukhopadhyay and D. N. Basu, Indian J. Phys **91**, 235 (2017).

[65] P. E. Hodgson, Nuclear Heavy-Ion Reactions, Oxford Univ., Oxford (1978).

[66] R. Bass, Nuclear Reactions with Heavy Ions, Springer, Berlin (1980).

[67] W. Nörenberg and H. A.Weidenmüller, Introduction to the Theory of Heavy-Ion Collisions, Springer, Berlin (1980).

[68] G. R. Satchler, Direct Nuclear Reactions, Oxford Univ., Oxford (1983).

[69] H. Feshbach, Theoretical Nuclear Physics: Nuclear Reactions, Wiley, New York (1992).

[70] P. Fröbrich and R. Lipperheide, Theory of Nuclear Reactions, Oxford Univ., Oxford (1996).

[71] N. Rowley, G. R. Satchler, and P. H. Stelson, Phys. Lett. **B 254**, 25 (1991).

[72] M. Dasgupta, D. J. Hinde, N. Rowley, and A. M. Stefanini, Annu. Rev. Nucl. Part. Sci. **48**, 401 (1998).

[73] G. Wallerstein et al., Rev. Mod. Phys. **69**, 995 (1997).

[74] J. X. Wei, J. R. Leigh, D. J. Hinde, J. O. Newton, R. C. Lemmon, S. Elfstrom, J. X. Chen, and N. Rowley,Phys. Rev. Lett. **67**, 3368 (1991).

[75] A. M. Stefanini et al., Phys. Rev. Lett. **74**, 864 (1995).

[76] H. Timmers, D. Ackermann, S. Beghini, L. Corradi, J. H. He, G. Montagnoli, F. Scarlassara, A. M. Stefanini, and N. Rowley, Nucl. Phys. **A 633**, 421 (1998).

[77] M. Trotta, A.M. Stefanini, L. Corradi, A. Gadea, F. Scarlassara, S. Beghini, and G. Montagnoli, Phys. Rev. **C 65**, 011601(R) (2001).

[78] A. M. Stefanini, F. Scarlassara, S. Beghini, G. Montagnoli, R. Silvestri, M. Trotta, B. R. Behera, L. Corradi, E. Fioretto, A. Gadea, Y. W. Wu, S. Szilner, H. Q. Zhang, Z. H. Liu, M. Ruan, F. Yang, and N. Rowley, Phys. Rev. **C 73**, 034606 (2006).

[79] A. M. Stefanini et al., Phys. Rev. **C 76**, 014610 (2007).

[80] Dao T. Khoa and W. von Oertzen, Phys. Lett. **B 304**, 8 (1993).

[81] Dao T. Khoa, W. von Oertzen and A. A. Ogloblin, Nucl. Phys. **A 602**, 98 (1996).

[82] Dao T. Khoa, G. R. Satchler and W. von Oertzen, Phys. Rev. **C 56**, 954 (1997).

[83] H. Nakada, Phys. Rev. **C 68**, 014315 (2003).

[84] H. Nakada, Phys. Rev. **C 78**, 054301 (2008).

[85] H. Nakada, Phys. Rev. **C 81**, 027301 (2010).

[86] A. K. Chaudhuri, D. N. Basu and Bikash Sinha, Nucl. Phys. **A 439**, 415 (1985).

[87] D. N. Basu, P. Roy Chowdhury and C. Samanta, Nucl. Phys. **A 811**, 140 (2008).

[88] W. D. Myers, Nucl. Phys. **A 204** 465 (1973).

[89] P. Roy Chowdhury and D. N. Basu, Acta Phys. Pol. **B 37**,1833 (2006).

[90] G. Audi, A.H. Wapstra and C. Thibault, Nucl. Phys. A 729, 337 (2003).

[91] D. Lunney, J. M. Pearson and C. Thibault, Rev. Mod. Phys. **75**, 1021 (2003).

[92] G. Royer and C. Gautier, Phys. Rev. **C 73**, 067302 (2006).

[93] G. A. Lalazissis, J. Konig and P. Ring, Phys. Rev. **C 55**, 540 (1997).

[94] G. A. Lalazissis, S. Raman, and P. Ring, At. Data and Nucl. Data Tables **71**, 1 (1999).

[95] S. Shlomo, V.M. Kolomietz and G. Colo, Eur. Phys. Jour. A **30**, 23 (2006).

[96] Y.W. Lui, D.H. Youngblood, Y. Tokimoto, H.L. Clark and B. John, Phys. Rev. C **69**, 034611 (2004).

[97] D.H. Youngblood, Y.W. Lui, B. John, Y. Tokimoto, H.L. Clark and X. Chen, Phys. Rev. C **69**, 054312 (2004).

[98] Y.W.Lui, D.H. Youngblood, H.L. Clark, Y. Tokimoto and B. John, Acta Phys. Pol. B **36**, 1107 (2005).

[99] J. P. Blaizot, Phys. Rep. **64**, 171 (1980).

[100] J. P. Blaizot, J. E. Berger, J. Dechargé and M. Girod, Nucl. Phys. **A 591**, 435 (1995).

[101] D. Vretenar, T. Nikśić and P. Ring, Phys. Rev. **C 68**, 024310 (2003).

[102] M. M. Sharma, Nucl. Phys. **A 816**, 65 (2009).

[103] T. Klähn et al., Phys. Rev. **C 74**, 035802 (2006).

[104] A. Akmal, V.R. Pandharipande and D.G. Ravenhall, Phys. Rev. C 58, 1804 (1998).

[105] Zhigang Xiao, Bao-An Li, Lie-Wen Chen, Gao-Chan Yong and Ming Zhang, Phys. Rev. Lett. **102**, 062502 (2009).

[106] T. Mukhopadhyay and D.N. Basu, Nucl. Phys. **A 789**, 201 (2007).

[107] P. Danielewicz, Nucl. Phys. **A 727**, 233 (2003).

[108] K. Pomorski and J. Dudek, Phys. Rev. **C 67**, 044316 (2003).

[109] L. Bennour et al., Phys. Rev. C **40**, 2834 (1989).

[110] D. N. Basu, Partha Roy Chowdhury and Abhishek Mishra, Eur. Phys. J. Plus **129**, 62 (2014).

[111] P. Roy Chowdhury, D. N. Basu and C. Samanta, Phys. Rev. **C 80**, 011305(R) (2009); D. N. Basu, P. Roy Chowdhury and C. Samanta, Phys. Rev. **C 80**, 057304 (2009).

[112] M. B. Tsang, Yingxun Zhang, P. Danielewicz, M. Famiano, Zhuxia Li, W. G. Lynch and A.W. Steiner, Phys. Rev. Lett. **102**, 122701 (2009).

[113] J. Piekarewicz and M. Centelles, Phys. Rev. **C 79**, 054311 (2009).

[114] M. Dutra, O. Lourenco, J. S. Sa Martins, A. Delfino, J. R. Stone and P. D. Stevenson, Phys. Rev. **C 85**, 035201 (2012).

[115] Hiroyuki Sagawa, Satoshi Yoshida, Guo-Mo Zeng, Jian-Zhong Gu and Xi-Zhen Zhang, Phys. Rev. **C 76**, 034327 (2007).

[116] M. Warda, X. Viñas, X. Roca-Maza and M. Centelles, Phys. Rev. **C 80**, 024316 (2009).

[117] B. K. Agrawal, J. N. De, S. K. Samaddar, G. Colò and A. Sulaksono, Phys. Rev. **C 87**, 051306(R) (2013).

[118] Bao-An Li and Xiao Han, Phys. Lett. **B 727**, 276 (2013).

[119] C. Mondal, B. K. Agrawal, J. N. De, S. K. Samaddar, M. Centelles and X. Viñas, Phys. Rev. **C 96**, 021302(R) (2017).

[120] M. Oertel, M. Hempel, T. Klähn and S. Typel, Rev. Mod. Phys. **89**, 015007 (2017).

[121] P. Roy Chowdhury, C. Samanta and D. N. Basu, Phys. Rev. **C 73**, 014612 (2006); *ibid* Phys. Rev. **C 77**, 044603 (2008); *ibid* Atomic Data and Nuclear Data Tables **94**, 781 (2008).

[122] C. Samanta, P. Roy Chowdhury and D.N. Basu, Nucl. Phys. **A789**, 142 (2007).

[123] De-Hua Wen, Bao-An Li and Lie-Wen Chen, Phys. Rev. Lett. **103**, 211102 (2009).

[124] H. Komatsu, Y. Eriguchi, I. Hachisu, Mon. Not. R. Astron. Soc. **237**, 355 (1989).

[125] R. C. Tolman, Phys. Rev. **55**, 364 (1939); J. R. Oppenheimer and G. M. Volkoff Phys. Rev. **55**, 374 (1939).

[126] N. Stergioulas, J. L. Friedman, Astrophys. J. **444**, 306 (1995).

[127] R. P. Feynman, N. Metropolis and E. Teller, Phys. Rev. **75**, 1561 (1949).

[128] N. Stergioulas, Living Rev. Rel. **6**, 3 (2006).

[129] J. W. T. Hessels et al., Science **311**, 1901 (2006).

[130] P. R. Chowdhury, A. Bhattacharyya and D. N. Basu, Phys. Rev. **C 81**, 062801(R) (2010).

[131] A. Kurkela, P. Romatschke, A. Vuorinen, Phys. Rev. **D 81**, 105021 (2010).

[132] A. Chodos, R. L. Jaffe, K. Johnson and C. B. Thorn, Phys. Rev. **D 10**, 2599 (1974).

[133] H. Heiselberg, C. J. Pethick and E. F. Staubo, Phys. Rev. Lett. **70**, 1355 (1993).

[134] S. Weissenborn, I. Sagert, G. Pagliara, M. Hempel and J. Schaffner-Bielich, Astrophys. J. Lett. **740**, L14 (2011).

[135] Abhishek Mishra, P. R. Chowdhury and D. N. Basu, Astropart. Phys. **36**, 42 (2012).

[136] J. M. Lattimer, C. J. Pethick, M. Prakash and P. Haensel, Phys. Rev. Lett. **66**, 2701 (1991).

[137] Andrew W. Steiner, Phys. Rev. **C 74**, 045808 (2006).

[138] E. M. Cackett et al., Mon. Not. Roy. Astron. Soc. **372**, 479 (2006).

[139] Craig O. Heinke and Wynn C. G. Ho, Astrophys. J. Lett. **719**, L167 (2010).

[140] Dany Page, Madappa Prakash, James M. Lattimer and Andrew W. Steiner, Phys. Rev. Lett. **106**, 081101 (2011).

[141] Dmitry G. Yakovlev, Wynn C. G. Ho, Peter S. Shternin, Craig O. Heinke and Alexander Y. Potekhin, Mon. Not. Roy. Astron. Soc. **411**, 1977 (2011).

[142] Peter S. Shternin, Dmitry G. Yakovlev, Craig O. Heinke, Wynn C. G. Ho and Daniel J. Patnaude, Mon. Not. Lett. Roy. Astron. Soc. **412**, L108 (2011).

[143] C. Ducoin, J. Margueron and C. Providência, Eur. Phys. Lett. **91**, 32001 (2010).

[144] F. Sammarruca and P. Krastev, Phys. Rev. **C 73**, 014001 (2006).

[145] B. Sinha, Phys. Rev. Lett. **50**, 91 (1983).

[146] J. R. Stone, N. J. Stone and S. A. Moszkowski, Phys. Rev. **C 89**, 044316 (2014).

[147] Lie-Wen Chen, Bao-Jun Cai, Che Ming Ko, Bao-An Li, Chun Shen and Jun Xu, Phys. Rev. **C 80**, 014322 (2009).

[148] V. S. Uma Maheswari, D..N. Basu, J. N. De and S. K. Samaddar, Nucl. Phys. **A 615**, 516 (1997).

[149] W. D. Arnett and R. L. Bowers, Astrophys. J. Suppl. **33**, 415 (1977).

[150] N. Andersson, K. Glampedakis, W. C. G. Ho and C. M. Espinoza, Phys. Rev. Lett. **109**, 241103 (2012).

[151] N. Chamel, Phys. Rev. Lett. **110**, 011101 (2013).

[152] J. Piekarewicz, F. J. Fattoyev and C. J. Horowitz, Phys. Rev. **C 90**, 015803 (2014).

[153] A. W. Steiner, S. Gandolfi, F. J. Fattoyev and W. G. Newton, Phys. Rev. **C 91**, 015804 (2015).

[154] Wynn C. G. Ho and Nils Andersson, Nature Physics **8**, 787 (2012).

[155] G. G. Pavlov, V. E. Zavlin, D. Sanwal, V. Burwitz and G. P. Garmire, Astrophys. J. **552**, L129 (2001).

[156] J. Hooker, W. G. Newton, Bao-An Li, Mon. Not. R. Astron. Soc. **449**, 3559 (2015).

[157] T. Delsate, N. Chamel, N. Gürlebeck, A. F. Fantina, J. M. Pearson, C. Ducoin, Phys. Rev. **D 94**, 023008 (2016).

[158] A. Li, J. M. Dong, J. B. Wang, R. X. Xu, Astrophys. J. Suppl. Ser. **223**, 16 (2016).

[159] F. Gulminelli, Ad. R. Raduta, *Phys. Rev.* **C 92**, 055803 (2015).

[160] H. Pais, A. Sulaksono, B. K. Agrawal and C. Providência, *Phys. Rev.* **C 93**, 045802 (2016).

[161] C. Ducoin, J. Margueron, and P. Chomaz, *Nucl. Phys.* **A 809**, 30 (2008).

[162] C. J. Horowitz and G. Shen, *Phys. Rev.* **C 78**, 015801 (2008).

[163] C. Ducoin, J. Margueron, C. Providência and I. Vidaña, *Phys. Rev.* **C 83**, 045810 (2011).

[164] K. Siwek-Wilczyńska and J. Wilczyński, Phys. Rev. **C 69**, 024611 (2004).

[165] T. Cap, K. Siwek-Wilczyńska and J. Wilczyński, Phys. Rev. **C 83**, 054602 (2011).

[166] Roman Wolski, Phys. Rev. **C 88**, 041603(R) (2013).

[167] H. Esbensen, Nucl. Phys. **A 352**, 147 (1981).

[168] P. Möller, J. R. Nix, W. D. Myers and W. J. Swiatecki, At. Data Nucl. Data Tables **59**, 185 (1995).

[169] S. Raman, C. W. Nestor, JR. and P. Tikkanen, At. Data Nucl. Data Tables **78**, 1 (2001).

[170] V. V. Sargsyan, G. G. Adamian, N. V. Antonenko, W. Scheid and H. Q. Zhang, Phys. Rev. **C 84**, 064614 (2011).

[171] V. V. Sargsyan, G. G. Adamian, N. V. Antonenko, W. Scheid and H. Q. Zhang, Phys. Rev. **C 85**, 024616 (2012).

[172] V. V. Sargsyan, G. Scamps, G. G. Adamian, N. V. Antonenko and D. Lacroix, Phys. Rev. **C 88**, 064601 (2013).

[173] N. V. Antonenko, E. A. Cherepanov, A. K. Nasirov, V. P. Permjakov, and V. V. Volkov, Phys. Lett. **B 319**, 425 (1993).

[174] J. R. Leigh, M. Dasgupta, D. J. Hinde, J. C. Mein, C. R. Morton, R. C. Lemmon, J. P. Lestone, J. O. Newton, H. Timmers, J. X. Wei, and N. Rowley, Phys. Rev. **C 52**, 3151 (1995).

[175] A. M. Stefanini, D. Ackermann, L. Corradi, J. H. He, G. Montagnoli, S. Beghini, F. Scarlassara, and G. F. Segato, Phys. Rev. **C 52**, R1727 (1995).

[176] A. M. Stefanini, F. Scarlassara, S. Beghini, G. Montagnoli, R. Silvestri, M. Trotta, B. R. Behera, L. Corradi, E. Fioretto, A. Gadea, Y. W. Wu, S. Szilner, H. Q. Zhang, Z. H. Liu, M. Ruan, F. Yang, and N. Rowley, Phys. Rev. **C 73**, 034606 (2006).

[177] J. J. Kolata, A. Roberts, A. M. Howard, D. Shapira, J. F. Liang, C. J. Gross, R. L. Varner, Z. Kohley, A. N. Villano, H. Amro, W. Loveland, and E. Chavez, Phys. Rev. **C 85**, 054603 (2012).

[178] F. Scarlassara, S. Beghini, G. Montagnoli, G. F. Segato, D. Ackermann, L. Corradi, C. J. Lin, A. M. Stefanini, and L. F. Zheng, Nucl. Phys. **A 672**, 99 (2000).

[179] A. M. Stefanini, L. Corradi, A. M. Vinodkumar, Yang Feng, F. Scarlassara, G. Montagnoli, S. Beghini, and M. Bisogno, Phys. Rev. **C 62**, 014601 (2000).

[180] H. Q. Zhang, C. J. Lin, F. Yang, H. M. Jia, X. X. Xu, Z. D. Wu, F. Jia, S. T. Zhang, Z. H. Liu, A. Richard, and C. Beck, Phys. Rev. **C 82**, 054609 (2010).

[181] E. M. Burbidge, G. R. Burbidge, W. A. Fowler and F. Hoyle, Rev. Mod. Phys. **29**, 547 (1957).

[182] W. A. Fowler and F. Hoyle, Astrophys. J. Suppl. **9**, 201 (1964); Appendix C.

[183] D. D. Clayton, *Principles of Stellar Evolution and Nucleosynthesis* (University of Chicago Press, Chicago, 1983).

[184] R. N. Boyd, *An Introduction to Nuclear Astrophysics* (University of Chicago, Chicago, 2008), 1st ed.

[185] J. M. Blatt and V. F. Weisskopf, *Theoretical Nuclear Physics* (John Wiley & Sons, New York; Chapman & Hall Limited, London.)

[186] Tapan Mukhopadhyay, Joydev Lahiri and D. N. Basu, Phys. Rev. **C 82**, 044613 (2010); *ibid* Phys. Rev. **C 83**, 067603 (2011).

[187] G. Gamow, Phys. Rev. **53**, 595 (1938).

[188] G. Gamow, Zeits. f. Physik. **51**, 204 (1928).

[189] X. Z. Li, Czechoslovak Journal of Physics **49**, 985 (1999).

[190] X. Z. Li, C. X. Li and H. F. Huang, Fusion Technology **36**, 324 (1999).

[191] Xing Zhong Li, Jian Tian, Ming Yuan Mei and Chong Xin Li, Phys. Rev. **C 61**, 024610 (2000).

[192] Xing Z. Li, Bin Liu, Si Chen, Qing M. Wei and Heinrich Hora, Laser and Particle Beams **22**, 469 (2004).

[193] Xing Z. Li, Qing M. Wei and Bin Liu, Nucl. Fusion **48**, 125003 (2008).

[194] Vinay Singh, Debasis Atta and Md. A. Khan, Proceedings of the DAE-BRNS Symp. on Nucl. Phys. **61**, 930 (2016).

[195] Chadwick M.B. et al. ENDF/B-VII.0: Next generation evaluated nuclear data library for nuclear science and technology Nucl. Data Sheets **107**, 29313060 (2006).

[196] Vinay Singh, Debasis Atta, Md. A. Khan and D. N. Basu, arXiv:1807.05815.

[197] Debasis Atta and D. N. Basu, Phys. Rev. **C 90**, 064622 (2014).

[198] K. Riisager, Rev. Mod. Phys. **66**, 1105 (1994).